Master's Theses and Capstones   Student Scholarship

2014

A Field Method for Backscatter Calibration Applied to NOAA's Reson 7125

Briana Welton
University of New Hampshire - Main Campus

Follow this and additional works at: https://scholars.unh.edu/thesis

A Field Method for Backscatter Calibration Applied to NOAA's Reson 7125

Multibeam Echo-Sounders

BY

Briana Welton

B.A., Mathematics, Smith College, 2002

THESIS

Submitted to the University of New Hampshire

in Partial Fulfillment of

the Requirements for the Degree of
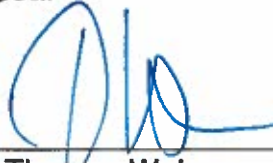

Master of Science

In

Ocean Engineering

May, 2014

This thesis has been examined and approved.

_____
Thesis Director, Dr. Jonathan Beaudoin
Research Assistant Professor, UNH

_____
Dr. Thomas Weber
Assistant Professor, UNH

_____
Capt. Andrew Armstrong III, NOAA (ret)
Co-Director, Joint Hydrographic Center
Affiliate Professor, UNH

April 28, 2014
_____
Date

DEDICATION

This thesis is dedicated to my hydro friends, and to the others who read it.

ACKNOWLEDGEMENTS

TABLE OF CONTENTS

LIST OF TABLES

LIST OF FIGURES

LIST OF ACRONYMS

CTD   Conductivity, Temperature, & Depth

ERDDM   Ellipsoid-Referenced Dynamic Draft Measurement

FMGT   Fledermaus Geocoder Toolbox

IMU   Inertial Measurement Unit

JD   Julian Day

LUT   Look-up Table

MBES   Multibeam Echo-Sounder

MRA   Maximum Response Axis

NM   Nautical Mile

NOAA   National Oceanic and Atmospheric Administration

OCS   Office of Coast Survey

PDF   Probability Density Function

POSMV   Position and Orientation System for Marine Vessels

RPM   Revolutions per Minute

S1   South One Survey Line

SOP   Standard Operating Procedure

SSP   Sound Speed Profile

SSS   Surface Sound Speed

SV   Surface Vessel

TVG   Time Varying Gain

UNH	University of New Hampshire
UTC	Coordinated Universal Time

ABSTRACT

A Field Method for Backscatter Calibration Applied to NOAA's Reson 7125

Multibeam Echo-Sounders

by

Briana Welton

University of New Hampshire, May, 2014

Acoustic seafloor backscatter measurements made by multiple Reson multibeam echo-sounders (MBES) used for hydrographic survey are observed to be inconsistent, affecting the quality of data products and impeding large-scale processing efforts. A method to conduct a relative *inter* and *intra* sonar calibration in the field using dual frequency Reson 7125 MBES has been developed, tested, and evaluated to improve the consistency of backscatter measurements made from multiple MBES systems. The approach is unique in that it determines a set of corrections for power, gain, pulse length, and an angle dependent calibration term relative to a single Reson 7125 MBES calibrated in an acoustic test tank. These corrections for each MBES can then be applied during processing for any acquisition setting combination. This approach seeks to reduce the need for subjective and inefficient manual data or data product manipulation during post processing, providing a foundation for improved automated seafloor characterization using data from more than one MBES system.

CHAPTER 1

Introduction

<u>**Problem Statement**</u>

Acoustic seafloor backscatter is used for diverse applications with a wide variety of techniques and approaches. Backscatter has been used to segment or cluster the seafloor into like areas or "themes" to estimate the acoustic impedance of the seafloor, which can be used to predict physical properties of the seafloor such as mean grain size and porosity (Fonseca and Mayer, 2007). Backscatter mosaics can be used to aid point sample selection for charting purposes (NOAA, 2013a), and might also be used to inform the time uncertainty of charted depths and re-survey schedules. Geological oceanographers have used backscatter to help understand seafloor provenance (Mitchell and Clarke, 1994, Dartnell and Gardner, 2004). Ocean engineers and resource managers have used backscatter to inform underwater construction and engineering projects such as cables, pipelines, wind farms, and geological storage (Paton et al., 1997, Pearce et al., Kinney, 2006, Heap et al., 2014). Modelers have used backscatter to inform transport models and estimate seafloor stability (Goff et al., 2002, Hughes Clarke et al., 1996). Fisheries scientists have used backscatter for habitat and population modeling (Brown and Blondel, 2009). Defense and government agencies have also used backscatter for the detection of unexploded ordnance (Wilson et al., 2009), and marine debris (Masetti and Calder, 2012). Backscatter might also be used

as an indicator of sonar health since problems with sonar sub-systems can cause artifacts in backscatter that can sometimes go unnoticed in bathymetric measurements.

Because of the diverse array of scientific and engineering applications, seafloor backscatter measurements are increasingly being recorded in conjunction with bathymetric measurements to capitalize on vessel time during hydrographic surveys. However, although acoustic scattering is a stochastic physical process, the difference in the central tendency of measurements made by different multibeam echo-sounders (MBES) of the same manufactured model over the same seafloor are observed to be inconsistent. Since the use of multiple MBES on a single hydrographic survey is a common operational paradigm within large hydrographic survey organizations, backscatter measurement inconsistencies significantly detract from the visual quality of backscatter products such as mosaics, and impede the use of manual and automated seafloor segmentation and/or characterization routines. The goal of this work is to reduce this kind of backscatter measurement inconsistency.

The problem is regularly apparent in backscatter mosaics at the geographic junction of adjacent data acquired with multiple systems, a situation further complicated by the use of different acquisition settings with each system. Figure 1 is an example of a typical backscatter mosaic made from data from four different Reson 7125 MBES in which the backscatter measurement inconsistencies between systems and settings are visually apparent.
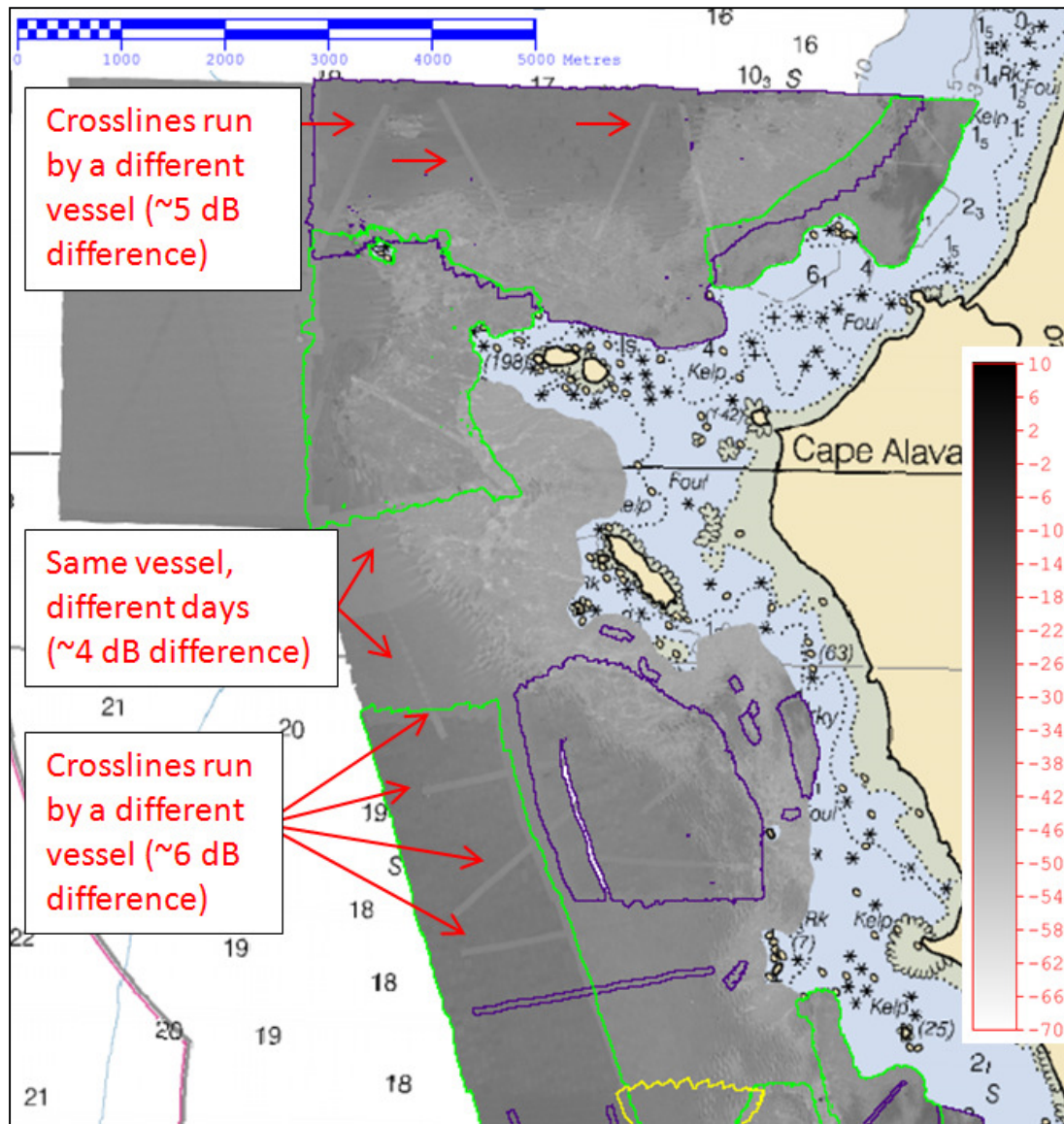
Figure 1: Backscatter mosaics from a NOAA hydrographic survey H12221 off the coast of Washington state. Data acquired in 2010 processed with Fledermaus Geocoding Toolbox (FMGT) using data from four different 400-kHz Reson 7125 MBES systems mounted on different vessels: Launch 2805 (no outline), Launch 2806 (purple), Launch 2807 (green), Launch 2808 (yellow).

Figure 2 shows the average beam backscatter value by the mean angle of incidence nominally corrected for settings and beam geometry from survey line files run over the same patch of seafloor by four survey launches with Reson 7125 MBES over the course of several years. Each unique survey launch is distinguished by vessel hull number

(Launch 280X, with X indicating a unique vessel hull number). Significant relative differences of up to 5 dB for the 200-kHz frequency and 7.5 dB for the 400-kHz frequency are observed. A mosaic processed and created in Fledermaus Geocoder Toolbox (FMGT) with a single line file from the set of lines shown in Figure 2 is presented in Figure 3. Data from both the 200 and 400-kHz projectors for every year available are shown. (The survey line is from a test site in Puget Sound, Washington, which is described in more detail in Chapter 4. Though an attempt was made to run all lines from this location using the same power, gain, and pulse length settings year to year, some of the lines were logged using different settings and courses. The individual MBES components such as projectors and receivers on each launch were not the same year to year either.)
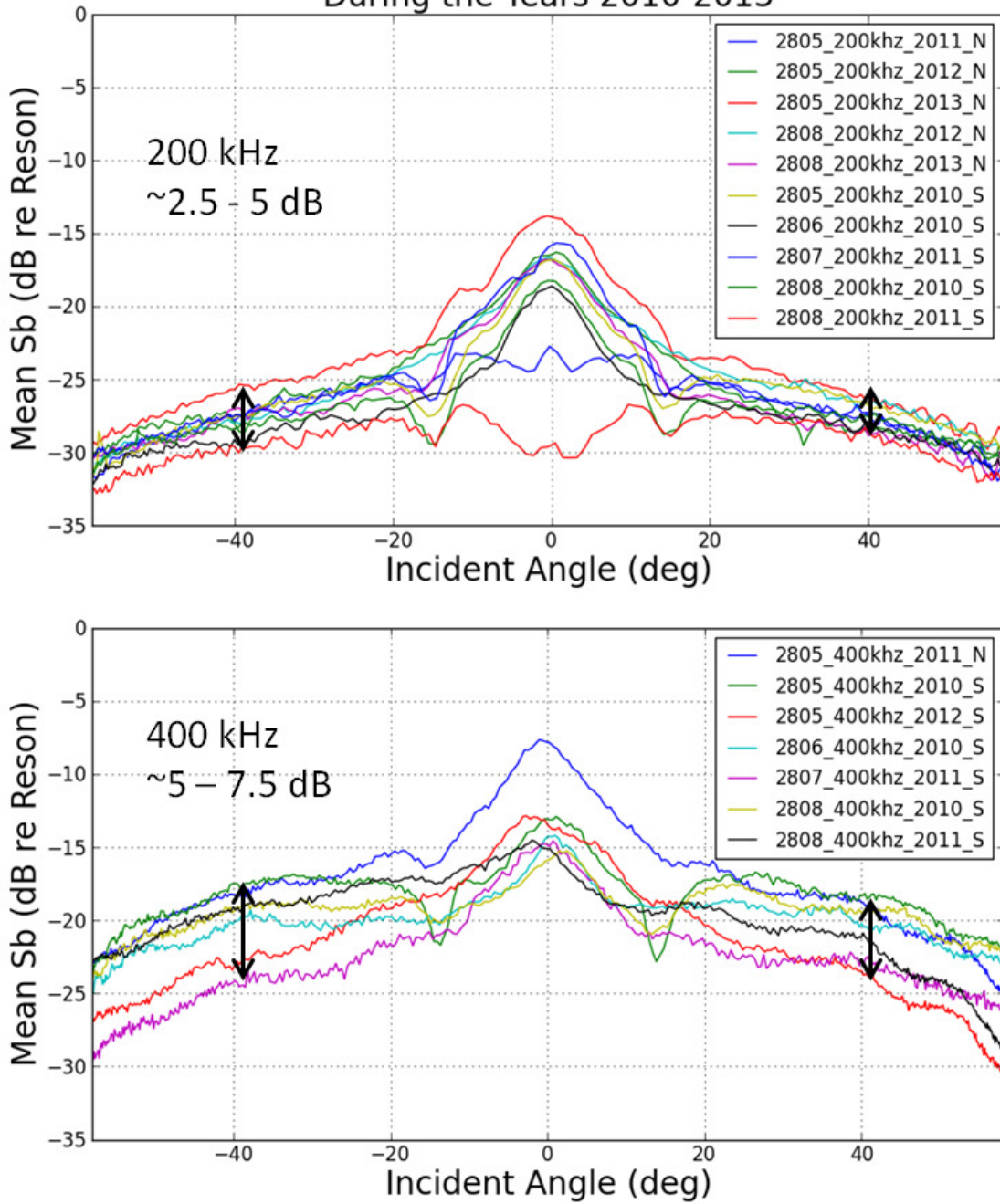
Figure 2: Beam average backscatter values from a single survey line from a reference area in Shilshole Bay, Puget Sound, run multiple times over four years by four survey launches, each with dual frequency Reson 7125s (200 kHz top, 400 kHz bottom, line direction indicated by "N" for north and "S" for south).
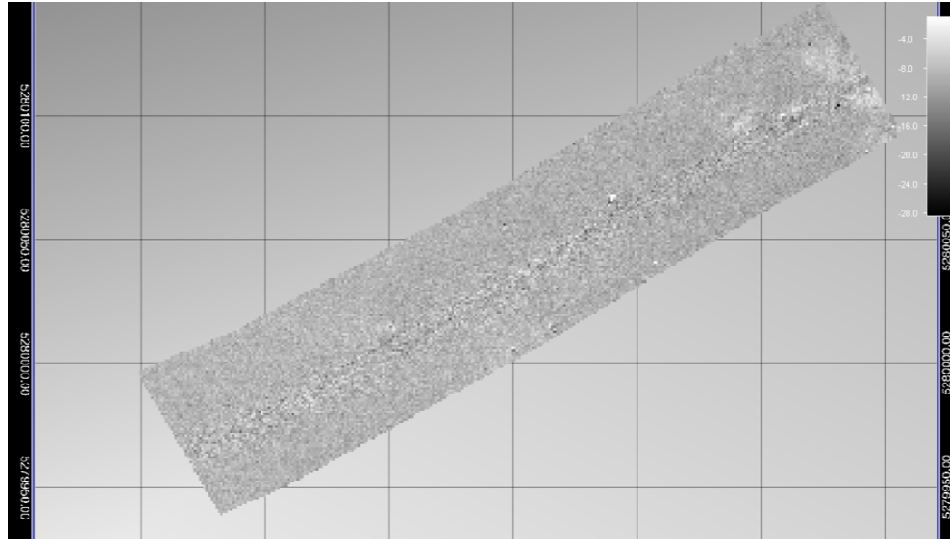
Figure 3: Mosaic of a single survey line file from a standard reference area in Shilshole Bay, Puget Sound, Washington (~13 m of water, ~500 m long) processed in FMGT.

Assuming the backscatter reduction process incorporates well measured and/or well modeled water column and seafloor geometry, and that any biases introduced by the processing reduction routine employed such as the insonified area estimate or sample selection are the same for all MBES systems, then the lack of radiometric calibrations is a reasonable explanation for measurement inconsistency. The solution to this is, of course, to acoustically calibrate the systems, however, absolute acoustic calibration in a test tank for every MBES is cost-and-time-prohibitive. A standard target calibration, in the field, with shallow water MBES mounted on small vessels poses physical challenges to positioning the target in the far field of all the beams. The field calibration proposed by Lanzoni (Lanzoni and Weber, 2011) requires a calibrated split-beam echo-sounder to position the target, the mounting for which also poses a challenge for use on small vessels, and has not yet been tested in the field. The additional effort required to set up these kinds of calibrations also scales with each additional system to be calibrated, and is excessive if all that is desired is consistency in measurements between systems.

6

A relative calibration is a reasonable alternative. Greenaway and Rice derived a single-value offset between two Reson 7125 SV2 MBES operating simultaneously on the same ship by differencing the averaged backscatter data acquired over a large geographic area that was processed in commercially available software (Greenaway, 2013). However, the systems were operating on the same hull at the same time and the derived offsets between the two systems were found to vary with time and/or location, likely due to different settings and system normalizations (a specific feature of Reson 7125 MBES to normalize amplitude and phase differences between the receiver elements).

Proposed Solution

This work proposes a compromise between existing absolute and relative calibration approaches to achieve consistent absolute backscatter estimates from multiple MBES systems via a field method devised to relatively calibrate multiple MBES systems against an absolute tank-calibrated system. A procedure with accompanying data reduction and analysis tools to conduct an *inter-* and *intra-* sonar calibration in the field, geared toward Reson 7125 MBES, has been created and explored using multiple NOAA launches, each of the same design and build, all outfitted with Reson 7125 SV1 MBES, one of which was calibrated in an acoustic test tank at the University of New Hampshire. The approach is unique in that it: 1) Applies acoustic tank measurements of the angular-dependent calibration coefficient, source level, gain, and beam widths performed at a fixed range and a single power, gain, and pulse length setting to reflectivity field data collected by the tank calibrated MBES to estimate the absolute scattering strength of a particular patch of seafloor; 2) Uses the absolute scattering strength estimate of the seafloor from the tank calibrated system to transfer the absolute

calibration to an uncalibrated system by using the uncalibrated system to measure the same patch of "calibrated seafloor" for one single set of settings (*inter* calibration); and 3) Measures the response of the field calibrated system at all other possible settings other than those used to measure the "calibrated seafloor" and develops corrections for them (*intra* calibration). The proposed result is a set of four correction look-up tables (LUT): one to account for the angle-dependent calibration coefficient at a single, fixed set of settings relative to the tank-calibrated system; and the other three to account for how the field calibrated system responds to changes in power, gain and pulse length settings relative to those used to measure the calibrated seafloor. Though the ability to apply such corrections does not currently exist in commercial processing software, the set of four correction tables are envisioned to be incorporated into the backscatter reduction process for any operational setting combination and are expected to eliminate the need for setting specific data processing (e.g. unique single-value combined corrections for each setting combination), or data product manipulation such as the use of non-linear color maps.

CHAPTER 2

Background

Backscatter from Hydrographic MBES for Seafloor Characterization

Multibeam echo sounders have been a common tool used in hydrographic survey to make bathymetric seafloor measurements since the 1980s. They typically consist of an acoustic projector and receiver array oriented in a Mill's cross orientation fixed to a watercraft such as a small boat, ship, autonomous or remotely operated vehicle, with electronic components to drive transduction, receive auxiliary data inputs (e.g. time synchronization, navigation, attitude, and sound speed), control operation, and record data. Hundreds of beams are formed over a wide angular sector in the across-track direction by coherently summing time delayed signals originating from the elements within a transmit array reflected from the water column and seafloor and received by elements in a receiver array. Range and angle measurements from hundreds of beams formed over swaths on the order of 120-150$^{\text{o}}$ are the primary measurements used to derive seafloor depths from hydrographic MBES. Most modern MBES also have the capability of recording some portion of the full beam-formed amplitude and phase time series output, allowing for measurement of water column and/or seafloor reflectivity as well. Seafloor backscatter from each beam can be derived from the amplitude of the portion of the complex envelope time series associated with

9

the seafloor and can be corrected for the radiometric and geometric parameters associated with it to estimate seafloor acoustic backscattering strength (Lurton, 2010).

The use of MBES backscatter measurements to characterize seafloor properties remotely was proposed as early as 1993 by De Moustier and Matsumoto (1993). A full coverage map of seafloor properties using a remote measurement approach is appealing for a number of reasons. For large areas, comprehensive geospatial imagery is more cost effective than high-resolution discrete point sampling with cameras, grab-samplers, cores, divers, or ROVs, and is often a complementary foundation for lower-resolution point sampling.

Large-scale hydrographic survey operations typically involve more than one vessel-MBES acquisition platform from which bathymetric and backscatter data are acquired. Bathymetric data are corrected for vessel navigation and attitude, sound speed, water levels, and misalignment between sensor reference frames and are combined into a single data set to produce a bathymetric surface. Bathymetric surfaces from multiple surveys or other seafloor mapping efforts can be joined with one another to make large scale mapping products such as those made available by Google Earth or the Global Bathymetric Chart of Oceans (GEBCO), and are limited only by resolution and computing capacity. This practice results in high quality geospatial map products useful for a variety of scientific, social, geographic, and political uses when the seafloor depth measurements and the gridded surfaces are corrected and reduced to a common vertical and horizontal datum.

A similar paradigm for acoustic seafloor backscatter products does not currently exist. The inconsistencies observed in backscatter measurements between different makes and models of MBES and a lack of standardized processing procedures and uses of the data are obstacles to realizing this kind of paradigm (Brown and Blondel,

2009, Parnum and Gavrilov, 2012). Multibeam echo-sounders are also operated at a range of different frequencies that span hundreds of kHz. Data collected using different frequencies makes little sense to directly combine due to the frequency dependence of acoustic scattering. Tools in commercially available software to make radiometric and geometric corrections to compensate for operating settings and to apply acoustic calibration information are in developmental stages. Best practices for data processing and manipulation are also emerging. The present situation hinders efforts to create synthesized data products from multiple measuring devices, limiting data products to relative measurements from a single MBES operated at a single frequency on small geographic and time scales. A detailed look into the reduction of raw MBES data into seafloor backscatter and the ways in which measurement inconsistency occurs are explored in the next section.

Sources of Backscatter Measurement Inconsistencies

"No man ever steps in the same river twice, for it is not the same river and he is not the same man" (Heraclitus), is an apt analogy for seafloor backscatter measurements. The seafloor can change. The water column can change. And MBES can change, all at varying time scales. Measurement inconsistencies can occur from imperfect measurement and/or modeling of any of these physical processes. Decoupling every possible inferred, measured, and modeled input that might be used in estimating backscatter measurements is beyond the scope of this work. However, examining the sources of backscatter measurement inconsistency from the physical perspective and from the sonar equation perspective is helpful to understand and appreciate the many possible ways inconsistencies might occur, and to provide a

foundation for how to go about isolating the sonar characteristics from the characteristics of the water column and the seafloor.

Each individual backscatter estimate is the result of accounting for a collection of stochastic processes associated with the equipment, the medium, and the target (Urick, 1967). That is, each measurement is affected by the MBES's ability to transmit and receive sound, the vehicle on which the MBES is mounted, and the collective response to the environmental conditions in which the system is operated; the media through with the sound is propagated; and the properties of the seafloor. The goal is to correct for the equipment and media such that the measurement only represents the seafloor.

Though there are many acoustic models that can be used to resolve seafloor backscatter (Etter, 2013), the sonar equation is a common, simple way to account for the individual physical processes described in the previous section. It is favorable for estimating backscatter because all terms are in dB, logarithmic units, allowing for easy addition and subtraction of terms representing an extreme range of numeric values. Starting from the perspective of a modified conventional sonar equation in which the units are all in dB (Urick, 1967):

$$\mathrm{EL} = \mathrm{SL} - 2\mathrm{TL} + \mathrm{TS} \qquad\qquad [1]$$

where EL is the echo level:

$$\mathrm{EL} = \mathrm{DN} - \mathrm{G} - \mathrm{C} \qquad\qquad [2]$$

where DN is a digital number representing the complex amplitude envelope of the pulse on the seafloor recorded by the sonar, C is a calibration coefficient term that accounts for the way the sonar mechanically responds to pressure waves and converts them to electrical signals (i.e. the way the sonar transduces, digitizes, steers beams, etc), and G is the applied gain, which can be time-varying or fixed; SL is the source level emitted from the sonar; TL is the transmission loss through the water column:

$$TL = 20 \log_{10} r + \alpha r \qquad\qquad [3]$$

where r is the slant range to the seafloor and α is the absorption coefficient; and TS is the target strength:

$$TS = S_b + 10 \log_{10}(\text{Area}) \qquad\qquad [4]$$

where S_b is the unit area scattering strength and Area is the insonified area of the beam. Solving:

$$DN - G - C = SL - 2TL + [S_b + 10 \log_{10}(\text{Area})] \qquad\qquad [5]$$

for S_b, we arrive at what is here referred to as the backscatter measurement:

$$S_b = DN - C - SL + 2TL - 10 \log_{10}(\text{Area}) - G \qquad\qquad [6]$$

Each individual term in equation [6] is the result of measured, estimated or modeled information and each has an associated uncertainty and possible biases, both of which contribute to the final accuracy of the estimate of S_b. The ways in which each term can be derived and the possible sources of uncertainty and/or associated biases that potentially lead to backscatter measurement inconsistency are discussed here.

Digital Number Selection (DN)

There are several ways in which the complex envelope (amplitude, intensity, or the digital number) of the signal can be selected. Examples of different selection approaches that have been used include the normalized integral of the pulse, the peak amplitude of the pulse, the complete time series of the pulse, or the amplitude associated with the seafloor detection (i.e. the centroid of the pulse). Using different selection criteria for the DN can result in inconsistencies in the backscatter measurement upwards of 0.5 dB (Penrose et al., 2008).

Calibration (C)

The calibration coefficient is typically a single value for all steering angles for all beams that has been estimated for un-calibrated systems and set as a default value in commercially available backscatter processing software. Each sonar has a unique value for C. The Reson 7125 MBES it is typically -100 dB. This default is not commonly changed during processing, but would contribute to measurement inconsistencies if inaccurate or different values were used for different systems and overlooked. A rudimentary way to make consistent mosaics from multiple MBES is to process the data, estimate the differences at the junctions, and reprocess the data using a value for C that is offset by the estimated difference.

Source Level (SL) and Gain (G)

The source level is formally the transmitted acoustic pressure level relative to 1 μPa referenced to a 1 m range from the transducer (Lurton, 2010). For un-calibrated Reson 7125 MBES, SL is typically taken to be the value of the power setting used at transmission as this value is reported directly in dB re 1 μPa at 1 m. The difference in the actual output of the individual MBES system relative to the operator's selected power setting leads to a bias in the estimate of the backscatter measurement which Lanzoni has shown can be as high as 5 dB (Lanzoni, 2012). Furthermore, it is not a single value fixed bias for all settings. Differences in the MBES system outputs relative to the power settings will result in measurement inconsistency between systems assuming the reported power setting value is used for the SL correction.

Similarly, mis-estimation or misuse of gain values result in a direct misestimate of S_b. The proprietary Reson time-varied gain is a function of the range, gain, absorption, and spreading settings, and has the greatest affect on the outer beams. Without any

additional radiometric calibration information, G is typically taken to be the gain setting value, which Lanzoni (2012) showed can differ from tenths of a dB to several dB.

Transmission Loss (TL) – Range (r) and Absorption (α)

The transmission loss term accounts for the energy loss due to absorption and spherical spreading that occurs as the sound propagates through the water column. To correct for this effect, the TL term relies on discrete point measurements along a vertical profile of the water column to model the way sound propagates through it. It is assumed that the vertical profile is representative of the water mass for the entire survey area. The term is only as accurate as how well the properties of the water column are measured and/or modeled at any point in time and space. The ways in which the range and absorption can be determined and how they affect the backscatter measurement are considered.

The range is estimated from the modeled ray path of each beam to the detected seabed. This can require knowledge of the two-way travel time from the detected seafloor, the sound speed profile through the water column, the attitude and position of the transmit and receive arrays of the MBES depending on how beam steering is implemented, and the sound speed at the face of the transducer at the time of transmit. The attitude and position of the sonar is generally determined from sensors mounted on the vessel, introducing potential measurement uncertainty from the sensors themselves and the alignment of up to four reference frames (beam pattern reference frame, sonar reference frame, vessel reference frame, position and orientation sensor reference frame discussed later). The sound speed profile can be directly measured acoustically, or computed with mathematical models from best available measurements of pressure, temperature and salinity. For example, the Chen-Millero model (UNESCO equation),

15

most commonly used for near shore applications in the United States has an estimated uncertainty of 0.5 m/s (Chen and Millero, 1977). This estimate does not include the uncertainty of the pressure, temperature, and salinity sensors themselves. Given that the TL term in the sonar equation is a function of range, and that the uncertainty scales with range, the uncertainty of the backscatter measurement also scales with range.

Absorption is also typically measured indirectly and computed from a model, of which several are available. The 1982 Francois Garrison Model reports an uncertainty of 5-10% using the parameters of frequency, temperature, depth, salinity, and acidity, all of which have their own measurement uncertainties (Francois and Garrison, 1982). The effect of uncertainty in calculation of absorption on backscatter measurements scales with range in the TL term. However, if the same estimate of absorption is used for MBES data collected by two systems over the same seafloor at the same time, this represents a bias of the same magnitude for both systems and cannot be considered a cause of measurement inconsistency between the two systems.

Discrete marine phenomenon such as fish, bubbles, or debris in the water column can also affect the amount of sound pressure attenuated during transmission. Accurately accounting for energy losses associated with attenuation blunders is difficult due to the ephemeral nature of such phenomenon in the insonified portion of the water column and these effects are commonly ignored in backscatter reduction models.

Insonified Area ($Area$)

The insonified area is estimated using the projected pulse shape on the seafloor and its intersection with the transmit and/or receiver beam patterns. Depending on how this is derived, it might require knowledge of the directivity of the MBES; the arrival angle of the beam at the seafloor, which might also require knowledge about the local shape of

the seafloor (i.e. the bathymetry) and the ray path of the beam; the pulse length; sound speed near the seafloor; and the shape of the beam. Ignoring or misestimating of any of these results in a mis-measurement of S_b.

While there are a number of ways the insonified Area can be calculated (Amiri-Simkooei et al., 2009, Simons and Snellen, 2009, Parnum and Gavrilov, 2012, Hammerstad, 2000), a common approach is to take the minimum of either:

$$\frac{\psi_{tx}\, c\tau r}{2\sin(\theta_{ix})\cos(\theta_{iy})} ,$$ [7]

the pulse length limited area (typically applicable for the outer beams), or

$$\frac{\psi_{tx}\psi_{rx}r^2}{\cos(\theta_{ix})\cos(\theta_{iy})},$$ [8]

the beam width limited area (typically applicable for near-nadir beams), where c is the sound speed in m/s, τ is the pulse length in s, r is the slant range from the MBES reference point to the seafloor in m, ψ_{tx} and ψ_{rx} are the -3 dB (half power) transmit and receive beam widths in radians, θ_{ix} is the angle of incidence in the across-track direction and θ_{iy} is the incidence angle in the along-track direction in radians (Lurton et al., 1994). Errors on the order of 5 to 10% of any of the variables in the numerator result in inconsistencies in on the order of tenths of a dB (e.g. 0.22 dB for a 5% error and 0.46 dB for 10% error in any of the parameters in the numerator). Misestimates of the angles in the denominator are more consequential (on the order of 3 dB or so for 1-10% errors).

Reson 7125 Operational Modes, Settings, and Saturation

Nearly all MBES allow some level of operator control and/or have automated setting controls. Whether controlled by an operator or by an algorithm, not every operational setting selection will be perfectly tuned for every environmental condition and/or cause the system to respond as expected.

For Reson SeaBat 7k series systems, the user selectable beam-forming mode should not affect the relative quality of beam pattern beyond the natural widening of the beam that comes from steering. This was explained in a manufacturer technical note theoretically and through empirical simulation (Maillard, 2010).

Greenaway showed that Reson 7125 MBES are capable of being operated in a saturated condition in which the amplitude of the received signal does not vary in direct proportion to the transmitted signal (Greenaway, 2010). Data acquisition by systems operated in a saturated state effectively renders radiometric corrections useless.

Lanzoni showed that there are some operational settings for which the Reson 7125 SV1 does not perform in a predicable way, particularly at power settings below 200 dB and pulse length settings below 100 μs (Lanzoni, 2012). Radiometric corrections when such settings are used also result in backscatter measurement inconsistencies. Lanzoni furthermore showed that relative setting changes do not result in equivalent received responses; though the received signals are proportional and correctable (e.g. a power setting change from 200 to 205 does not result in a variation of 5 dB in SL).

Finally, setting changes are not instantaneous, and require some amount of time for the MBES electronics to stabilize. Radiometric corrections do not exist for data acquired during setting adjustment periods, resulting in short period inconsistencies for several successive pings during which the new settings are stabilizing.

Sonar Calibration

Radiometric calibrations can be relative and/or absolute, for which many methods have been proposed. The standard target method is well-known for single-beam echo-sounders (Foote and MacLennan, 1984, Foote, 1983, Foote, 1982), and can be performed in the open ocean or in a tank. This method has also been adapted for

small MBES in a tank (Foote et al., 2005). Lanzoni and Weber proposed a method for conducting a standard target calibration with MBES in the field (Lanzoni and Weber, 2011) and Heaton et al. are exploring the use of an extended target for high frequency MBES as an alternative to the standard sphere approach (Heaton et al., 2013). Pocwiardowski et al. proposed an alternative to the standard target for large sonar based on measurement of individual channel characteristics during the manufacturing process (Pocwiardowski et al., 2006). Greenaway and Rice introduced a relative inter vessel normalization approach by cross correlating processed backscatter measurements from two simultaneously operating MBES over a large geographic area (Greenaway, 2013)

Reson 7125 Calibration

A dual frequency Reson 7125 SV1 with independent projectors for each frequency (200 kHz and 400 kHz) was calibrated in the test tank at the University of New Hampshire in the spring of 2012 using the standard sphere approach with a TC 4034 calibrated hydrophone. A technical report describes each tank calibration measurement and its results (Lanzoni, 2012). The tank calibration measurements that were used for this work are the system responses to power and gain settings, the calibration term as function of beam steering angle, and the combined 3-dB beam widths, all performed at a range of 8 m with the same relative settings. Calibration measurements not used included independent transmitted and received pulses at fixed ranges and settings, and an evaluation of saturation. Uncertainty estimates were not reported. A more detailed description of how each calibration is used specifically for this work is provided in the *inter* calibration data processing section in Chapter 3.

19

CHAPTER 3

Methodology

As the goal of this work is to develop a method to achieve consistent backscatter measurements from hydrographic surveys conducted with more than one MBES-survey-vessel pairing, each MBES is assumed to be mounted on its own unique platform. Recognizing that each vessel introduces its own acoustic noise characteristics to the problem from vibrating machinery such as engines, generators, and propellers (Burdic, 1984), each relative calibration between "systems" pertains to the collective difference between each MBES-vessel pairing. If MBES-vessel components were to be separated, reconfigured, or replaced, the relative calibration is expected to change, but could be reacquired with the new configurations. The idea is analogous to orthometric leveling of benchmarks in which a vertical reference is transferred from one mark to another (NOAA, 2013c).

The field calibration procedure is conceived to take place in two stages: one in which the reference MBES (tank calibrated 7125 in this case) acquires data over the same patch of seafloor as the MBES to be calibrated, as near in time as possible to determine the angle-dependent calibration term C; and the second in which each vessel is stationary while the uncalibrated MBES pings through a range of system setting combinations over the same seafloor with as little acoustic interference as possible to

determine setting corrections for power, gain, and pulse length relative to those used to acquire C (referred to here as "pivot settings"). The pivot settings are the unique power, gain, and pulse length settings used to acquire the *inter* calibration data. The *intra* calibration is designed to measure how the system responds to settings relative to the pivot settings and to develop corrections for them. The corrections for the pivot settings within the LUTs that are the result of the *intra* calibration are necessarily zero by design.

The *inter* calibration transfers a reference standard level to the uncalibrated system for a single setting combination of power, gain and pulse length. If the newly calibrated system were only to be operated at these settings, the system would produce measurements that are calibrated. Operating only using a single set of setting combinations or performing an *inter* calibration for all setting combinations is an impractical imposition upon field operations; thus the calibration standard must be transferred to all other possible settings of power, gain and pulse length in the newly calibrated system. The *intra* calibration is a procedure that seeks to transfer the *inter* calibration to other power, gain, and pulse length settings by measuring how the sonar responds when operated at all other setting combinations. The *intra* calibration results in correction tables relative to the *inter* calibration pivot settings (pivot settings have a zero correction) that account for how the system responds when settings other than the pivot settings are used. The *inter* sonar calibration is a function of the beam steering angle and the resulting calibration is applicable regardless of the beam forming mode (e.g. equiangular or equidistant with or without roll stabilization enabled). The *inter* and *intra* calibrations for the same pivot settings are taken as a set. The considerations for where and how to acquire the data, the recommended processing approach, and how the results are expected to be used are explained below.

Baseline Reference MBES/Vessel Selection

While this effort was undertaken with the intention of relatively calibrating multiple un-calibrated MBES systems relative to a tank-calibrated MBES system, this method could be employed using only un-calibrated MBES or semi-calibrated MBES (a sonar for which only a subset of calibration information is known) as a baseline MBES. When selecting a baseline MBES to which all other MBES are to be referenced, the characteristics of each MBES and vessel on which it is mounted should be considered. The MBES that is most acoustically and operationally stable should be used as the baseline since the reference is tied to a particular system. That is, the system whose components are most stable and least likely to be dismantled from the vessel on which it is mounted or reconfigured in any way.

Inter Calibration

Site Selection

Two MBES on two separate vessels are used to measure the same area of seafloor as near in time as possible and the difference between the two is used to determine $C(\theta_s)$ for the uncalibrated system using a single set of settings. The seafloor is the calibration target. This exposes the result of the test to uncertainty from nearly all of the terms in the backscatter reduction calculation presented in equation [6]. It is therefore necessary to carefully consider the conditions of the seafloor, water column, and surface dynamics, as well as how well each can be measured and/or modeled when selecting the location and time to acquire the data using a standard planned survey line. In general, it is desirable to select a time and location at which the seafloor, water column, and sea surface properties are most stable; and where this cannot be achieved, a line length, ping rate, and depth to obtain a sufficient number of pings such that the

biases in potential sources of interference are the same for each system, or are negligible. Adhering to certain site criteria also allow some of the backscatter processing steps to be simplified, thereby reducing the possibility of human-induced processing error. Using these guiding principles, the practical considerations are discussed here.

Ideally the coincident line would be over a flat, stationary (e.g. not undergoing active transport), homogenous seafloor composed of the same sediment in terms of type, grain size, roughness, porosity, and cohesion with as little biological activity as possible both in and on the seafloor as well as the water column. The line should be run in areas with minimal spatial gradients in temperature, salinity, and sound speed profiles of the water column. A site that meets these criteria will minimize biases from vessel navigational errors, discrete targets on the seafloor or in the water column (e.g. fish, aquatic debris, etc), and discrete oceanographic events (e.g. moving salinity wedges or thermoclines). If a zero-slope seafloor is not an option, running the line parallel to contours on the most gradually slopping seafloor available is preferred to avoid error associated with imperfect geometric corrections in the processing routine such as those associate with reference frame alignment, ray tracing, and seafloor slope. (For the case study, the coincident lines were only run parallel to the bathymetric contour because the along-track seafloor slope was assumed to be zero during processing.) If active transport is suspected, the line should be run at a time and for a duration over which the transport is expected to be minimal and most constant, though it should be clear that it is expected that this scenario is quite suboptimal and another location should be sought if possible.

Determining the ideal water level and current regime is not straightforward. On one hand, current will coherently carry propeller wash and vessel wake away from the test area, as well as any other particles or debris in the water column, a desirable

situation since these contaminants will have a reduced impact on the follow up observations collected immediately afterward by the second system. On the other hand, current can also induce sediment transport depending on the characteristics of the seabed (Le Roux, 2005). A low magnitude current is generally thought preferable, with the survey line oriented parallel to the direction of flow, ideally with similar flow structure on either side of the line.

Bubbles in the water column are also a potential source of bias. Bubbles change the sound speed and attenuation and can be acoustic targets many times larger than their physical size depending on their resonant frequencies (Novarini et al., 1998). Waves and wakes of vessels are a major source of bubbles, so care should be taken to select an area and/or time with little vessel traffic when surface conditions are calm (less than 10 knots of wind and no recent history of breaking waves). Areas of venting, seeping, or biological off-gassing would not be favorable locations for the coincident line either. Assuming that the test can be performed in a calm area, the remaining causes of bubbles during this test are propeller wash and vessel wake from the test vessels. While it is desirable to run the coincident line with both systems as near in time as possible to reduce the chance of induced bias due to seafloor or water column dynamics, waiting 5-10 minutes for vessel wake to dissipate between passes is suggested. Though dispersion of bubbles in the upper water column is a poorly understood process affected by boundary dynamics at the ocean-atmosphere interface, this wait time was selected because Thorpe and Hall showed nearly complete dissipation of acoustically perceptible bubbles after 5-10 minutes of a discrete breaking wave using an upward looking 248 kHz side scan sonar placed on the seafloor (Thorpe and Hall, 1983). This observation is consistent with Thorpe's earlier predicted 400 s life span of an air bubble 100 µm in diameter originating at a depth of 8 m in the water column (Thorpe, 1982). While the

size of bubbles produced from propellers vary in size by the depth, water chemistry, rotational velocity, and vessel and propeller design and size, a 100 μm bubble is within the range of modeled bubble sizes for a five-blade, 0.4 m diameter propeller (similar in size to those on the survey vessels used in the case studies described in Chapter 4) using various parameters (Hsiao et al., 2006). However, bubbles from a much larger vessel with a larger propeller have been observed to last much longer (Weber et al., 2005). Of additional note, a one-knot surface current would carry the wake and propeller wash 300 m in 10 minutes.

Selecting an area with little vessel traffic and anthropogenic activity is preferred since acoustic interference from other vessels and their possible activities (fishing, trawling, diving, etc) are other potential sources of biases. In such an area cannot be found, waiting for periods of light traffic and anthropogenic activity is preferred.

The general water depth is another factor to consider with the primary consideration being that the test site depth need be within the operational depth range of the MBES. In other words, the depth must be shallower than the extinction depth of the outer beams, and the system should be able to maintain coverage over its entire angular sector so as to allow for measurements of C across the full swath. Conversely, the water depth should not be so shallow that the seafloor is not yet in the far field (the depth at which the acoustic wave is considered planar at the scale of the insonified area). A rough approximation of the far field of a linear array similar in length to a Reson 7125 is around 44 m for the 400-kHz frequency and around 22 m for the 200-kHz frequency, discounting transmit and receive focusing. The 200-kHz operational depth range is roughly 8 to 300 m and for the 400-kHz this range is roughly 4 -100 m. Deeper depth ranges impose lower ping rates thereby increasing the time to conduct the test and

potentially exposing the test results to more of the aforementioned biases in the water column.

Since a perfectly ideal location that meets all of these criteria may be difficult to find in the field, the potential sources of bias for the location should be recognized and the line length relative to depth and ping rate should be long enough such that these biases can be assumed to center on the same value over the course of data acquisition of each vessel. For instance, if breaking surface waves are present and assumed to be causing funnel shaped plumes of bubbles below the surface in randomly distributed geographic locations (Monahan and Lu, 1990), the coincident line should be long enough to support the assumption that bubble plume interference averages to the same value while logging data with each MBES, which in this example might be considered a function of the sea surface wave length. Isolating and quantifying individual bias such as this in practice is beyond the scope of this work but is worthwhile considering as an example of the many biases to which this method is exposed.

Careful consideration of the conditions of the seafloor, water column, and surface dynamics when selecting the time and location in which to run an *inter* calibration line is an important step in the process. As has been described, it desirable to select a time and location in which the seafloor, water column, and sea surface properties are most stable. When this cannot be achieved, a line length, ping rate, and depth to achieve a sufficient number of pings such that the potential sources of bias are the same for each system, and/or are negligible should be selected.

Data Acquisition

Once the site is selected and the line azimuth and length is determined, the coincident line is run in the same direction by both vessels with all the MBES and all

26

other ancillary echo-sounders not transmitting. A salinity and temperature water column

profile measurement (CTD) is taken immediately before and after MBES acquisition at a

minimum to verify the assumption of oceanographic stability of the water column. If the

MBES are at risk of being operated in a saturated setting regime, care should be taken

to select operational settings that ensure all systems are operating in a linear regime

while maximizing the number of quality bottom detections across the swath for most if

not all beams. While it is not necessary for all systems to use the same operational

settings, it is suggested as good practice to ease record keeping and calibration

tracking, especially when managing multiple systems and frequencies. The direction the

line is run is considered to be of little importance, but using the processing technique

proposed, running the lines in the same direction with each boat is preferred to be able

to develop a beam-to-beam calibration. The vessel speeds should be the same, and

careful navigation of the line is of course desirable. The beam-forming mode (e.g.

equidistant, equiangular, number of beams, swath angle range, dynamic steering, etc.)

should be the same such that the same number of beams is formed in the same way

over the same angular sector or at least averages to the same values over the number

of pings in each sample set.

Data Processing

The data from each line acquired by each system is processed using the

backscatter reduction process described in this section. As this work is geared toward

working with multiple Reson 7125 systems operated by NOAA, the Reson .s7k sonar file

(Reson, 2011); a Seabird conductivity, temperature, and depth (CTD) .cnv profile file

(Sea-Bird Electronics, 2013); and a CARIS .svp sound speed profile file (CARIS, 2012)

are all used to reduce the raw digital number associated with the seafloor detections

recorded in the Reson .s7k files into estimates of seafloor scattering strength, S_b. The respective data definition documents should be referenced for additional information about each record and data format. While much of the approach is specific to operational controls and parameters of the Reson 7125, and to file types and data acquisition and processing workflows currently used by NOAA hydrographic field units, this approach is theoretically adaptable to other data formats and acquisition workflows.

Using the basic sonar equation solved for the scattering strengths of each beam, S_b, as described in Chapter 2:

$$S_b \ = \ DN - C - SL + \ 2TL - \ 10\log_{10}(\text{Area}) - \ G \qquad [9]$$

the way in which the values of each term are selected or derived using the raw data files are:

$$DN = 20\log_{10}(\text{dn}) \qquad [10]$$

where dn is a unitless digital number from the Reson 7006 amplitude record associated with the seafloor detection of each beam; $C(\theta_s)$ is either derived from tank calibration: $C_{tank}(\theta_s)$; field calibration: $C_{field}(\theta_s)$, if available; or a commonly used fixed value: $C_{default}(\theta_s)$ = -100 dB for Reson 7125 MBES, where θ_s is the beam steering angle in the sonar reference frame; SL is taken to be the operator-selectable Reson power setting from the Reson 7000 record plus a setting correction either derived from tank calibration measurements, SL_{tank}, or field calibration measurements, SL_{field} if available, both in dB re Reson;

$$TL \ = \ 20\log_{10}\text{r} \ + \ \alpha r/1000 \qquad [11]$$

where r is the ray traced slant range to the seafloor for each beam in m and α is the harmonic mean of the absorption coefficient profile calculated for each SSP depth bin in dB/km; Area is the minimum of either:

$$\frac{\psi_{tx}\,c\tau r}{2\sin(\theta_{ix})\cos(\theta_{iy})}\,,\qquad\qquad[12]$$

the pulse length limited area (typically applicable for the outer beams), or

$$\frac{\psi_{tx}\psi_{rx}r^2}{\cos(\theta_{ix})\cos(\theta_{iy})},\qquad\qquad[13]$$

the beam width limited area (typically applicable for near-nadir beams where ψ_{tx} and ψ_{rx} are the -3 dB (half power) transmit and receive beam widths in radians taken to be either those specified by the manufacturer or those measured in the tank, c is the sound speed at the depth of the seabed measured by the CTD profile in m/s, τ is the pulse length setting in s, θ_i is the true angle of incidence with the seafloor accounting for the beam ray path and the local across-track slope of the seafloor in radians, and θ_s is the steering angle corrected for vessel mounting biases relative to the inertial measurement unit (IMU) and possibly real time vessel roll, depending on the data record version used and whether roll stabilization is enabled (for earlier data formats, the steering angles are taken from the Reson 7004 record and are in the vertical reference frame if roll stabilization is enabled and are in the MBES reference frame if roll stabilization is disabled; and in later data formats the steering angles are taken from the Reson 7027 record and are in the MBES reference frame regardless of whether roll stabilization is enabled); G is the time-varying Reson applied gain derived from a proprietary formula for each beam plus a setting correction from tank calibration measurements, $G_{tank,}$ or field calibration measurements, G_{field}, if available.

For each ping: the user-selected single setting value for power, gain, absorption, spreading, and pulse length, as well as the frequency, f, the surface sound speed, c_s, and roll compensation status and datagram version are obtained from the Reson 7000 record; the vessel navigation is taken from the Reson 1003 record; vessel heave, pitch, and roll are taken from the Reson 1012 record; and vessel heading is taken from the

29

Reson 1013 record. For each beam in each ping: the digital sample associated with the Reson seafloor detection (dn) is taken from the Reson 7008 record; the two-way travel time (*twtt*) is taken from the Reson 7006 record; and the steering angle (θ_s) is taken from the Reson 7004 record for earlier datagram versions or the 7027 for later datagram versions.

For instances in which the raw data have been logged using Hypack, a multibeam data acquisition software (.7k/.hsx file format), the files are rewritten to Reson file format (.s7k). Beam data for which quality seafloor detections (passes Reson filters for brightness, colinearity, and depth) are not achieved and pings for which navigation information does not exist are removed from the dataset prior to processing.

Ray Traced Range, Depth, and Seafloor Incidence Angle

The stratified ray-tracing method (Lurton, 2010) is employed to compute *r;* using the *twtt,* θ_s, and sound speed profile (SSP) modeled by Chen-Millero's formulation applied to the CTD temperature and salinity depth profile measurement made near in time and space to the MBES data. The surface sound speed measurements made by an auxiliary sensor mounted near the transducer face are used in place of the SSP measurement for the concurrent depth layer of the transducer in the water column. The ray-traced seafloor depth in m is the cumulative depth traveled in each sound speed layer plus, z_{tx}, the transducer depth below the vessel waterline.

The incidence angle of the beam to the seafloor, θ_i, is calculated using the entrance angle of the beam into the SSP depth layer nearest above the seafloor calculated using the stratified ray-tracing method, and the across track slope of the seafloor, calculated using a best fit line of each depth swath. The slope of the seafloor in the fore/aft direction of the vessel reference frame is assumed to be zero by design

30

(recall that the survey lines are run parallel to the depth contours), and is a criterion of the field site selection. Otherwise a 3D seafloor slope correction should be considered for computing the insonified area.

Absorption

The absorption coefficient, α, is the harmonic mean of an absorption coefficient profile computed at each CTD depth layer using the model proposed by Francois and Garrison (Francois and Garrison, 1982), using a fixed value for pH 8.0, and the Reson system frequency of either 200 or 400 kHz. Acidity was not directly measured but ocean observing buoys in the North Pacific show variability between 7.8 and 8.3 over the course of the last the last three years (NOAA, 2013b), which affects absorption estimates by no more than a tenth of a dB at the frequency and depth ranges of concern.

Calibration Data $- C(\theta_s), SL, G, \psi_{tx}, \psi_{rx}$

The processing code was designed to be able to use calibrated or uncalibrated values for the $C(\theta_s), SL, G, \psi_{tx}, \psi_{rx}$ terms in equation [6] or subsets thereof in the backscatter reduction process. The code also distinguishes between the source of the calibration files (e.g. tank or field) and whether or not to apply what is being referred to as a pseudo pulse length (PL) correction, which will be introduced and discussed in more detail in following sections. The way in which each correction term has been derived and how it is applied is explained here. All applied tank calibration corrections refer to those derived from the tank calibration report (Lanzoni, 2012).

The tank calibration term results for $C(\theta_s), SL, G$ for the reference MBES as reported by Lanzoni (2012) have been altered to accommodate the proposed method, which derives $C_{tank}(\theta_s), SL_{tank}, G_{tank}$ at a reference range of 8 m, despite a subset of

other tank calibration measurements made at other ranges. The calibration values at a range of 8 m were recalculated (see below) using the SL and G tank calibration measurements at 8 m for the associated power and gain settings used to compute the $C_{tank}(\theta_s)$ term that is used in this method:

$$C_{tank}(\theta_s) = C_{tank@8m}(\theta_s) - \text{Power Setting} + SL_{tank@8m,210} \\ - \text{Gain Setting} + G_{tank@8m,40} \qquad [14]$$

where $SL_{tank@8m,210}$ is 206.58 dB for the 400-kHz projector and 205.39 dB for the 200-kHz projector at a power setting of 210; and $G_{tank@8m,40}$ is 41.93 dB for the 400-kHz projector 39.75 dB for the 200-kHz projector at a gain setting of 40. Figure 4 shows the tank calibration results at all four ranges for both the 200-kHz and 400-kHz projector, with the values of $C_{tank}(\theta_s)$ that are used in this method highlighted in black.

The 400-kHz $C_{tank}(\theta_s)$ measurements at the reference range of 8 m are not considered accurate. The 2-4 dB fluctuations over 2-5 degree steering angles that are most notable in the port outer beams and the inconsistent pattern over the range of steering angles compared to the results for the other three reference ranges call into question the validity of the results. Further evidence to discount the 8 m calibration curve is provided by the general pattern of the 2, 4, and 6 m calibration curves which compare well with raw data (DN) collected in the field by the tank-calibrated MBES over homogenous seafloors that does not compare well with the 8 m calibration curve. As the use of a reference range other than 8 m was not a viable alternative because the tank SL and G calibrations were not measured at a reference range of 8 m, the calibration curve at 4 m was shifted to the 8 m curve at beam number 130 and smoothed and recalculated using equation [14].
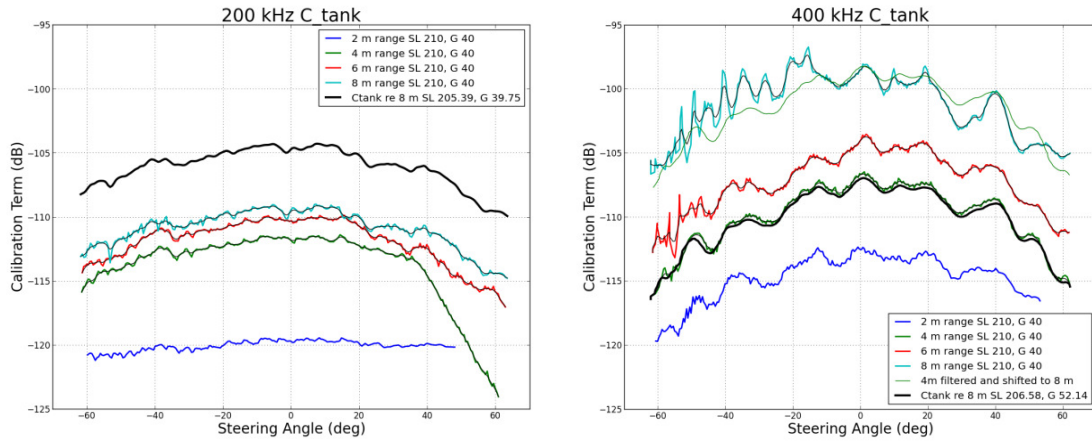
Figure 4: Smoothed tank calibration curves as measured at 4, 6, 8, and 12 m for 200 kHz (left) and 400 kHz (right).

In turn, the tank power and gain setting calibration corrections in Figure 5 relative to the reference settings used to measure the calibration curve (power setting of 210, gain setting of 40, and a pulse length of 110 μs) are used exactly as they are reported by Lanzoni.
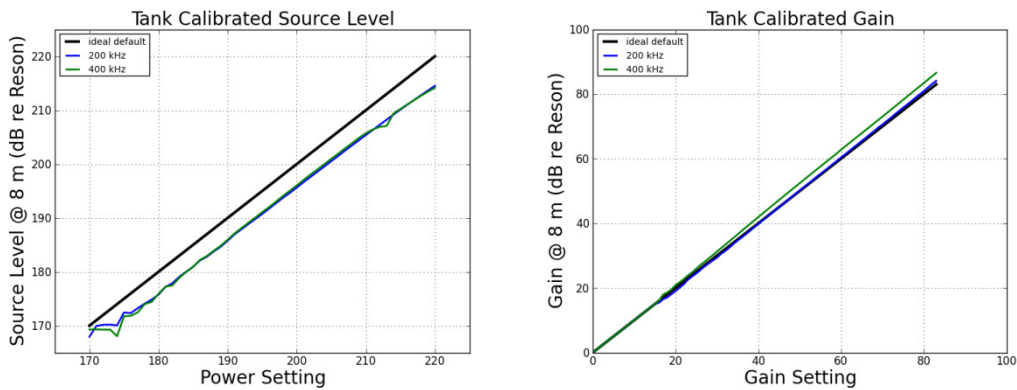
Figure 5: Power (left) and gain (right) setting tank calibrations at 8 m.

This allows for a single difference between a pair of lines to determine $C_{field}(\theta_s)$ relative to the pivot settings used to acquire them. This is significant because it eliminates the need to run a coincident line for each setting combination, which is considered impractical for a field method.

Look up tables (LUTs) similar to $C_{tank}(\theta_s)$, SL_{tank}, G_{tank} are the result of the *inter* and *intra* calibration and are referred to as $C_{field}(\theta_s)$, SL_{field}, G_{field}. The development of the LUTs is described in following sections, and the application of them in the code used in the development and evaluation of this method is the same. Despite being accounted for in equation [6] in the same way, it is important to note that they do not represent the same measurements.

An interpolated value for $C(\theta_s)$ is computed given θ_s. If neither $C_{tank}(\theta_s)$, and $C_{field}(\theta_s)$ do not exist or are not desired to be applied, a default value of -100 dB is used for all θ_s. The default value of -100 dB is used because it is commonly found in commercial seafloor backscatter processing software packages for Reson 7125 MBES, and has been considered an acceptable approximation in lieu of tank measurements. The default value of -100 is presumed to be a legacy value from the original Geocoder tool (Fonseca and Calder, 2005) value for a Reson 8125.

Similarly, if tank or field calibration information is to be used to correct the setting values for power and gain, the interpolated value from the setting calibration LUT is applied. If setting corrections are unavailable for either power and/or gain, then the reported power setting is used for SL and the true applied gain is applied as returned from the proprietary Reson time varying gain (TVG) function.

The polynomial approximations given by Lanzoni (2012) are used for ψ_{tx}, ψ_{rx}:

$$p(x) = p_1 x^n + p_2 x^{n-1} + \ldots + p_n x + p_{n+1} \qquad [15]$$

where p is either ψ_{tx}, ψ_{rx} in degrees as a function of the athwartship steering angle, x, and p_n is given by the values in Table 1.

34

RX	p_1	p_2	p_3	p_4	p_5
200 kHz	6.2807×10^{-8}	-1.5369×10^{-7}	1.3436×10^{-4}	2.1162×10^{-4}	1.1469
400 kHz	2.9281×10^{-8}	8.2353×10^{-8}	6.4674×10^{-5}	-1.0116×10^{-4}	0.5843
TX	p_1	p_2	p_3	p_4	
200 kHz	-4.1976×10^{-7}	3.3590×10^{-5}	3.6067×10^{-4}	2.0915	
400 kHz	-1.5035×10^{-6}	2.1751×10^{-5}	0.002	1.1785	

Table 1: Polynomial values for tank calibrated transmit and receive beam widths: ψ_{tx}, ψ_{rx}.

Otherwise $\psi_{tx\text{-appx}}$ is 1° for 400 kHz and 2° for 200 kHz, and $\psi_{rx\text{-appx}}$ is approximated by dividing the nadir beam width (0.5° for 400 kHz and 1° for 200 kHz) by $cosine(\theta_s)$ to account for the growth of the receiver beam width with increasing beam steering angles. The maximum response axis (MRA) of each beam is assumed to be aligned on axis with the sonar reference frame. However, the MRA of the outer beams appears to curve in the along-track axis of the sonar reference frame, suggesting the existence of a unique beam pattern reference frame separate from the sonar reference frame. Corrections for this are not made since the along-track angles cannot be resolved from the beam pattern measurement.

Instead of using the calibrated transmit and receive pulse lengths that were measured independently in the tank (Lanzoni, 2012), a pseudo pulse correction is suggested in the form of a deviation from the ideal setting length (described in the *intra* calibration data processing section). The pseudo pulse length correction is added as a quantity in dB to equation [6] to account for how the MBES responds to the use of pulse length settings other than the pivot setting. This approach was conceived after it was unexpectedly found that the raw recorded amplitude around the seafloor detection is higher (on the order of 2-5 dB) for pulse lengths below 200 µs. The tank-calibrated

transmit pulse lengths were not used because they do not appear to have a relationship with what is actually recorded by the receiver.

Across-Swath Scattering Strength Differences

Once the coincident *inter* calibration lines are processed into scattering strengths using the method described, the central tendencies of the scattering strengths by beam number, S_{b_n}, and by incidence angle $S_b(\theta_i)$ are computed for both the tank calibrated reference system, $S_{b_{ref}}$, and the system being field calibrated, $S_{b_{uncal}}$. Depending on the distributions of the scattering strengths, the mean, median, or mode of the scattering strengths by beam or by incident angle might be used to describe the central tendency of each MBES backscatter measurements.

For the Reson 7125 data acquired during the case studies described below in Chapter 4, the difference between the across-swath mean calibrated scattering strengths and the mean uncalibrated scattering strengths is taken to be C_{field} for the field calibrated systems, adjusted for $C_{default}$:

$$C_{field}(\overline{\theta_{uncal}}) = [\overline{S_{b_{uncal}}} - \overline{S_{b_{ref}}}] + C_{default} \qquad [16]$$

The difference between the median and mode of the scattering strengths by beam and incidence angle are also computed for comparison. The mean DNs are also differenced. Additionally the standard deviations and DN differences are computed, as well as a subset of the mean S_b and DN differences from incidence angles 15° to 30° to compare alternative methods for deriving C_{field}.

The difference in the across-swath central tendencies $C_{field}(\overline{\theta_{uncal}})$ is finally smoothed, similar to the smoothing of C_{tank}. Smoothing $C(\theta_s)$ is important to prevent adding noise to future data processed with this correction. The uncertainty of $C_{field}(\theta_s)$ is estimated by calculating the standard deviation of two sample means:

$$\sigma_{C(\theta_s)field} = \sqrt{\frac{\sigma^2_{S_b(\theta_s)uncal}}{\sqrt{n_{uncal}}} + \frac{\sigma^2_{S_b(\theta_s)ref}}{\sqrt{n_{ref}}}} \qquad [17]$$

Though this is a simple computation, it is based on many underlying assumptions so a number of checks are necessary to evaluate how well the criteria of the field calibration were met. Descriptive sample statistics (mean, median, mode, standard deviation) of the scattering strengths of all the pings for each beam are computed as a simple check that the beam distributions are close to symmetric. The mean and power spectra of each vessel's heave, pitch, and roll over the successive sample pings are computed to check that each vessel was operated under similar sea surface conditions.

Example

The following figures illustrate the data comparisons that are made during the evaluation of each *inter* calibration line pair and creation of $C_{field}(\overline{\theta_s})$ using the "South 1" (S1) 400-kHz set of lines for Launch 2805 and Launch 2807 at Site 2 (Offshore 20 m) which is described in detail in Chapter 4. Figure 6 is a plot of the three CTD casts made during the particular calibration, all taken within approximately 1.5 hours of one another in the vicinity of the survey line. Launch 2805 started the S1 survey line at 1818 UTC, and Launch 2807 started it at 1825 UTC. The CTD data are used to inform the criterion of a stable water column from a physical oceanography perspective. The harmonic mean absorption computed from each of these varies by 0.5 dB/km and the sound speed by no more than 0.5 m/s, which would result in small inconsistencies in the final computation of S_b, despite an apparent change near the bottom of the last CTD profile taken at 1838. The CTD taken at 1753 UTC was used for processing both files.
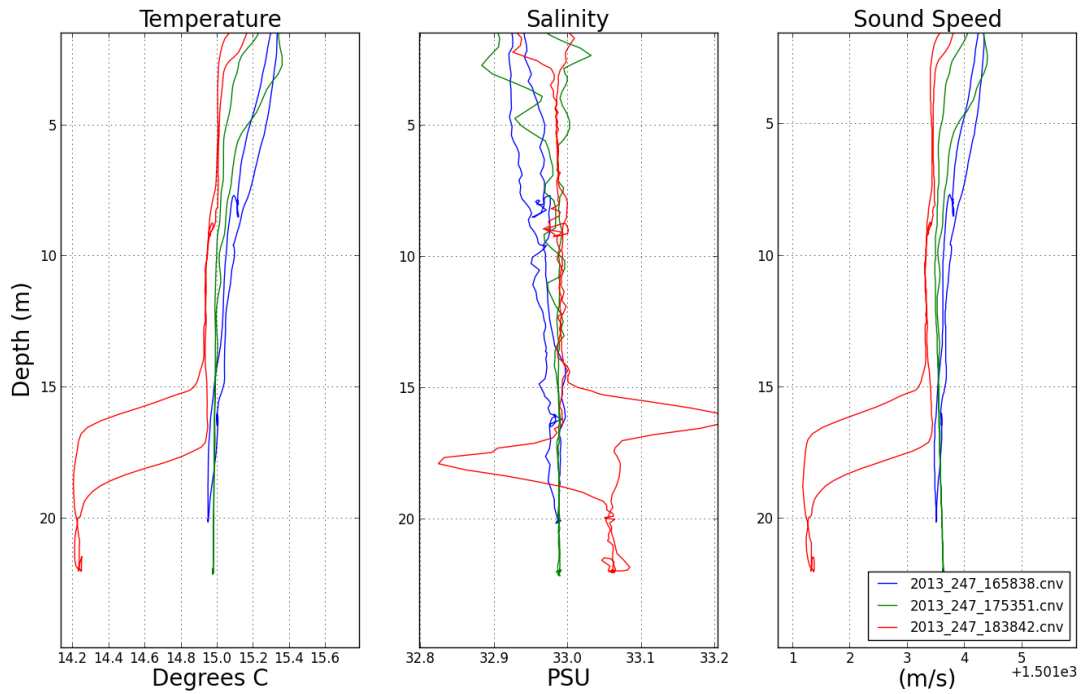
Figure 6: Comparison of the three CTD casts taken during the inter calibration at Site 2 (Year_JulianDay_HoursMinutesSeconds in UTC)

Figure 7 is a comparison plot used to visualize the data from the two systems in several different ways: the beam averages with the normalized PDF of each beam; a grayscale color map of each S_b measurement by beam and ping number, and the beam averages by their mean steering angles and incident angles. The beam distributions between systems appear similar, and the beam patterns by incidence angle and steering angle are similar.
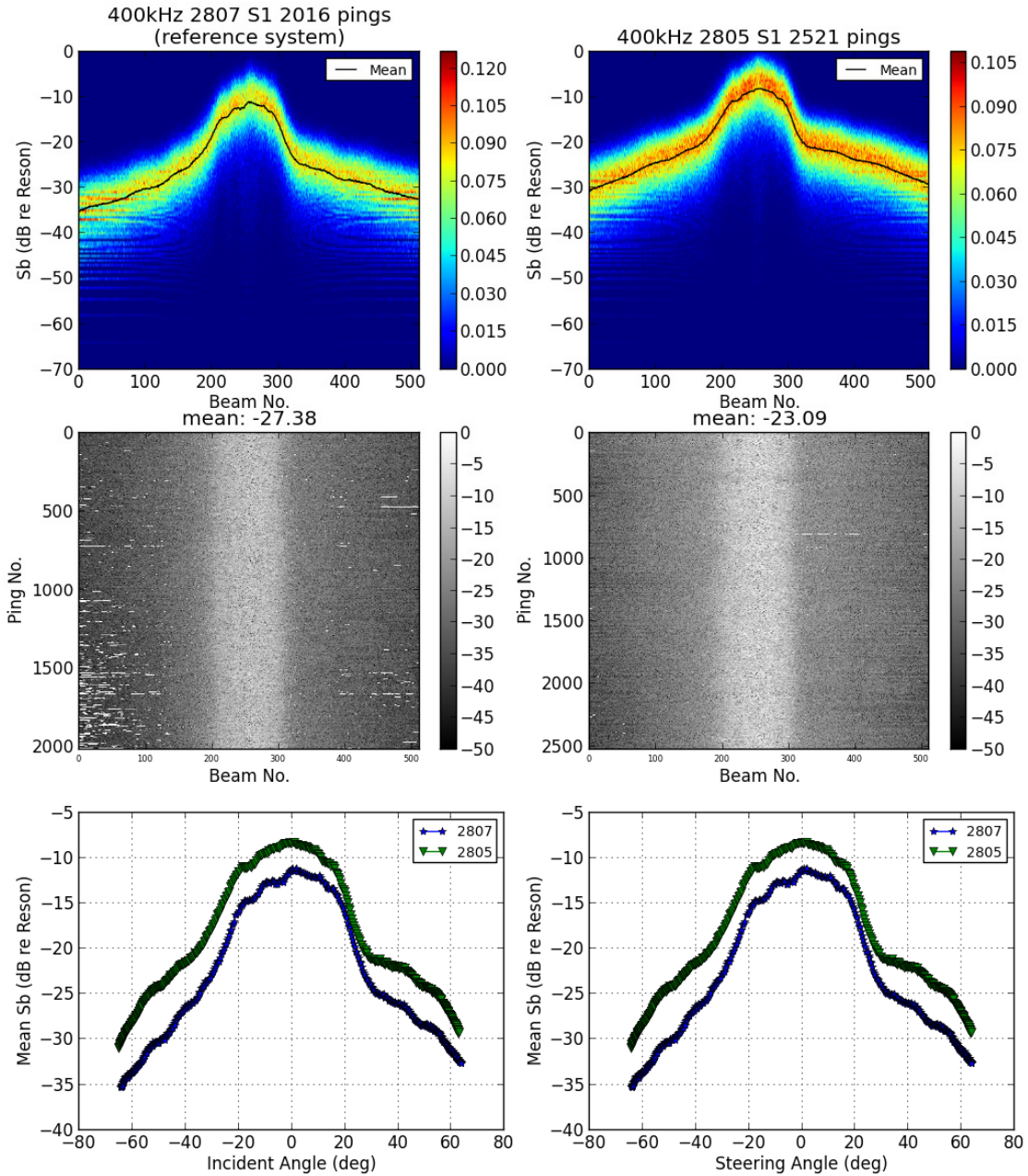
Figure 7: Comparison of data from two systems over the same patch of seafloor from the S1 Line at Site 2. Top Row: beam averaged S_b measurements (solid line) with the normalized PDF of each beam (color map), Launch 2807 system data (left), Launch 2805 system data (right). Middle Row: S_b by beam number and ping number made by two systems, Launch 2807 system (left), Launch 2805 system (right). Bottom Row: beam averages from the two systems plotted together by angles of incidence (left) and steering angle (right).

Figure 8 shows the quartile box plots, each representing eight beams binned together for Launch 2807 system data (top) and Launch 2805 system data (bottom).
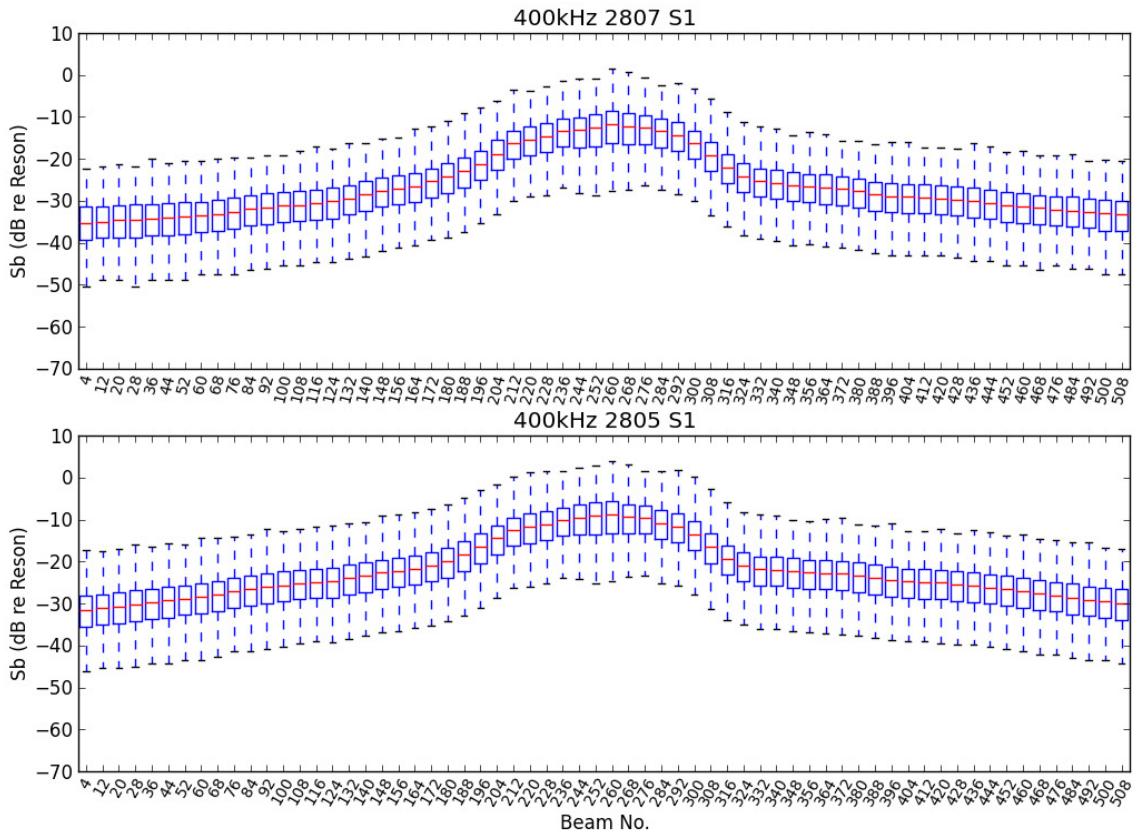
Figure 8: Eight-beam binned S_b box plots of two systems: Launch 2807 system data (top), Launch 2805 system data (bottom) from the S1 Line at Site 2.

Figure 8 is meant to show the measurement spread and central tendency of each region of the swath. Figure 9 shows the time series and the spectral densities of the heave, roll and pitch of each vessel during the S1 *inter* calibration at Site 2. It is meant to check for biases induced by the sea keeping of each launch, and shows that there are no apparent biases. Appendix A shows an example of how S_b is affected by changes to static pitch (vessel squat), which can be as much as several dB.
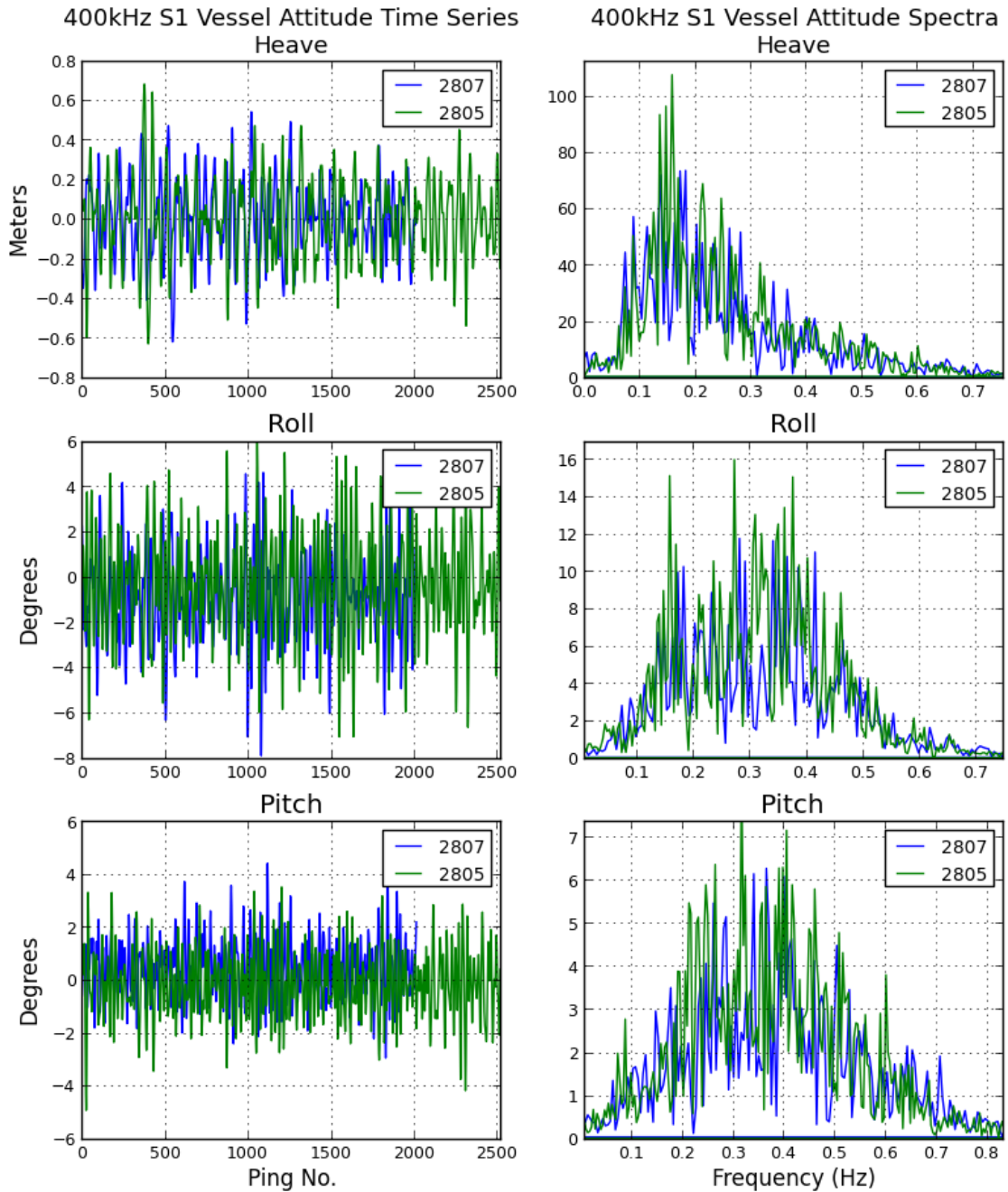
Figure 9: Vessel attitude by ping number (left) and their respective spectral densities (right) from two systems: heave (top), roll (middle), pitch (bottom).

Figure 10 shows the smoothed beam differences by steering angle, which is the result of the *inter* calibration as conceived. The smoothed beam mean difference by incidence angle is ultimately what is used in the case study explained in Chapter 4, but

the smoothed beam medians and modes are shown as well as comparative alternatives. Though statistical distribution testing has been forgone, the boxplots, PDFs and similarity between the mean, median, and mode are considered sufficient checks to proceed with the results.
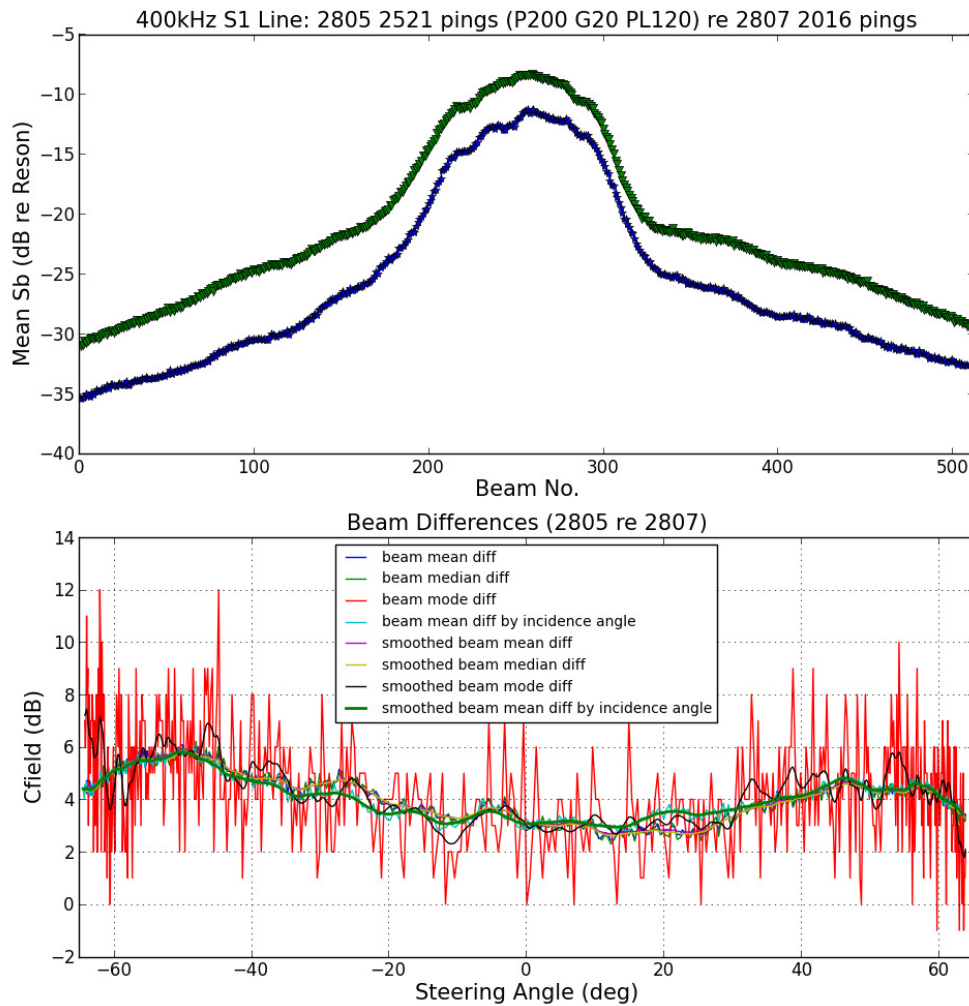
Figure 10: Beam means of two systems (top); and beam to beam differences by steering angle (bottom) taken to be the inter calibration results referenced to a power setting of 200, gain setting of 20, and a pulse length setting of 120.

<u>*Intra* Calibration</u>

Site Selection

The *intra* calibration uses the change in recorded amplitude of each seafloor detect for each setting change of either gain, power, and pulse length, holding the other two settings constant. The purpose of this test is to determine setting corrections for all possible setting combinations other than the pivot settings used during the *inter* calibration test. This method uses sample statistics to determine the central tendency of each MBES' response to changes in settings. Each amplitude measurement from each beam is assumed to be an independent sample described by a Normal distribution when the MBES is pinging at a stationary, ergodic, homogenous seafloor from a fixed position.

Many of the seafloor, water column, and sea surface characteristics desirable for the *inter* calibration site are also desirable for the *intra* calibration site. The physical set up is somewhat less constrained in that the requirement to have two vessels over the same patch of seafloor near in time does not exist, yet it is more sensitive to small perturbations on the seafloor, in the water column, or on the sea surface because a small number of pings are compared to successive set of pings at another set of settings.

Though the *intra* calibration was only conducted alongside a pier and underway during the field case studies, it is foreseeable that comparable results might be achieved when conducted from anchor or a mooring over a homogenous seafloor. The ways in which conducting the test underway, alongside a pier, at anchor, or from a mooring affects the assumption of seafloor and water column stability must be considered when selecting a site. Pier pilings, mooring lines, or anchor chain may affect the flow of current near the vessel causing a deviation from what the vessel might normally

experience underway or away from structures in the water column. Pier pilings, anchors, and mooring blocks will also affect the flow at the seabed, potentially altering the target seabed. Current also carries discrete targets in the water column, which can also foul on water column structures such as pilings, mooring lines, and anchor chains. Conducting the test underway introduces vessel motion, noise and water flow over the transducer into the problem, but might be considered a more realistic reflection of how the MBES responds while in normal operation. Vessel squat is expected to decrease the amplitudes by increasing the incidence angles of all beams with the seafloor over the course of an underway test, but the relative differences between setting combinations are expected to be the same as long as the squat and trim remain stable (see Appendix A). Dynamic vessel motion challenges the assumptions of the test, but low magnitude, long period motion might be acceptable (e.g. the outer beams can ping 30 times in 0.68 s in 7.5 m of water so a 10 s period roll or pitch of a few degrees might be tolerable). Conducting the test alongside a pier is potentially troublesome due to debris commonly found alongside piers (debris with differing acoustic impedances effectively renders the seafloor inhomogeneous), as well as acoustic noise from other vessels moored nearby.

An ideal depth and seafloor type that accommodates all setting combinations for the Reson 7125 has not been identified. That is, a depth for which the seafloor is detectable in the beam-formed amplitude using lower setting values, but does not saturate received signals made using higher settings has not been identified. From a practical perspective, shallower depths on the order of 5-10 m are preferable so that a faster ping rate can be used to decrease the overall length of time it takes to complete the test, and also to minimize exposure of each ping to discrete interference events in the water column (e.g. kelp leaf in the water column passing under the boat). Even if an ideal depth and seafloor type exists, finding it over a span of homogenous seafloor

alongside a pier, in a mooring field or anchorage area, or in a low trafficked area is unlikely. Ultimately the merits and limitations of each potential site available within a given area must be considered individually and weighed against each other to choose the best available site.

Sample Size and Setting Interval Selection

The sample size is the number of pings at each setting combination. A large number of pings at each setting combination theoretically increases the confidence in the result, but also increases the risk of induced biases from the dynamics of the water column or seafloor. If the assumptions of a homogenous, stationary seafloor and water column can be preserved for seconds at a time, a target confidence interval or precision of the sample mean can be used to determine the sample size. The number of pings at each setting combination used in the field case studies varied between 15-30 pings.

The particular model of Reson 7125 MBES (SV1) used in the case study allow users to select gain settings ranging from 0 to 83 dB in intervals of 1; power settings ranging from 170 to 220 dB in intervals of 1; and pulse length settings from 33 to 300 μs in intervals of 1 μs up to 100 μs, and in intervals of 10 μs up to 300 μs. Logging all possible combinations would be a lengthy process (on the order of days) and; therefore the *intra* calibration was performed during the case study using several different down-sampled setting selections with different setting step intervals. This is considered acceptable because the Reson 7125 amplitude response to gain and power setting changes is assumed to be linear as there are no previous observations to suggest otherwise.

45

Data Acquisition

A script to command setting changes after every 30 pings at each setting combination originally written by Rice for a saturation monitoring tool (Rice, 2012) was modified and used during the case study described later in this document. The *intra* calibration could be conducted manually albeit tediously and likely without a precise number of pings at each setting combination. To log a sample of pings at each setting combination, first the pulse length is set, then the power, and finally the system is then cycled through the range of gain settings. After logging through all gain settings with the pulse length and power fixed, then the power setting is changed, and the gain cycle is repeated. This process continues through all the remaining settings for power and pulse length. The spreading and absorption is set to zero throughout the test to avoid the need to correct for Reson applied TVG. The fixed Reson depth gates are also set tightly around the seafloor to avoid logging erroneous seafloor detections.

Several lessons were learned during the course of testing this method and are summarized here. Setting the pulse length first is recommended because it appears to be the slowest setting to stabilize, so changing the pulse length frequently in short time spans leads to noisier results. Using the highest possible ping rate does not appear to affect the results. The first several pings after a change in setting combination have been observed to have higher amplitudes than their successors for some systems and setting combinations, indicating that there is an adjustment period that should be considered for exclusion from logging and/or data analysis. Reson 7125 MBES have a real time depth/range gating option in which data outside the filters are not recorded, the use of which is recommended to reduce the quantity of poor quality data logged and to assist the bottom tracking when operating at low power and low gain settings.

Data Processing

The recorded amplitude associated with the bottom detection in the 7006 record is taken as the raw digital number, dn, of which the logarithmic quantity is, $DN = 20 \log_{10}(dn)$. The $dn's$ for which bottom detection with a Reson high quality flag is not achieved are first removed. Though data are logged for all setting combinations, the $dn's$ for all the beams logged using only the pivot settings of interest are extracted to determine how the system changes away from settings other than the pivot settings. That is, to create the SL_{field} LUT, all the pings logged using the single gain pivot setting, the single pivot pulse length setting, and all the power settings are selected. To create the G_{field} LUT, all the pings logged using the single power pivot setting, the single pivot pulse length setting, and all the gain settings are selected. To create the pseudo PL_{field} LUT, all the pings logged using the single gain pivot setting, the single power setting, and all the pulse settings are selected.

Figure 11 is an example of the raw data from a single set of pivot settings (power setting of 200, gain setting of 21, and a pulse length of 120 µs) logged by one MBES mounted on NOAA Launch 2805 while moored alongside a pier. The top panel shows the raw DN for all beams. The middle panel shows the mean of the $DN's$ for each ping at each setting using several different combinations of pings (all beams, five beams at nadir, five beams to port, and five beams to starboard), the expected change if all the settings were truly representative of their named values relative to the lowest value used for each setting, and a 16-bit max value in dB. Reson 7125 MBES are assumed to have a 16-bit digital range, meaning the raw recorded values in dB can range from zero to roughly $20 \log_{10}(2^{16} - 1) = 96.3$ dB. This maximum digital value is plotted in Figure 11

(middle panel) for comparison to the power and gain roll off points to understand whether digital or acoustic saturation is occurring at that setting combination.
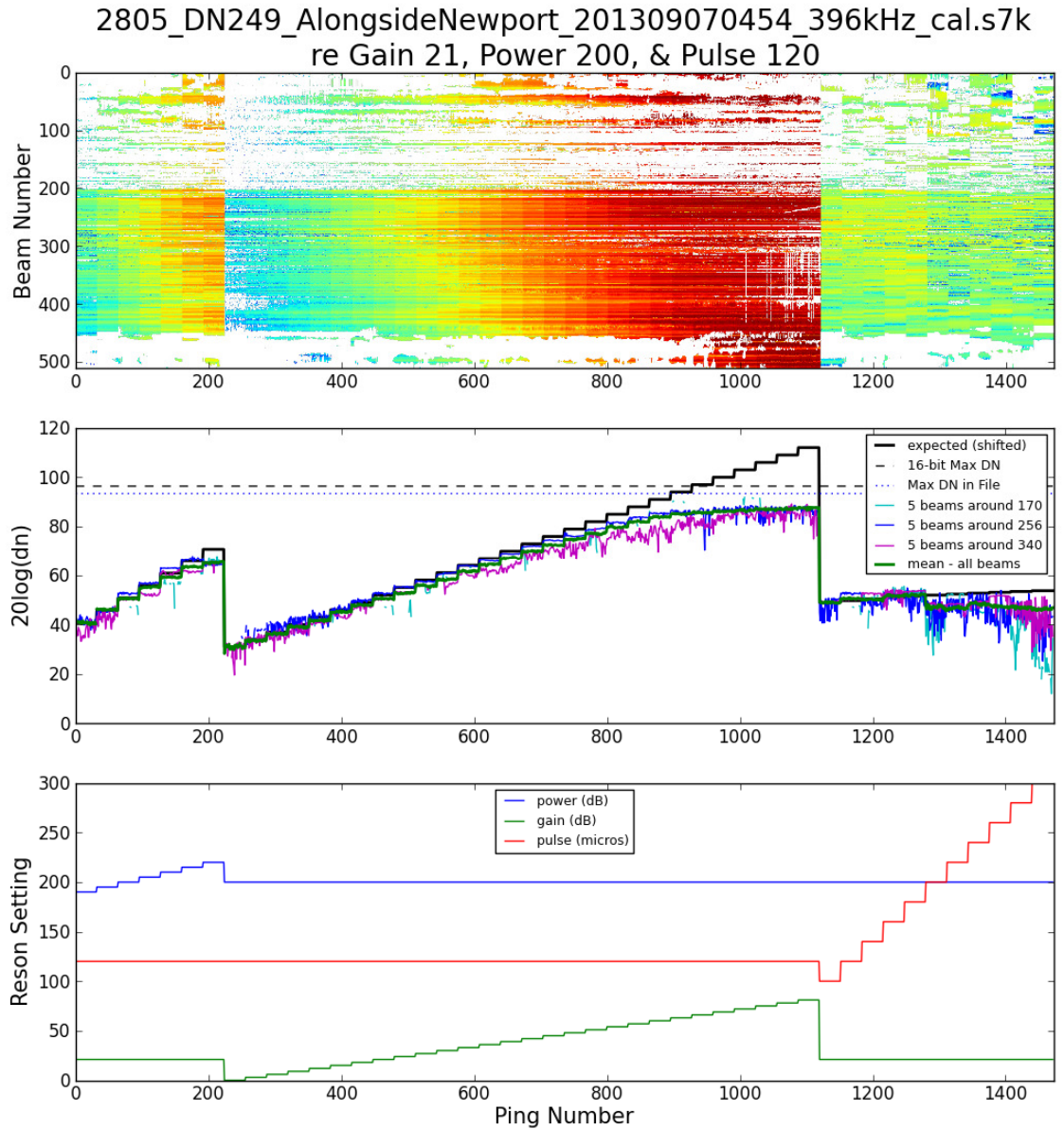
Figure 11: Sample set of raw data from the intra calibration using the pivot settings of gain = 21, power = 200, and pulse length of 120x10^-6 s. Top: raw digital numbers in dB. Middle: average values in dB. Bottom: setting values.

To create each setting correction LUT, the $dn's$ at each of the selected setting combinations for each beam are averaged:

$$\overline{dn_{p,g,\tau_j}} = \frac{1}{N_{pings}} \sum dn_{ij} \qquad [18]$$

where $\overline{dn_{p,g,\tau_j}}$ is the mean dn value for all pings at a particular power, gain, and pulse length setting for beam j; N_{pings} is the number of $dn's$ in the sample; and dn_{ij} is the digital number for beam j, ping i.

The mean digital number for each beam, $\overline{dn_{p,g,\tau_j}}$ at each setting combination is averaged with all other beams:

$$\overline{dn_{p,g,\tau}} = \frac{1}{N_{beams}} \sum \overline{dn_{p,g,\tau_j}} \qquad [19]$$

The mean digital number taken from all beams and all pings at each setting combination is converted to dB: $\overline{DN_{p,g,\tau}} = 20 \log_{10} \overline{dn_{p,g,\tau}}$. Treating the mean $\overline{DN_{p,g,\tau}}$ at the pivot setting for the particular LUT being created as the pivot point value, the difference between $\overline{DN_{p,g,\tau}}$ of the pivot setting and all other settings is computed such that the pivot setting is the setting value itself. Using the power settings as an example, to determine $SL_{field}@p_i, g, \tau$ at power setting i:

$$\Delta DN_{p_i,g,\tau} = \overline{DN_{p_i,g,\tau}} - \overline{DN_{p,g,\tau}} \qquad [20]$$

and

$$SL_{field}@p_i, g, \tau = p + \Delta DN_{p_i,g,\tau} \qquad [21]$$

where p is the pivot setting and p_i is any other possible power setting. (Numerically, if the pivot power setting p is 200, and the average DN at power setting 210 (p_{210}) is 8 dB more than the average DN at the power pivot setting of 200 ($\Delta DN_{p_i,g,\tau} = 8$), then $SL_{field}@p_{210}, g, \tau$ is taken to be 208.)

Because the *intra* calibration is expected to be performed in relatively shallow water depths, the systems are expected to saturate at higher setting values for power and gain. To find the linear region of the SL_{field} and G_{field} at which it is assumed saturation did not occur, the SL_{field} and G_{field} values are linearly regressed onto their

corresponding settings, first using all settings and then by successively removing the next highest setting. The R-squared value and 95% confidence interval (CI) for each regression are computed. The highest setting that results in the largest R-squared value (below 1, i.e. more than two settings) and minimum CI is taken to be the maximum setting within the linear operational regime of the MBES during the test. The minimum setting value is taken to be smallest operational value of the setting. The linear, non-saturated setting corrected values are extrapolated to derive corrections for the saturated settings, resulting in the final *intra* calibration LUTs for the power and gain settings. Alternately, the test could be performed in several depth ranges (e.g. shallow, medium, deep), and the linear setting regions of each could be combined. A full comparison between the two approaches has not been achieved. A linear approximation of the field data is considered suitable as that is what has been observed in the test tank.

The pseudo PL correction is determined by calculating the difference between the expected changes (EΔ) in dB for the pulse length used relative to the pivot pulse length where the expected change in dB is:

$$E\Delta = 10 \log_{10}(\tau_i) - 10 \log_{10}(\tau) \qquad [22]$$

which is what would be used in the insonified area term of the backscatter calculation in equation [6], all other terms being equal. The pseudo pulse length correction is the difference between what is expected and what was measured in the field:

$$\text{pseudoPL} = E\Delta - \Delta DN_{p,g,\tau_i} \qquad [23]$$

where $\Delta DN_{p,g,\tau i}$ is the change in dB when using other pulse lengths other than the pivot pulse length at the pivot power and gain settings. The pseudo PL correction is intended for all beams, regardless of how the insonified area is defined, as the correction

accounts for an observed system amplitude response to all beams and is not a correction for the length of time the pulse is emitted or for the shape of the pulse.

Figure 12, Figure 13, and Figure 14 show the resulting look up tables of the *intra* calibration associated with the raw data presented in Figure 11. The red line is $\Delta DN_{pi,g,\tau}$ for each setting away from the pivot setting (indicated in back) with 95% CIs around it. As expected, the system diverges from a linear response at higher power and gain settings. The blue lines in the power and gain plots show the extrapolated linear regression. The green line for the power and gain plots is the extrapolated linear regression shifted to pass through the pivot setting, resulting in a zero correction when the MBES is operated at the pivot setting. The green line shown in each of the three plots is what is used to generate the LUTs for SL_{field}, G_{field}, and pseudo PL_{field} for this system relative to a power setting of 200, gain setting of 21, and a pulse length setting of 120. The pulse length correction above 200 μs is as has been aforementioned several dB less than expected value relative to the pivot setting, which is below 200 μs.
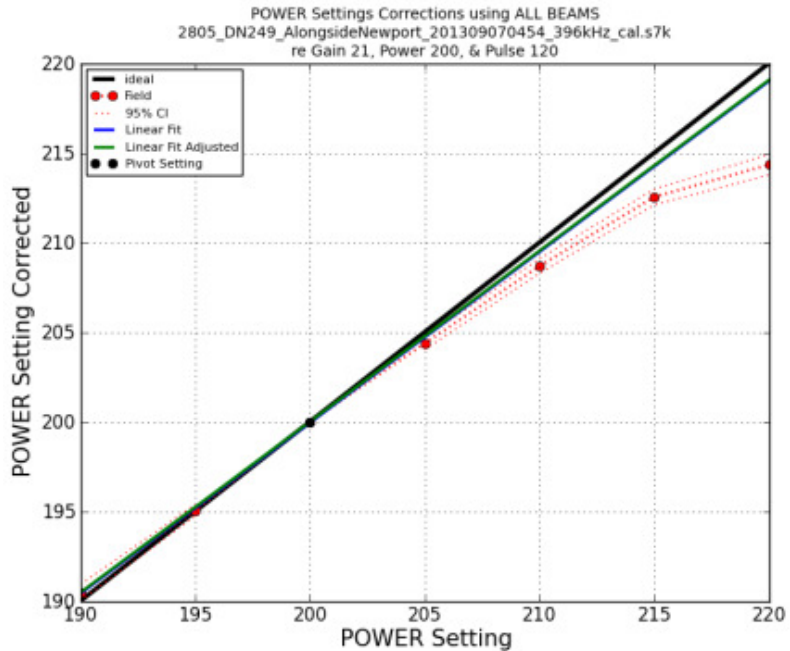
Figure 12: Power setting correction table relative to the pivot settings of gain = 21, power = 200, and pulse = 120x10^{-6}.
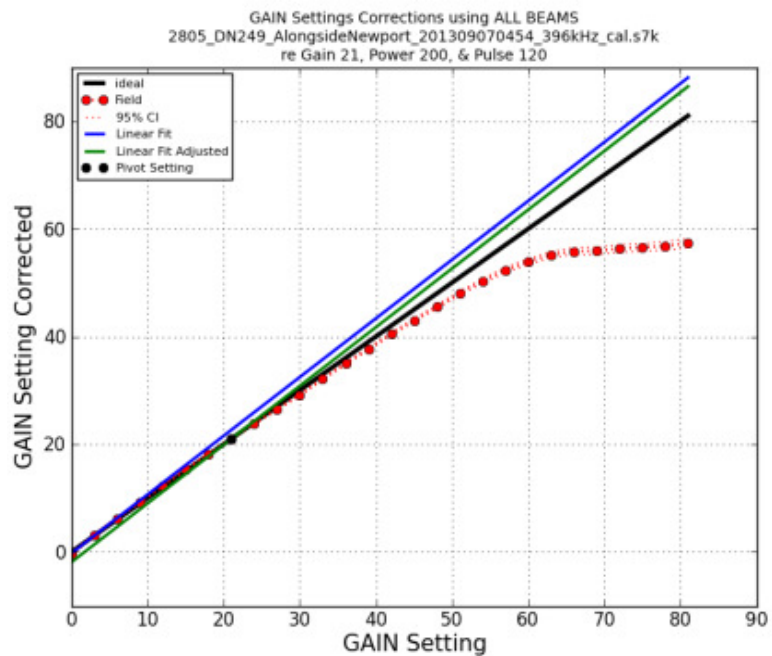
Figure 13: Gain setting correction table relative to the pivot settings of gain = 21, power = 200, and pulse = 120x10^{-6}.

PULSE LENGTH Settings Corrections using ALL BEAMS
2805_DN249_AlongsideNewport_201309070454_396kHz_cal.s7k
re Gain 21, Power 200, & Pulse 120
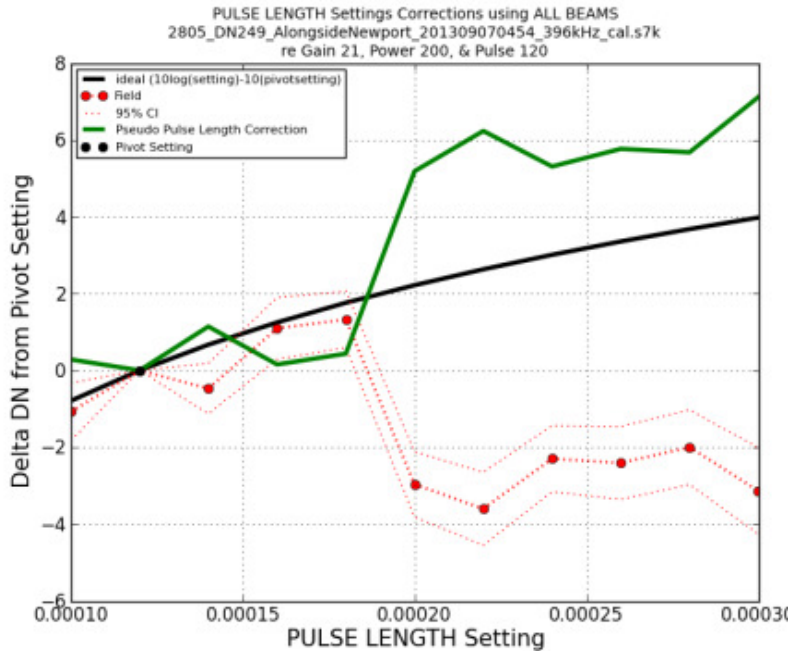
Figure 14: Pseudo pulse length setting correction table relative to the pivot settings of gain = 21, power = 200, and pulse = 120x10^{-6}.

The resulting four LUTs from the *inter* and *intra* calibrations ($C_{field}(\theta_s)$, SL_{field}, and G_{field}, and pseudo PL_{field}) are saved as text files and are expected to be used as a set during processing data from that system, similar to the way in which the tank calibration data are applied. Figure 15 summarizes the processing steps for both the *inter* and *intra* calibration data and how they are expected to be used. Appendix C provides a conceptualized schema for handling calibration files, application, and associated metadata.

Inter Calibration Data Processing Flow Chart

Intra Calibration Data Processing Flow Chart

Raw Data Files: .s7k, .cnv, .svp

Calibration Files: $C(\Theta_{sa})$, SL(power setting), G(gain setting), $\psi_{tx}(\Theta_{sa})$, $\psi_{rx}(\Theta_{sa})$, pseudoPL(pulse length setting)

Raw Data Files: .s7k

Process Backscatter

Select which calibration corrections to apply to which system? How many pings to compare?

Make SL, G, and pseudo PL Look-up Tables

Processed Backscatter Files: .npy

SL(power setting), G(gain setting), pseudoPL(pulse length setting)

Compare Backscatter (CTD, Attitude, & Ss Comparisons; Compute Statistics, etc)

$C_{field}(\Theta_{sa})$ or single value C_{field} made with mean DN or S_b

Figure 15: Inter and intra calibration data processing flow chart.

54

CHAPTER 4

Case Studies

NOAA Ship *Fairweather* carries four hydrographic survey launches equipped with dual-frequency Reson 7125 SV1 MBES that were the primary platforms used in the development of this field calibration procedure. *Fairweather's* operational area is Alaska and the west coast of the contiguous United States, so data collected in four different geographic locations were used. The permutations of launches, frequencies, pivot settings, and testing sites add an undesirable complexity to this work. However, all were deemed necessary to substantiate the method. The systems and field case studies are presented in this chapter. (Several assumptions that were made in the formulation of this method were explored using other data sets from systems of opportunity that are presented in Appendix A.)

Launches

NOAA Ship *Fairweather* carries four 10-m survey launches of the same design, all of which were built in 2009 by All American Marine. Each launch is referred to by its unique hull number: 2805, 2806, 2807 and 2808. Figure 16 shows the launches alongside the NOAA small boat pier in Newport, Oregon.

Figure 16: NOAA Survey Launches 2805, 2806, 2807, and 2808 in Newport, Oregon.

Each launch is equipped with a dual-frequency Reson 7125 SV1 MBES with separate 200-kHz and 400-kHz projectors, a Reson real-time surface sound speed sensor, an Applanix POSMV position and attitude sensor, and a Seabird CTD for conductivity, temperature, and pressure profiling with which to model the sound speed profile through the water column. Figure 17 shows the Reson 7125 as mounted on each launch.
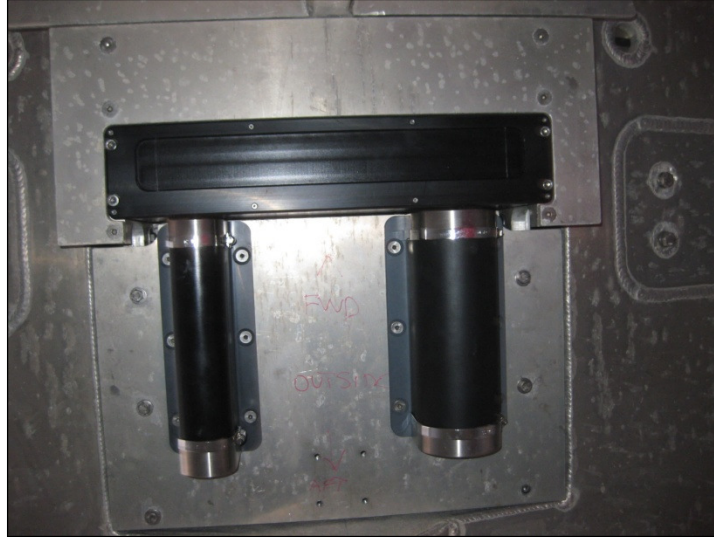
Figure 17: Reson 7125 SV1 Mounted to the Hull of Launch

The tank-calibrated Reson 7125 was mounted on Launch 2805 in 2012 and on Launch 2807 in 2013. The NOAA Ship *Fairweather* Data Acquisition and Processing Reports from 2010-2013 explain the complete configurations in detail for each year (NOAA Ship Fairweather, 2010 - 2013).

Field Data

Though the systems and launches are used regularly during the course of *Fairweather's* field survey seasons (NOAA Ship Fairweather, 2010 - 2013), the conceived field procedure was developed and evaluated using data acquired at four locations on the West Coast of the United States as shown in Figure 18: Shilshole Bay, in Puget Sound, Washington; Duck Bay, near Kodiak Island, Alaska; Newport, Oregon; and Los Angeles, Long Beach, CA (LALB).
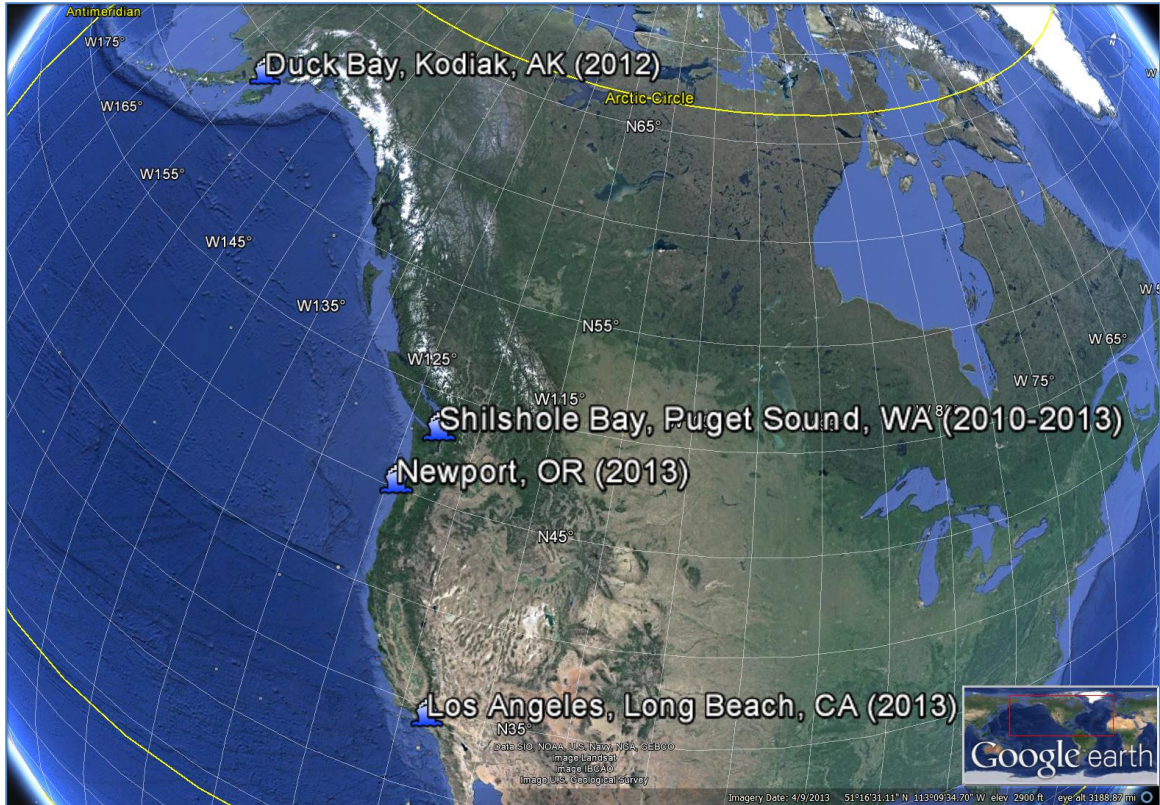
Figure 18: Four locations where data used in the development of this method were acquired: Shilshole Bay, in Puget Sound, Washington; Duck Bay, near Kodiak Island, Alaska; Newport, Oregon; and Los Angeles, Long Beach, CA

Shilshole Bay, Puget Sound, Washington

Shilshole Bay is a well-established test site that has been used for a number of years for reference-frame calibration by NOAA hydrographic field units and contractors. Many of *Fairweather's* systems were tested there each spring during the years 2010-2013. Though the individual hardware components of each system, such as projectors and receivers, were not the same on each launch year to year, the data that were logged while running the same survey line over the same area of seafloor were first used to provide a baseline estimate of the magnitude of the backscatter measurement inconsistencies between systems over time. As mentioned in the introduction, a ~2-2.5

dB spread was observed between the 200-kHz systems and a ~5-7.5 dB spread was found in the 400-kHz systems.

Duck Bay, Kodiak, Alaska

The system that was acoustically calibrated in the tank at UNH in January 2012 was used during *Fairweather's* 2012 field season on Launch 2805. Two systems that year, Launch 2805 (the tank calibrated system) and Launch 2808, logged data over the same patch of seafloor using the same line run in the same direction using the same settings both at the Shilshole test site in April (JD105, power = 200, gain = 25, pulse length = 38) and again on two different days at the Duck Bay location in August and September (JD242 and JD264, power = 200, gain = 21, pulse length = 50). The data from the coincident lines run at these two locations were used to verify the consistency of the difference between the beam mean S_b of the two systems. Figure 19 shows the beam averages of Launch 2805 and Launch 2808 at both locations on all days. (The Shilshole line file contains approximately 1100 pings while the Duck Bay line file contains approximately 100 pings, which accounts for the relative across-swath noise in the Duck Bay lines. The Duck Bay lines are saturated at nadir.) Though these two particular systems at the 200-kHz frequency are not notably inconsistent, the differences support the possibility of a consistent beam pattern difference of a few dB between systems from two different geographically distinct areas. (The 400-kHz lines are not shown because the files from Shilshole are corrupt.)
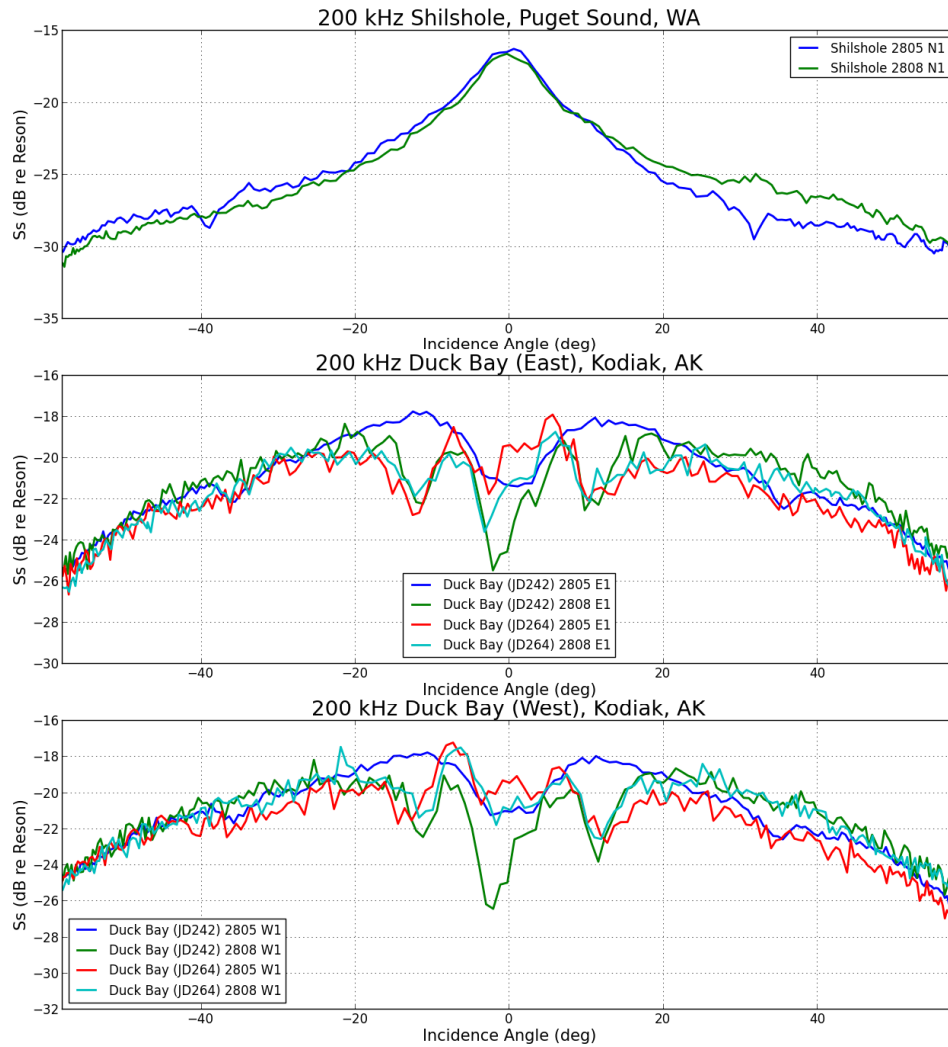
Figure 19: Mean beam S_b by incidence angle for launches 2805 and 2808 (no tank calibrations applied) in two different locations during the 2012 field season. Relative difference roughly less than a dB for the stable regions of the swath.

Newport Field Calibration

Finally, both the *inter* and *intra* calibration procedures were tested in 2013 using three vessels – Launch 2805, Launch 2806, and Launch 2807 – in Newport, Oregon, in August and September (JD246 – JD250). In this case, the tank calibrated MBES was mounted on Launch 2807.

Newport, Oregon, is on the Yaquina River near where the river meets the Pacific Ocean. Yaquina Bay is an estuary that extends 23 miles inland and is influenced by mixed semi-diurnal tides. The mean tidal range at the nearest water level station at South Beach is 1.9 m, and the predicted current at the US 1 Highway Bridge ranges from 1 to 3.5 knots. The river is flanked by gently sloping beaches and coastal dunes, with a man-made breakwater at the entrance. The sediment sizes range from coarse sand to silt (Kulm, 1965). The Port of Newport is supported primarily by the lumber and fishing industry, but the area is also popular for recreational boating and fishing. Considering the ideal attributes of a field calibration location described in Chapter 3, Newport, Oregon, is not ideal. However, Newport is the homeport of NOAA's pacific fleet and the most likely place all NOAA MBES systems will be at one point in time. It also serves as a worst-case scenario in which to evaluate the effectiveness of the method proposed in this work.

All calibrations were performed on clear days with winds less than 10 knots. Small fishing vessels were encountered at all sites, but every attempt was made to wait until transiting vessels cleared the area. Sub-aquatic vegetation debris was visually observed in the water column at all sites. The calibrations in the river were all performed on days with maximum flood tide currents less than 1.2 knots.

Inter Calibration

The *inter* calibration procedure was executed at three different sites – in 10 m water depth in the Yaquina River (Site 1), in 20 m water depth 2 NM off the coast of Newport (Site 2); and in 40 m water depth 4 NM off the coast of Newport (Site 3) – with three systems using different pivot settings to verify the repeatability of the approach across a range of system settings and locations (Figure 20). The settings at each

location were selected in situ with a Saturation Monitor tool that estimates when the system is saturating (Rice, 2012). The *inter* calibration survey lines were run in both directions with each set of settings. The systems on Launch 2805 and Launch 2806 were calibrated against the tank-calibrated system on Launch 2807.
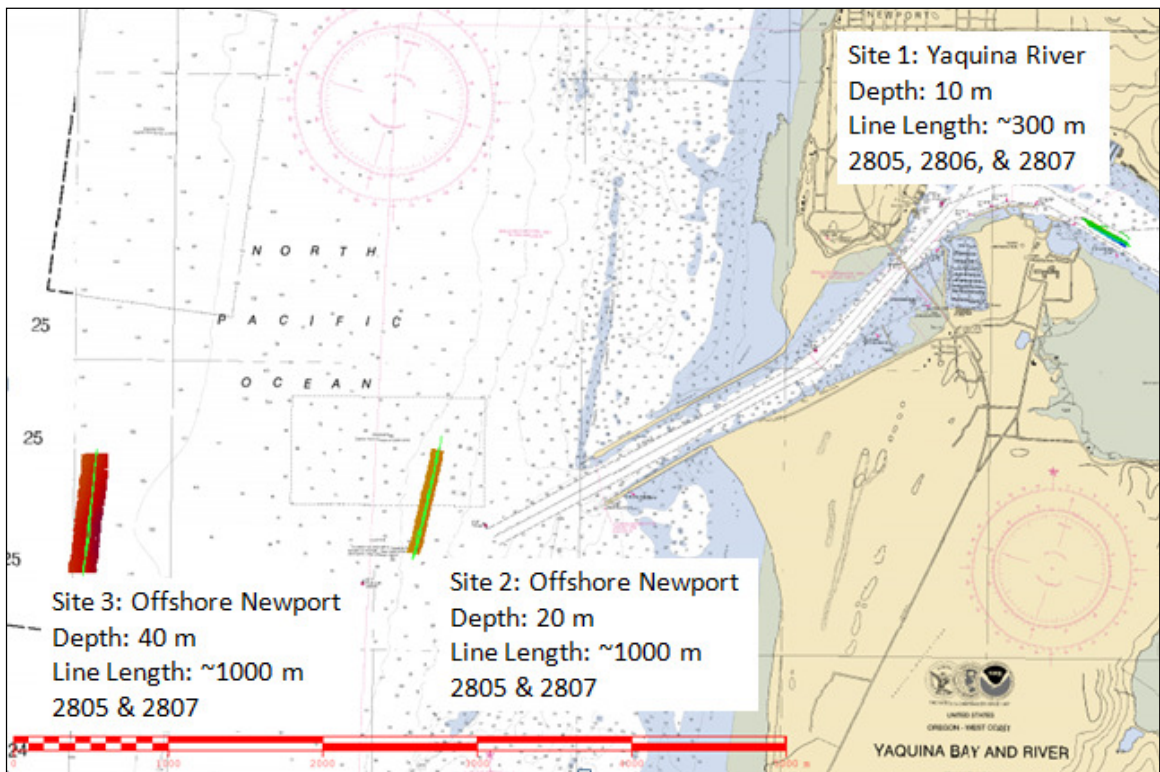
Figure 20: Inter calibration sites in and around Newport, Oregon (NOAA Chart 18746).

The Launch 2805 system was calibrated at all three sites using five setting combinations over the course of two days. The Launch 2806 system was calibrated at Site 1 only, using the same set of settings four times. All systems were calibrated at both frequencies in equidistant mode with roll stabilization enabled. During all tests, data were logged both in Hypack on a separate acquisition computer and by the Reson controller software on the Reson 7P processor. The data were logged in Hypack because that is the traditional acquisition method of the ship, but also with Reson

7kCenter to record water column data as well. In most cases, the Hypack .7k/.hsx file pair were used as the raw data because the file sizes are smaller and are easier to handle. However, some of the Hypack data that were logged were found to have not recorded about 1/3 to 1/2 of the pings (this problem was later traced to a Microsoft Windows Administrator setting). For those cases, the raw data from the Reson .s7k file were used. Table 2 contains the settings that were used for each line pair and the results of both the relative and relative absolute calibrations for both frequencies. The system on Launch 2807 was used as the reference system to which the other two systems were calibrated for both the relative and relative absolute *inter* calibration.

Relative Inter Calibration

The *inter* calibration data were first processed as a simple relative calibration without tank calibration corrections. This was done both to assess the initial differences between systems compared to what was previously observed at Shilshole, and to derive relative $C_{field}(\theta_s)$, for each launch at each site for all pivot settings used. Depending on the setting combinations used, the relative differences are consistent with those observed at Shilshole (system to system differences varying between tenths of a dB for 200 kHz and up to 5 dB for 400 kHz).

Figure 21 shows the results of the 200-kHz relative *inter* calibrations ($C_{field}(\theta_s)$, for the Launch 2805 system at all three sites using different pivot setting (A, B, and C), and for the Launch 2806 system at Site 3 using only one setting repeated several times (D). Figure 22 shows the same for the 400-kHz systems, though the pivot settings are different.
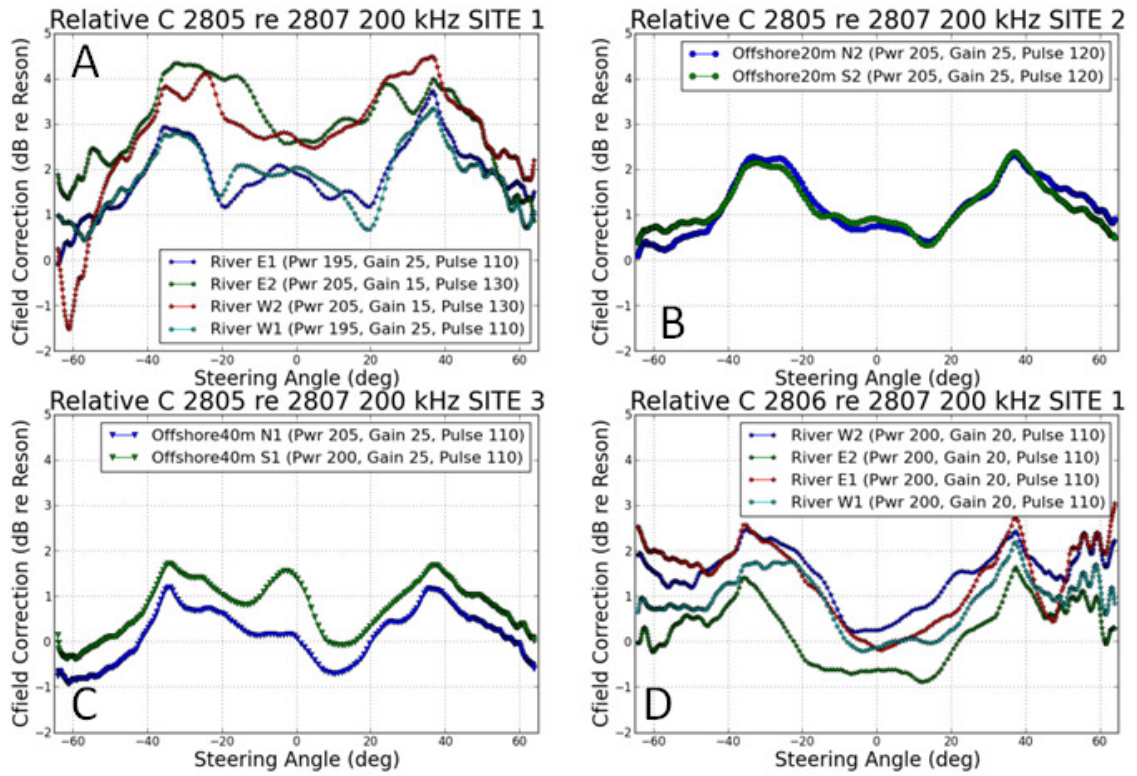
Figure 21: Relative 200-kHz $C_{field}(\theta_s)$, for Launch 2805 system at Site 1 (A), Site 2 (B), Site 3 (C) and for Launch 2806 system at Site 3 (D) relative to the pivot settings used.
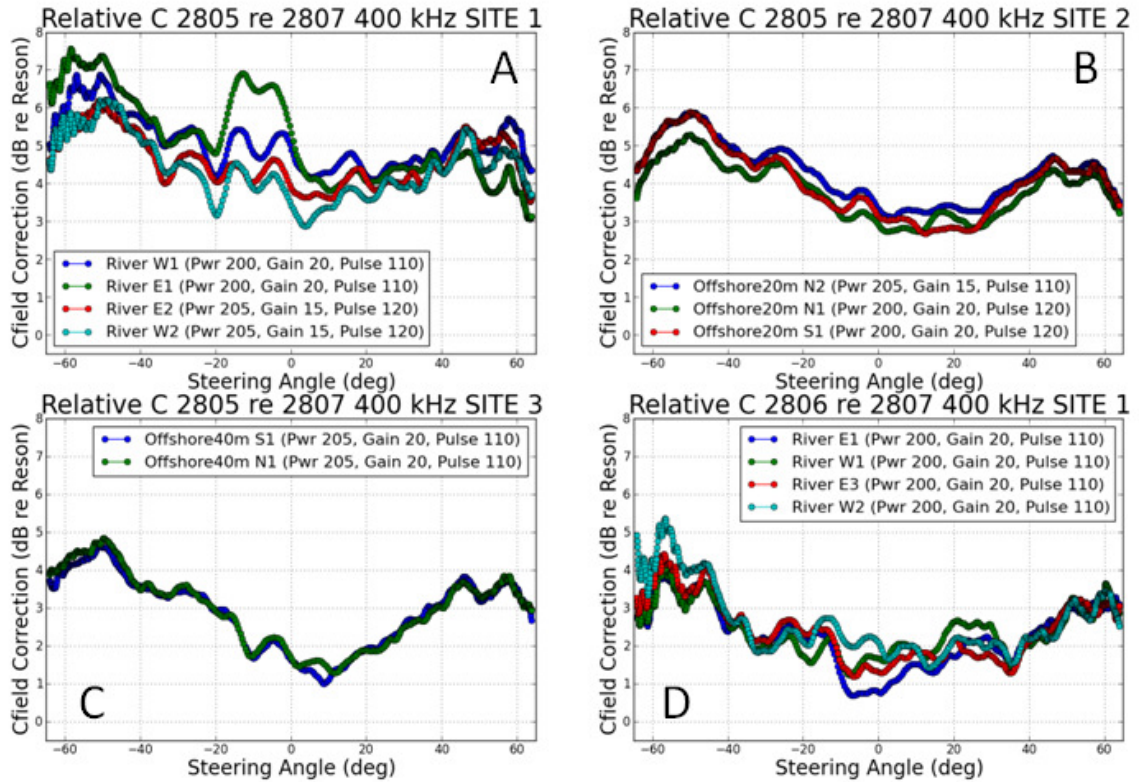
Figure 22: Relative 400-kHz $C_{field}(\theta_s)$ for Launch 2805 system at Site 1 (A), Site 2 (B), Site 3 (C) and for Launch 2806 system at Site 3 (D) relative to the pivot settings used.

With the exception of the 400-kHz E1 line at Site 1 (Figure 22A), the results show similar beam patterns from calibration to calibration for each system and each frequency. However, each frequency and system has its own unique beam pattern. The vertical offsets on the order of 0.5 - 2 dB between calibrations are the result of using different pivot settings (most prominently observed in Figure 21A). The differences between calibrations are on the order of a few tenths of a dB or less when the same settings are used with the exception of the 200-kHz-E2 calibration for the Launch 2806 system at Site 1 (Figure 21D), which is considered an anomaly that requires further investigation. The Launch 2806 system results at Site 1 show slightly higher variation for both frequencies even though the same settings were used multiple times. The

smoothest beam pattern (Site 2) comes from the survey lines with the most number of pings (~2000).

Relative Absolute Inter Calibration

The same *inter* calibration files were also processed as relative absolute *inter* calibrations, meaning that the tank calibration corrections were used to process the data from the Launch 2807 system. Figure 23 shows the 200-kHz and Figure 24 shows the 400-kHz relative absolute calibrations at all three sites for the Launch 2805 system (A, B, C) and at Site 1 for the Launch 2806 system (D).
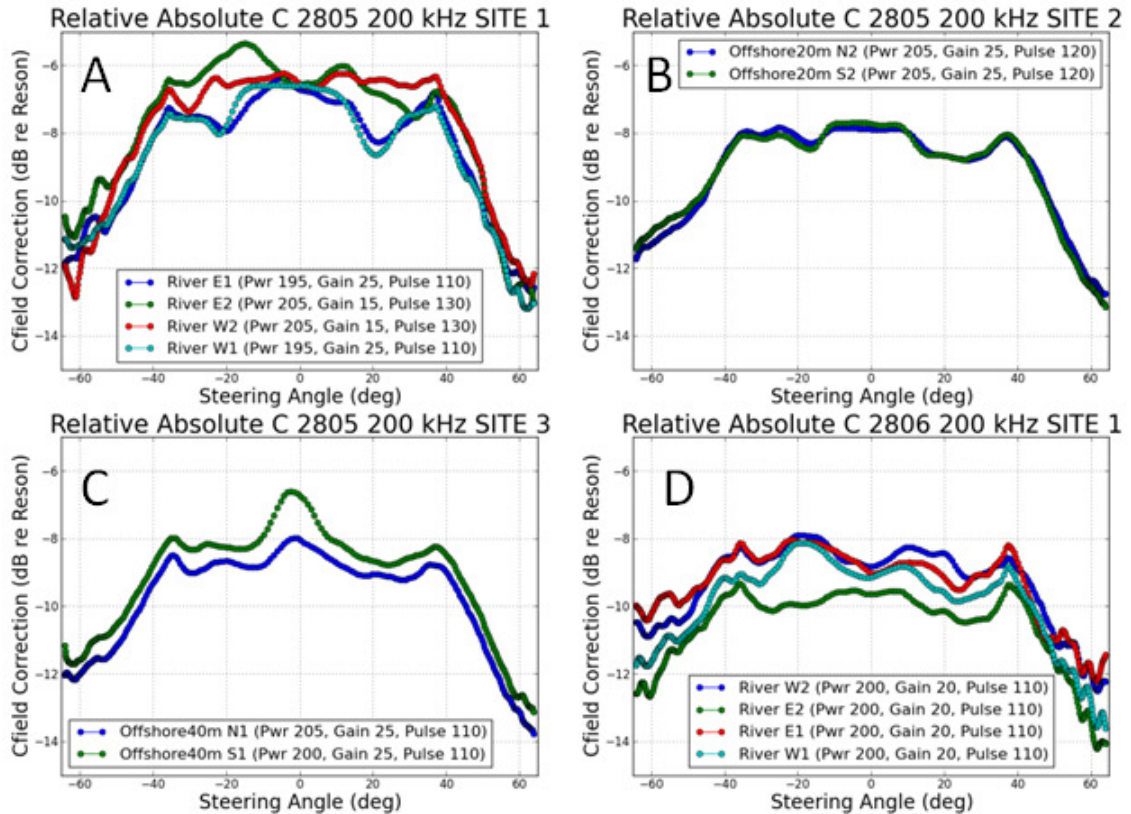
Figure 23: Relative absolute 200- kHz $C_{field}(\theta_s)$ for Launch 2805 system at Site 1 (A), Site 2 (B), Site 3 (C) and for Launch 2806 system at Site 3 (D) relative to the pivot settings used.
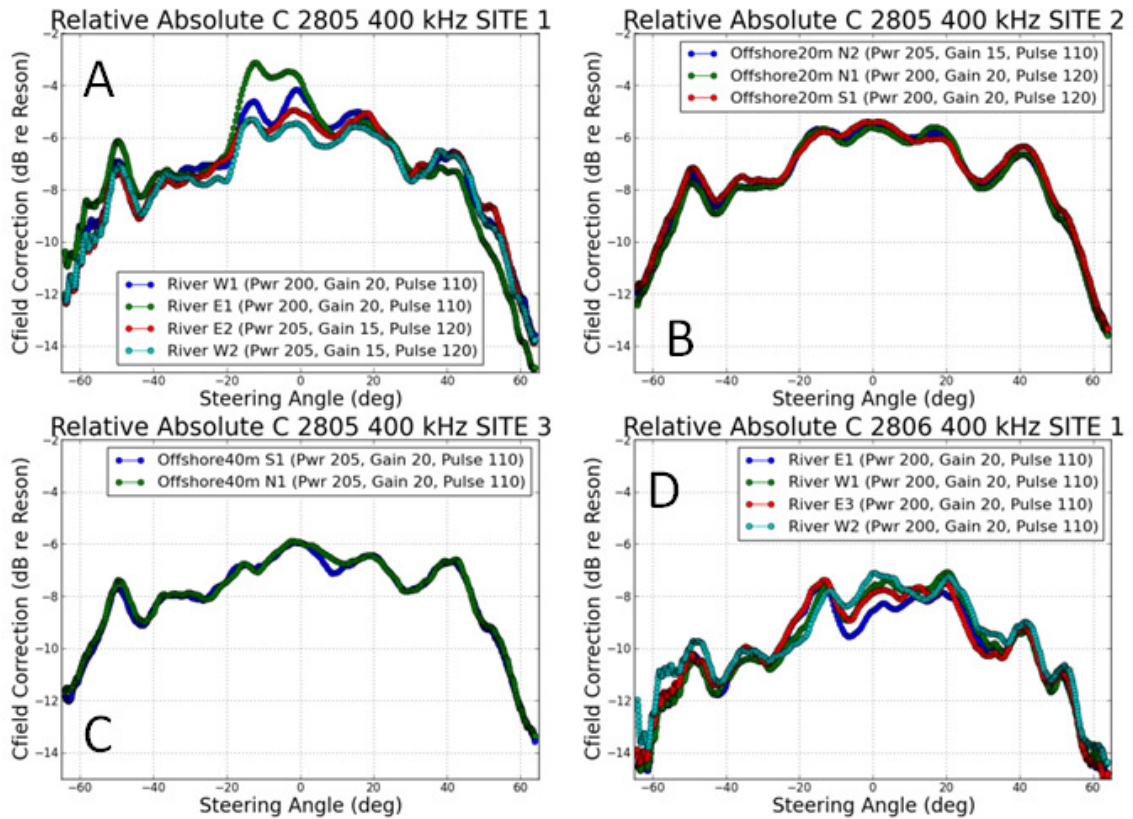
Figure 24: Relative absolute 400-kHz $C_{field}(\theta_s)$ for Launch 2805 system at Site 1 (A), Site 2 (B), Site 3 (C) and for Launch 2806 system at Site 3 (D) relative to the pivot settings used.

The two primary differences between the relative and the relative absolute *inter* calibrations are the shape of the beam patterns and the overall absolute values of the results. The comparative difference in the shape of the beam patterns comes from applying $C_{tank}(\theta_s)$, $\psi_{tx-tank}$, $\psi_{rx-tank}$ to the calibrated Launch 2807 system data as described in the Chapter 3 section on *inter* calibration data processing. The comparative difference in absolute value (1-5 dB for the relative calibration and an 8-10 dB difference for the relative absolute calibration) comes from applying $C_{tank}(\theta_s)$, SL_{tank}, and G_{tank} to Launch 2807 system data. The high frequency undulating pattern in the outer beams

are possible justification for additional smoothing to avoid along track banding artifacts in mosaics.

Table 2 summarizes how each line was acquired. It also shows the mean S_b for each line processed both as a relative and a relative absolute calibration, and the mean and standard deviation of the beam-to-beam difference between systems. It also shows the mean and standard deviation of the difference between the beam mean S_b and DN's for all beams with incidence angles between 15-30°. The beam-to-beam mean DN were differenced in the same way as S_b to compare the raw values recorded by each system. A mean and standard deviation of $C_{field}(15 - 30^o)$, the "oblique" columns in Table 2, was calculated because that region of the swath appears most consistent for all *inter* calibrations.

Table 2 (400 kHz). Column headers: label / Line / Power / Gain / Pulse | 400 kHz RELATIVE (2805 Mean Sb, 2807 Mean Sb, Mean Sb Diff, SD Sb Diff, Mean Obliq Sb, SD Obliq Sb, Mean DN Diff, SD DN Diff, Mean Obliq DN Diff, SD Obliq DN Diff) | 400 kHz RELATIVE ABSOLUTE (2805 Mean Sb, 2807 Mean Sb, Mean Sb Diff, SD Sb Diff, Mean Obliq Sb, SD Obliq Sb)

2805 re 2807	Line	Power	Gain	Pulse	2805 Mean Sb	2807 Mean Sb	Mean Sb Diff	SD Sb Diff	Mean Obliq Sb	SD Obliq Sb	Mean DN Diff	SD DN Diff	Mean Obliq DN Diff	SD Obliq DN Diff	2805 Mean Sb	2807 Mean Sb	Mean Sb Diff	SD Sb Diff	Mean Obliq Sb	SD Obliq Sb
Site 1 (JD246) River 10m	E1	200	20	110	-22.2	-27.5	5.28	1.33	4.79	0.67	5.32	1.43	4.91	0.63	-22.2	-13.8	-8.38	2.88	-6.41	0.85
Max Flood: 1027	W1	200	20	110	-22.2	-27.4	5.28	0.77	4.72	0.56	5.3	0.72	4.79	0.57	-22.2	-13.8	-8.39	2.44	-6.44	0.89
(1 kt)	E2	195/205	25/15	130/120	-21.8	-26.6	4.78	0.75	4.31	0.41	4.58	0.65	4.33	0.41	-21.8	-13.3	-8.51	2.43	-6.45	0.92
Slack: 1243	W2	195/205	25/15	130/120	-21.8	-26.4	4.64	0.87	3.96	0.52	4.44	0.73	4.03	0.53	-21.8	-13.2	-8.63	2.34	-6.83	0.96
Site 2 (JD247) Offshore 20m	N1	200	20	120	-21.9	-25.9	4.01	0.7	3.68	0.68	4	0.66	3.66	0.61	-21.9	-13.2	-8.72	2.26	-6.8	0.95
	S1	200	20	120	-21.5	-25.8	4.3	0.88	3.56	0.79	4.29	0.84	3.55	0.72	-21.5	-13.1	-8.42	2.16	-6.91	0.71
	N2	205	15	110	-22.1	-26.6	4.45	0.77	4.03	0.74	4.45	0.73	4.01	0.65	-22.1	-13.5	-8.62	2.23	-6.87	0.91
	S2	na	na	na	na	na	na	na	na	na	na	na	na	na	na	na	na	na	na	na
Site 3 (JD247) Offshore 40m	N1	205	20	110	-20.2	-24	3.29	0.95	2.59	0.76	3.29	0.92	2.59	0.63	-20.7	-12	-8.79	2.05	-7.33	0.66
	S1	205	20	110	-20.8	-24	3.22	0.9	2.61	0.68	3.23	0.87	2.62	0.54	-20.8	-11.9	-8.89	2.07	-7.31	0.68

2806 re 2807	Line	Power	Gain	Pulse	2806 Mean Sb	2807 Mean Sb	Mean Sb Diff	SD Sb Diff	Mean Obliq Sb	SD Obliq Sb	Mean DN Diff	SD DN Diff	Mean Obliq DN Diff	SD Obliq DN Diff	2806 Mean Sb	2807 Mean Sb	Mean Sb Diff	SD Sb Diff	Mean Obliq Sb	SD Obliq Sb
Site 1 (JD250) River 10m	E1	200	20	110	-24.6	-27.1	2.58	0.83	2.13	0.4	2.64	0.78	2.23	0.4	-24.6	-13.5	-11.1	2.17	-9.05	1.03
Slack: 0901	W1	200	20	110	-24.5	-27.1	2.65	0.77	2.16	0.47	2.73	0.73	2.29	0.47	-24.5	-13.4	-11.1	2.27	-8.91	1.27
Max Flood: 1243 (1.2 kt)	E2	200	20	110	-24.6	-27.3	2.71	0.88	2.13	0.47	2.78	0.82	2.24	0.47	-24.6	-13.6	-11	2.22	-8.98	1.1
	W2	200	20	110	-24.4	-27.5	3.09	1.05	2.1	0.54	2.94	1.07	1.88	0.55	-24.4	-13.8	-10.6	2.03	-8.93	1.16

Table 2 (200 kHz). 200 kHz RELATIVE | 200 kHz RELATIVE ABSOLUTE

2805 re 2807	Line	Power	Gain	Pulse	2805 Mean Sb	2807 Mean Sb	Mean Sb Diff	SD Sb Diff	Mean Obliq Sb	SD Obliq Sb	Mean DN Diff	SD DN Diff	Mean Obliq DN Diff	SD Obliq DN Diff	2805 Mean Sb	2807 Mean Sb	Mean Sb Diff	SD Sb Diff	Mean Obliq Sb	SD Obliq Sb
Site 1 (JD246) River 10m	E1	195	25	110	-29.4	-31.09	1.7	0.9	1.83	0.85	1.77	0.94	1.93	0.81	-29.42	-20.01	-9.41	2.05	-7.84	0.52
	W1	195	25	110	-29.41	-31.05	1.64	0.86	1.68	1.02	1.64	0.88	1.69	0.98	-29.42	-19.93	-9.49	2.14	-7.91	0.82
Max Flood: 1027 (1 kt) Slack: 1243	E2	200/205	20/15	110/130	-28.93	-31.61	2.67	1.06	3.84	0.61	3.26	1.01	4.17	0.74	-28.93	-19.82	-9.1			
	W2	200/205	20/15	110/130	-29.18	-31.51	2.32	1.55	3.59	0.69	2.93	1.56	3.94	0.83	-29.19	-20.24	-8.95	2.41	-6.57	0.43
Site 2 (JD247) Offshore 20m	N1	na	na	na					saturated								saturated			
	S1	na	na	na																
	N2	205	25	120	-28.64	-29.76	1.12	0.67	1.49	0.69	1.1	0.7	1.47	0.57	-28.64	-18.82	-9.82	1.64	-8.47	0.43
	S2	205	25	120	-28.79	-29.92	1.13	0.57	1.36	0.6	1.11	0.58	1.35	0.52	-28.79	-18.99	-9.81	1.66	-8.48	0.36
Site 3 (JD247) Offshore 40m	N1	205	25	110	-27.68	-27.69	-0.01	0.67	0.36	0.51	0.01	0.69	0.37	0.42	-27.68	-17.19	-10.49	1.73	-8.97	0.35
	S1	205	25	110	-27.23	-27.83	-0.6	0.7	0.86	0.54	-4.37	0.71	-4.1	0.44	-27.23	-17.33	-9.91	1.81	-8.49	0.33

2806 re 2807	Line	Power	Gain	Pulse	2806 Mean Sb	2807 Mean Sb	Mean Sb Diff	SD Sb Diff	Mean Obliq Sb	SD Obliq Sb	Mean DN Diff	SD DN Diff	Mean Obliq DN Diff	SD Obliq DN Diff	2806 Mean Sb	2807 Mean Sb	Mean Sb Diff	SD Sb Diff	Mean Obliq Sb	SD Obliq Sb
Site 1 (JD250) River 10m	E1	200	20	110	-31.57	-33.17	1.6	0.89	1.29	0.53	1.5	0.9	1.27	0.53	-31.57	-21.84	-9.73	1.28	-8.74	0.62
Slack: 0901	W1	200	20	110	-31.22	-32.18	0.98	0.69	1.02	0.78	0.88	0.7	0.91	0.75	-31.22	-20.75	-10.47	1.53	-9.09	0.79
Max Flood: 1243 (1.2 kt)	E2	200	20	110	-32.01	-32.35	0.33	0.73	0.05	0.52	0.34	0.75	0.04	0.52	-32.01	-20.91	-11.1	1.47	-10.18	0.3
	W2	200	20	110	-31.34	-32.95	1.6	0.66	1.69	0.5	1.5	0.69	1.57	0.45	-31.34	-21.51	-9.83	1.39	-8.52	0.56

Table 2: Summary table of the inter relative and relative absolute calibration for all realizations of the inter calibration.

These additional differencing methods might also be considered as options for use as $C_{tank}(\theta_s)$. The beam-to-beam differences between the mean S_b and mean DN are within several tenths of a dB of each other, and the standard deviation of differencing the mean DN are slightly lower. The oblique angle difference was computed for practical purposes. Considering that $C(\theta_s)$ captures and accounts for the largest single difference between systems and that single-value offsets are currently the only way to adjust data processed and handled by commercial processing software, a single value offset was computed and considered.

Intra Calibration Term, SL_{field}, G_{field}, pseudo PL_{field}

A complete *intra* calibration using the full range of system settings was repeated twice while the launches were moored alongside the NOAA small boat pier on JD242 and JD249 (Figure 16). On JD242 Launch 2805 and Launch 2807 were both moored port-side to the north face of the small boat pier in 7-8 m of water on an ebbing tide. On JD249 Launch 2805 and Launch 2807 were moored in the opposite orientation in similar conditions (starboard-side to the north face of the pier in 7-8 m of water on an ebbing tide) and Launch 2806 was moored port side-to on the south face of the pier in 4-5 m of water. The pier pilings are spaced approximately every 6 m on the north face with additional pilings several meters away from the pier as well, making it impossible to orient the launches such that pilings are not detected by the MBES. The gain setting step intervals were 3 dB on JD242 and 6 dB on JD249. The pulse length setting intervals were 10 μs JD242 and 20 μs JD249. The power setting intervals were always kept at 5 dB. The *intra* calibration was also conducted underway with Launch 2807 near Site 1 in the Yaquina River, and at Site 2 offshore (200 kHz only). The high-end setting values were not used at Site 1 and Site 2 because the systems saturate at high-end setting values in shallow water.

The setting SL_{field}, and G_{field}, and pseudo PL_field tables were created using all the sets of pivot settings used during the *inter* calibrations. Figure 25, Figure 26, and Figure 27 respectively show the 200-kHz *intra* calibration results. Figure 28, Figure 29, and Figure 30 respectively show the 400-kHz *intra* calibration results.

Figure 25: 200-kHz SL_{field} corrections for the systems on 2805 (top), 2806 (middle), and 2807 (bottom). LUTs are plotted on the left, and deviations from ideal are plotted on the right.

Figure 26: 200-kHz G_{field} corrections for the systems on 2805 (top), 2806 (middle), and 2807 (bottom). LUTs are plotted on the left, and deviations from ideal are plotted on the right.

Figure 27: 200-kHz pseudo PL_{field} corrections for the systems on 2805 (top), 2806 (middle), and 2807 (bottom).
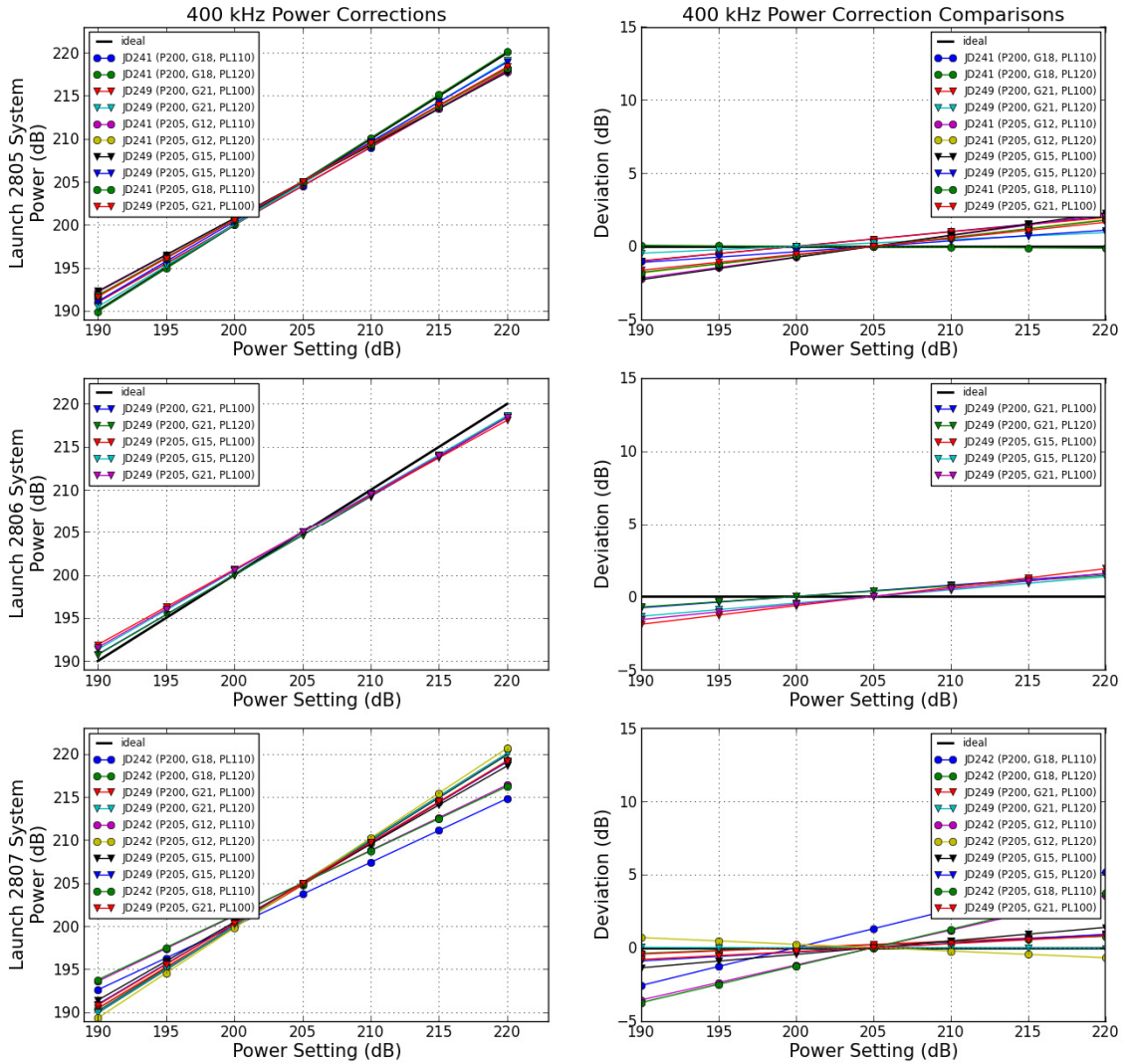
Figure 28: 400-kHz SL_{field} corrections for the systems on 2805 (top), 2806 (middle), and 2807 (bottom). LUTs are plotted on the left, and deviations from ideal are plotted on the right.
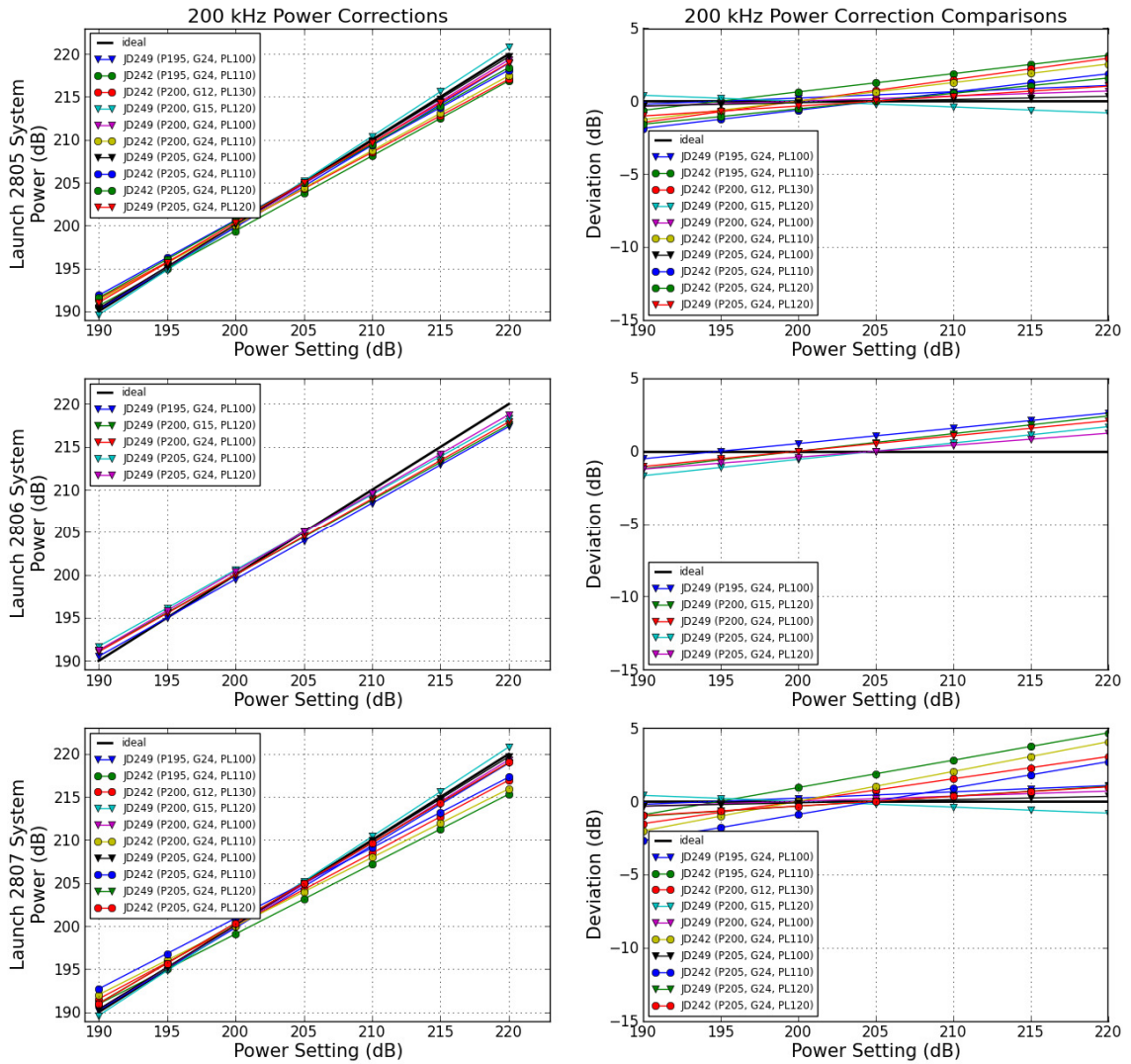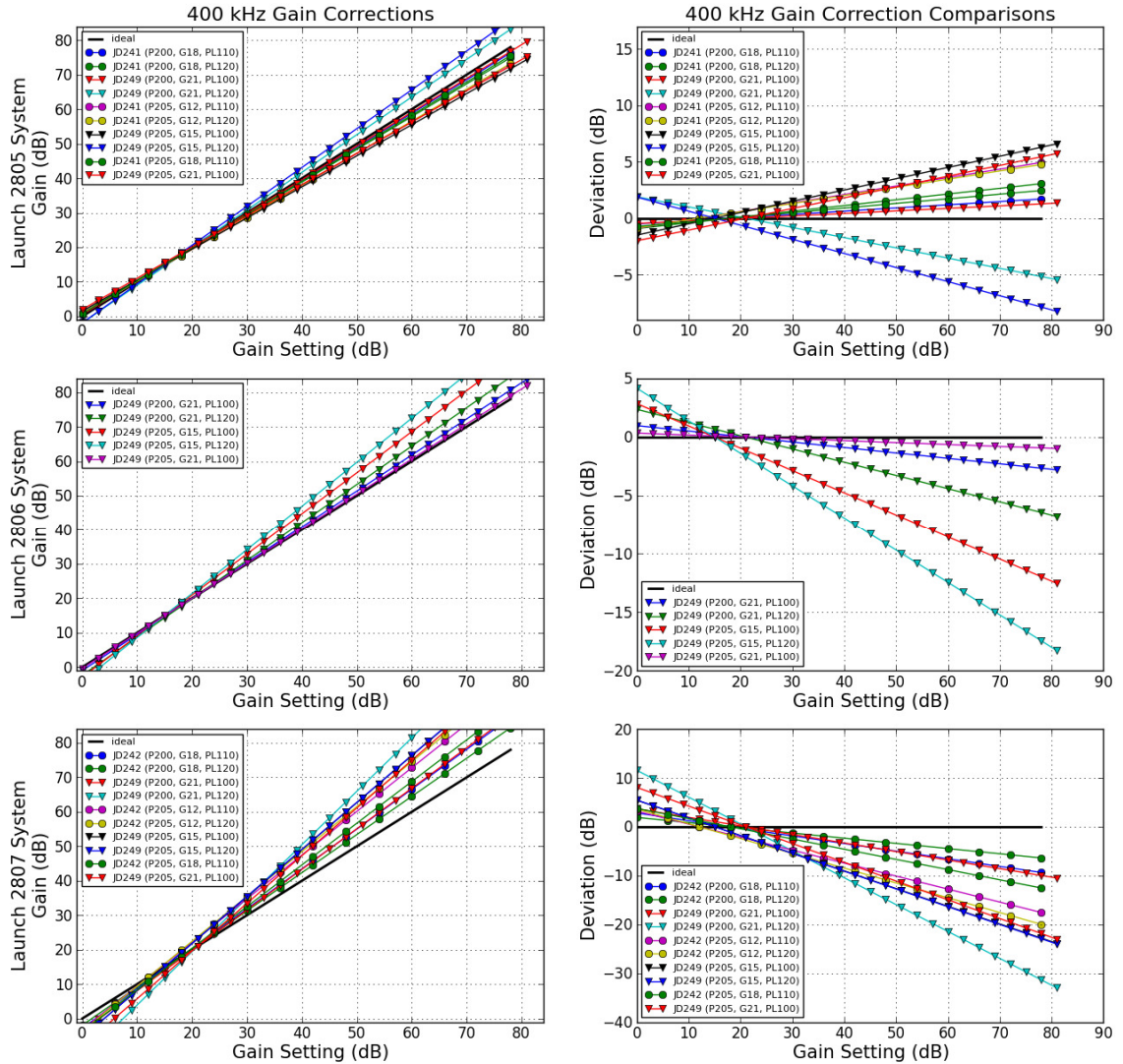
Figure 29: 400-kHz G_{field} corrections for the systems on 2805 (top), 2806 (middle), and 2807 (bottom). LUTs are plotted on the left, and deviation from ideal are plotted on the right.
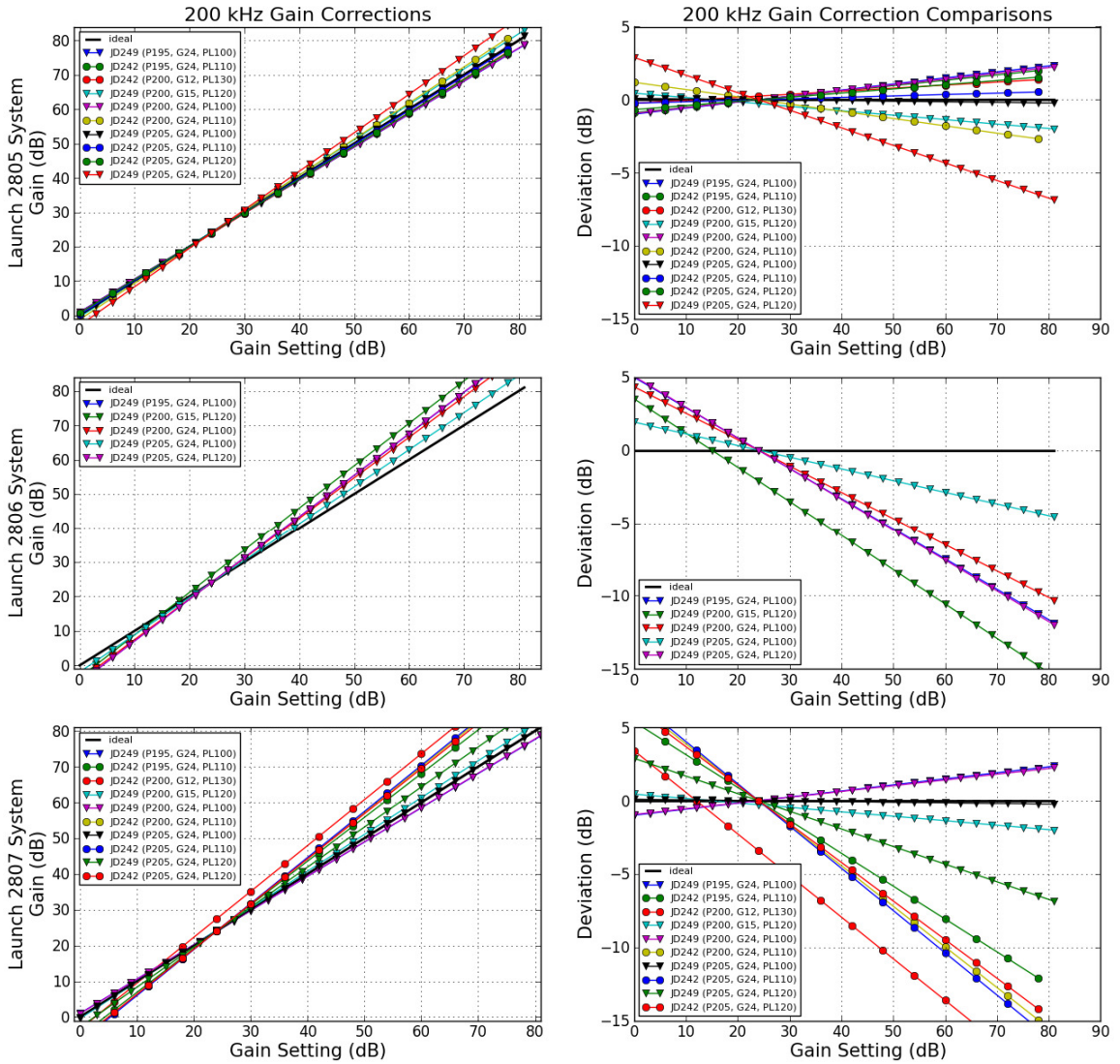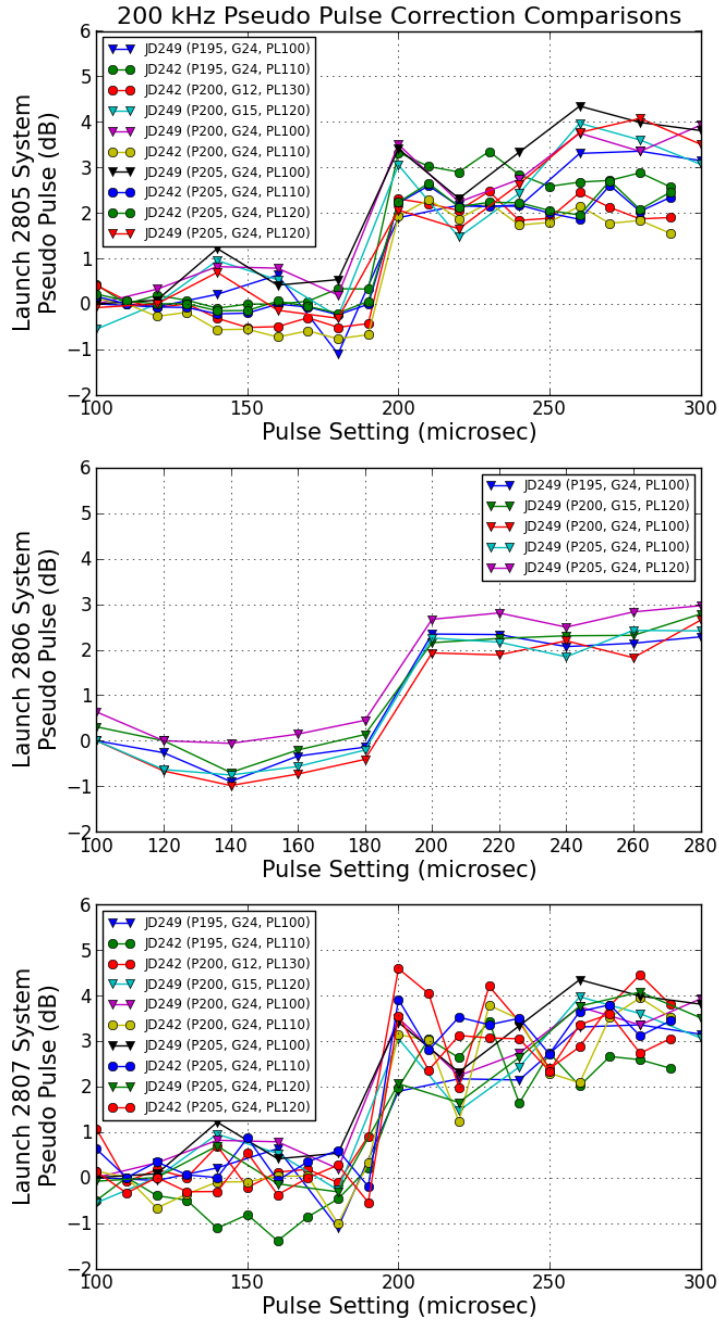
Figure 30: 400-kHz pseudo PL_{field} corrections for the systems on 2805 (top), 2806 (middle), and 2807 (bottom).

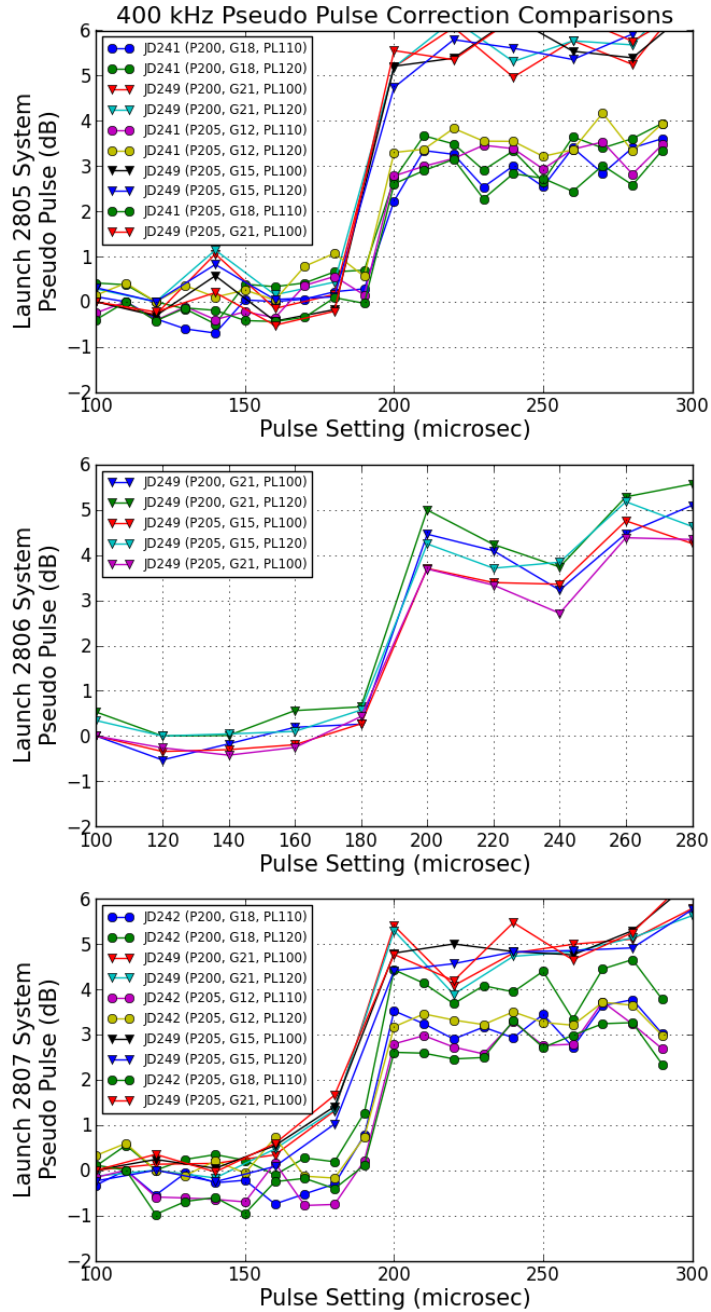All three systems respond similarly to all three settings. The slopes of the G_{field} calibrations are primarily above unity, and the slopes of the SL_{field} are slightly below unity. However, the G_{field} calibrations are much less consistent than SL_{field}, so much so

that it is questionable whether or not they are resolvable with any amount of fidelity in the field. Though the general trend of the slopes is similar, the corrections at the high and low-end settings can be many dB, particularly with gain.

The amplitude of the pulse drops at pulse length settings above 200 μs, resulting in pseudo PL_{field} corrections on the order of 3–5 dB for pulse length settings above 200 μs when the pivot setting is below 200 μs. If the pivot settings had been above 200 μs the corrections below 200 μs would have been negative corrections on the order of 3-5 dB. It was also observed that the pseudo corrections above 200 μs vary by 2 dB between JD242 and JD249.

The SL_{field} and G_{field} *intra* calibrations for the Launch 2807 system with the same or closest pivot settings that were used to conduct the tank calibration (power=210, gain=40, pulse length=130) are compared with one another in Figure 32.

Figure 31: Comparison of the SL_{field} intra calibrations with SL_{tank}, 200 kHz (top), 400 kHz (bottom). The setting correction (LUT) is plotted on the left and the deviation from ideal is plotted on the right.

The vertical discrepancy between SL_{field} and SL_{tank} for the Launch 2807 system is due to the absolute measurement of SL_{tank} with a calibrated hydrophone and the relative measurement of SL_{field} using only the system itself. As expected, the slopes of the SL_{field} calibrations are similar to SL_{tank} except for the 200-kHz calibration performed alongside the pier on JD242, which is slightly steeper for unknown reasons that warrant further investigation.
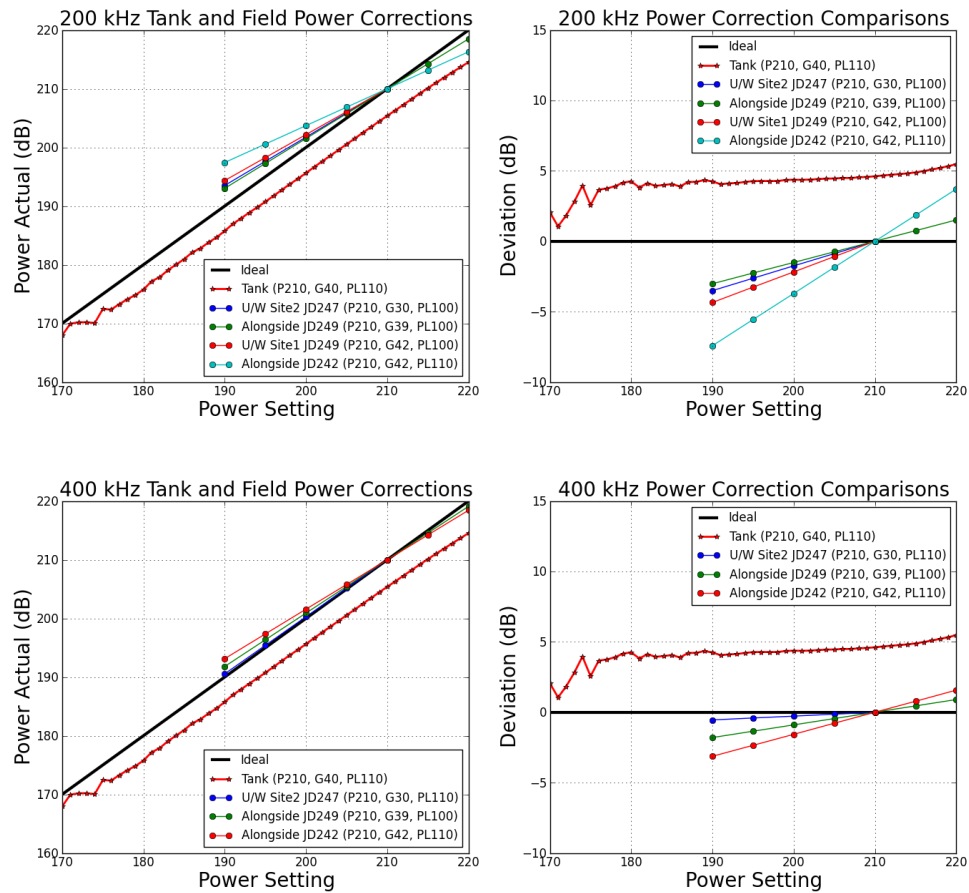
78
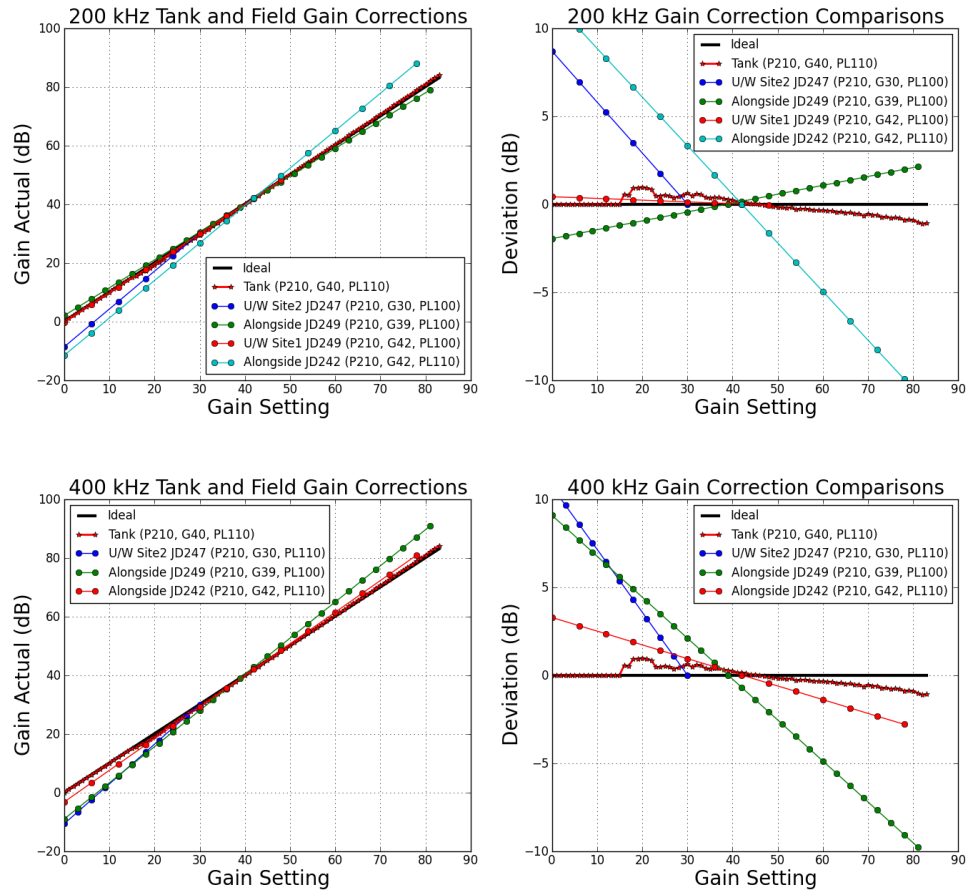
Figure 32: Comparison of the G_{field} intra calibrations with G_{tank}, 200 kHz (top), 400 kHz (bottom). The setting correction (LUT) is plotted on the left and the deviation from ideal is plotted on the right.

The slopes of the G_{field} calibration are less consistent than SL_{field} when compared to each other and to their tank counterparts. Contrary to the SL_{field} calibrations, the G_{field} that most closely agrees with G_{tank} is the 200-kHz calibration performed alongside the pier on JD242.

The factors observed to contribute to the variation between realizations of the *intra* calibration, primarily G_{field}, are the setting step interval (e.g. increasing the gain setting in steps of 6 dB), the pivot setting position within the full range of settings, and the algorithm used to identify and/or isolate the linear region of the setting response

79

curve. In general, reasonable *intra* calibration results are achieved when the linear region of the response is large; in other words, when saturation occurs at higher settings. This typically happens in deeper water, however, deeper water results in fewer samples at the lower range of settings. An improved balance between these two limitations is necessary. In some cases, the use of setting step intervals of 5-6 dB is considered too coarse in that the interval resolution limits the detection of the linear range of settings from which to extrapolate the LUT corrections. Furthermore, the algorithm used to identify the linear region of the system setting response assumes that the response is linear starting from the lowest settings, which is not necessarily appropriate as was observed in the tank (Lanzoni, 2012). This assumption leads to the undesirable result of producing unreasonable setting corrections whose slopes deviate substantially from unity. This is due to the least-squares approach favoring the response associated with lower setting values, particularly when the system saturates early, presumably due to the conditions in which the *intra* calibration was conducted (i.e. in shallow water or over particular seafloor types). This situation is confounded by coarse setting step intervals, which further limits the linear region over which to fit the correction line. Overall, the variation in the *intra* calibration results show that care and caution should be taken when deciding whether or not to pursue their use or whether to recalibrate in better conditions, such as deeper or shallower water or over a different seafloor type.

Application of Field Calibration Data to California Survey Data

The primary goal of this work is to develop a set of calibrations that can be used during processing that will result in consistent backscatter measurements for all systems for all operating settings. For this reason the $C_{field}(\theta_s)$, SL_{field}, and G_{field} tables were

applied to data selected from a traditional hydrographic survey conducted by *Fairweather* near Los Angeles, California, several weeks after the field calibration data were acquired. The pseudo PL corrections were not applied to the survey data because the pulse length settings used to acquire the data were less than 100 μs. (Pseudo PL corrections were not derived for settings below 100 μs because sonar response was shown to be non-linear below that value.) The 200-kHz field calibration sets could not be tested as 200-kHz data was not collected in California by the field calibrated launches.

Adjacent survey line files collected by Launch 2805 and Launch 2807 were selected from NOAA hydrographic survey H12620 for use in evaluating how well the *inter* and *intra* calibrations improve backscatter measurement consistency. Figure 33 shows the navigation lines from multiple launches where each field calibrated launch acquired survey data and the location of the two lines used in this case study.
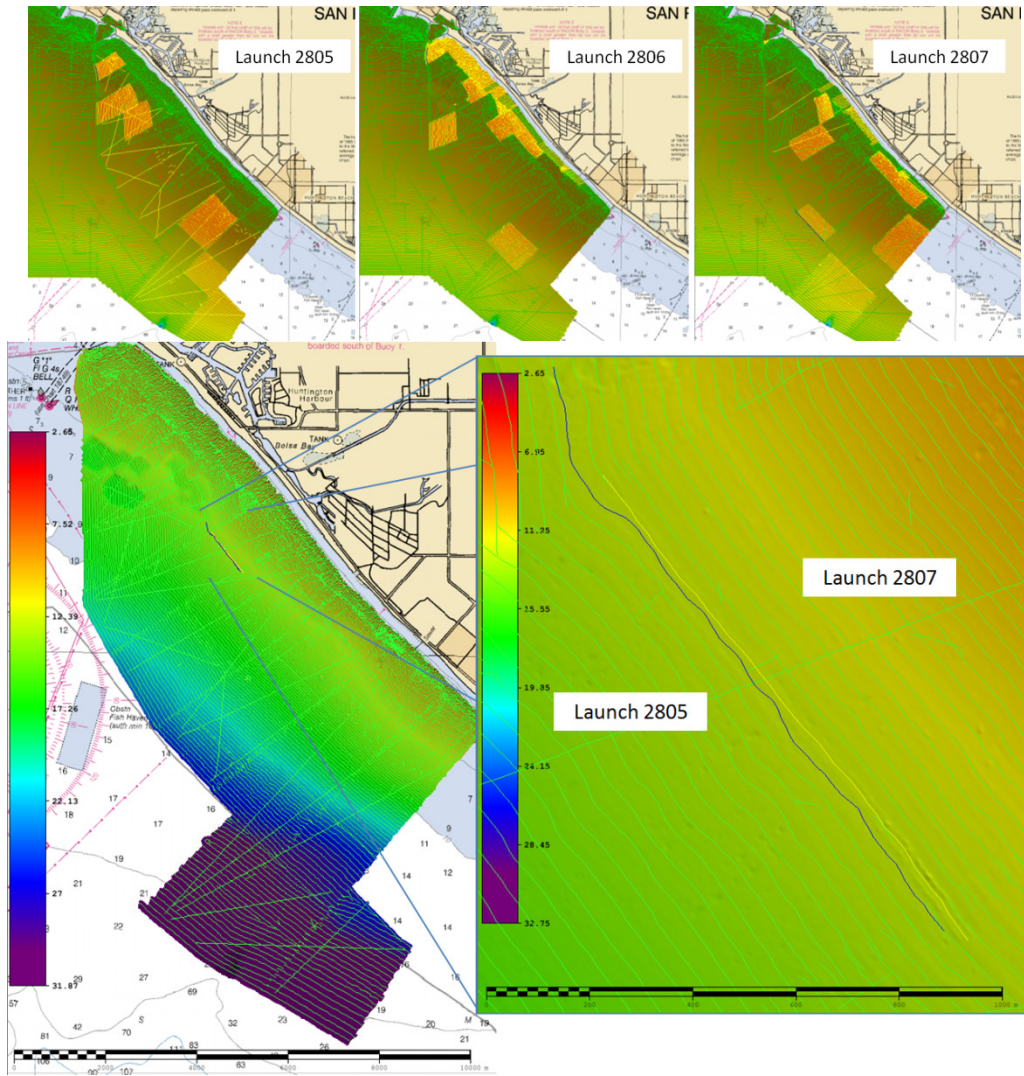
Figure 33: Hydrographic survey H12620 navigation lines segmented by launch.

Relative and Relative Absolute Calibrations Applied to Launch 2805 & Launch 2807

Figure 34 and Figure 35 depict two adjacent survey lines acquired by Launch 2805 system and Launch 2807 system as processed in FMGT (Figure 34) and with the processing method described in Chapter 3 (Figure 35). As observed in Newport, there is an approximate 4-5 dB difference between the two systems, which serves as an example of the initial problem this work seeks to address. The Launch 2805 system was

operated with a single set of settings throughout the duration of the line (power = 199, gain = 39, pulse = 50 µs), while the Launch 2807 system was operated using a variety of setting changes (power ranging from 205 to 220, gain ranging from 15 to 25, and a pulse length ranging from 50 to 80 µs). The nominal settings have been used for processing as described in Chapter 3.

Figure 34: Two adjacent lines run by Launch 2805 (mode: 30.5 dB) and Launch 2807 (mode: 35.7 dB) as processed and mosaiced in commercial software, FMGT (default color map, -70 to 10).

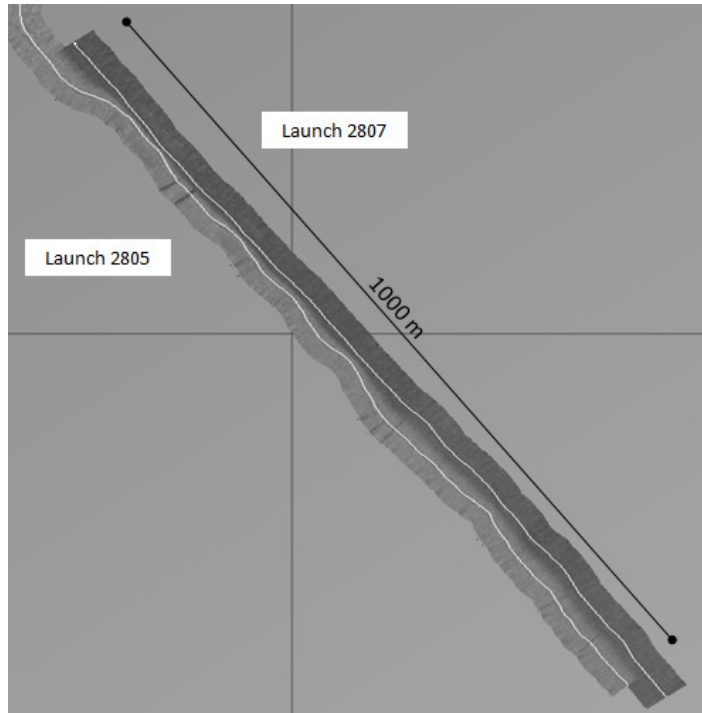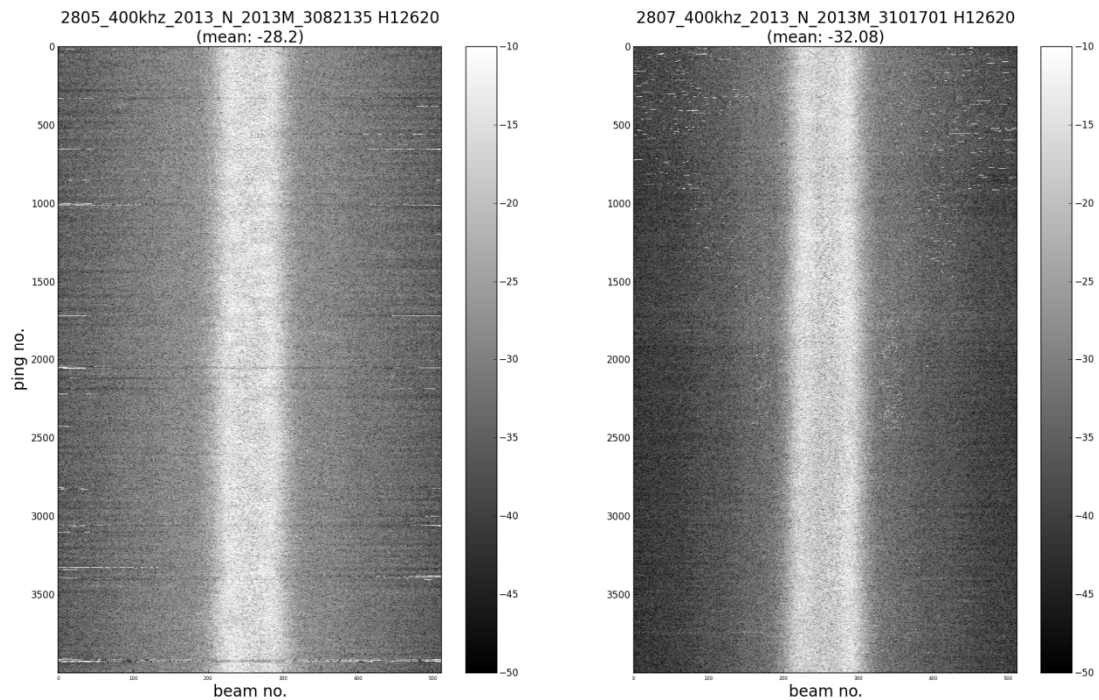***Figure 35: The same two lines shown in Figure 34 processed with research code without any field or tank calibrations applied to either file.***

The mode of the normalized histogram in FMGT of the data acquired by the launch 2805 system is -30.5 dB, and for the launch 2807 system it is -35.7 dB (a 5.2 dB difference). The mean of the beam means for the launch 2805 system data processed in the research code is -28.20 dB, and for the launch 2807 system it is -32.08 dB (a 3.9 dB difference). While it is not exactly known how FMGT processes backscatter data, the discrepancy between the data shown in Figure 35 (processed using research code) and data shown in Figure 34 (processed using FMGT) is suspected to come from normalizing the data to the mean between 30 and 60° as was done in the original Geocoder research tool (Fonseca and Calder, 2005). Through not exactly the same, Figure 34 and Figure 35 serve to corroborate the backscatter processing approach and establish a baseline from which to evaluate all the realizations of the relative and relative absolute field calibrations derived from the Newport case study data.

These two files were processed as a relative calibration and as a relative absolute calibration using all five *inter* calibrations for the launch 2805 system. The *intra* calibrations from JD249 for each unique *inter* calibration pivot setting set were used because they are more consistent with each other. Figure 36 shows the results of applying the five relative field calibrations. That is, the $C_{field}(\theta_s)$, SL_{field}, and G_{field} for the five unique pivot setting combinations were applied to the data file from the launch 2805 system, while no acoustic calibration data were applied to the launch 2807 system data besides the nominal setting values.

Figure 36: Launch 2805 and Launch 2807 system data processed without any calibration corrections, and Launch 2805 system data processed with five relative field calibration sets and without any calibrations: beam averages (top), mosaics (bottom).

The blue and green beam means for the systems on both launches do not have any calibrations applied (i.e. the initial case of doing nothing). The remaining colors show the result of applying the five realizations of the *inter* and *intra* field calibration sets acquired in Newport, OR. Though the field calibrations bring the Launch 2805 system

data closer to the Launch 2807 system data, variation between calibrations is on the order of 1-2 dB, likely due to the variability between their associated *intra* calibrations.

Figure 37 shows the results of applying the five relative absolute *inter* calibrations with their associated *intra* calibrations.   In this case $C_{tank}(\theta_s)$, SL_{tank}, and G_{tank} $\psi_{\text{tx-tank}}$, $\psi_{\text{rx-tank}}$ have been applied to the Launch 2807 system data file, and $C_{field}(\theta_s)$, SL_{field}, and G_{field} have been applied to the Launch 2805 system data file.
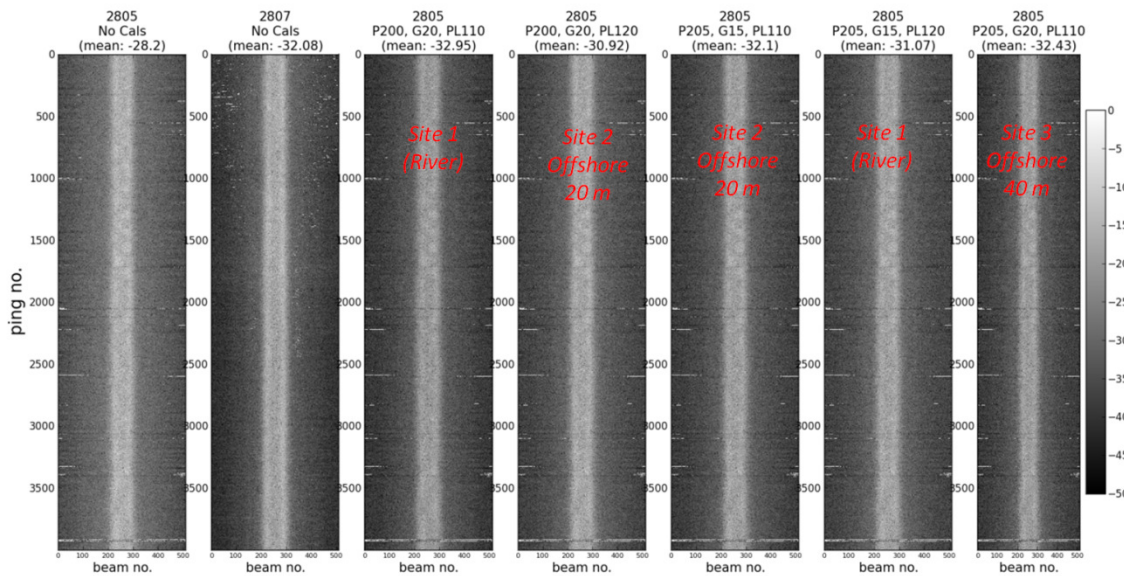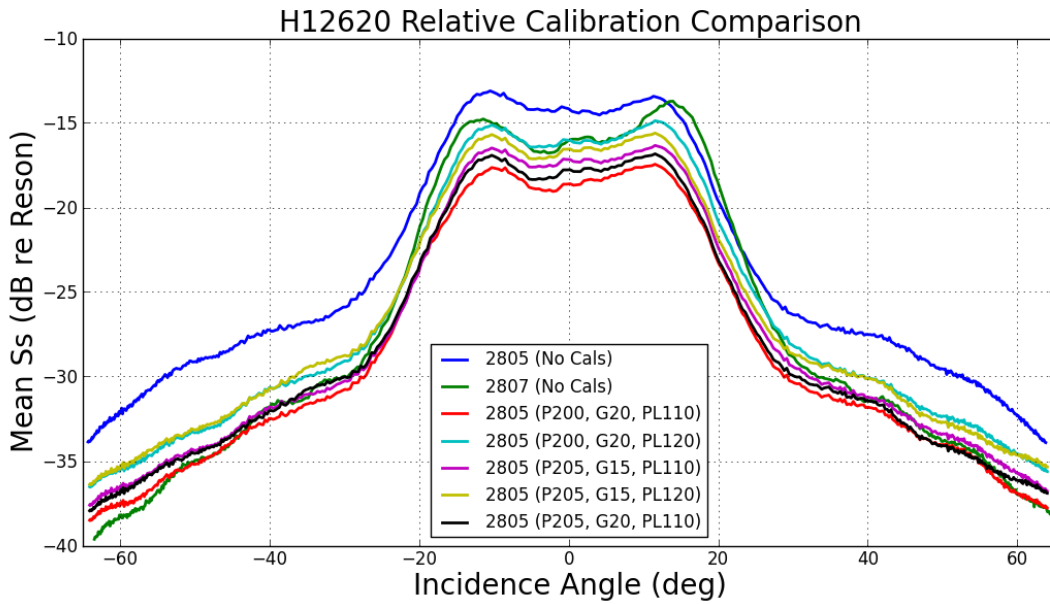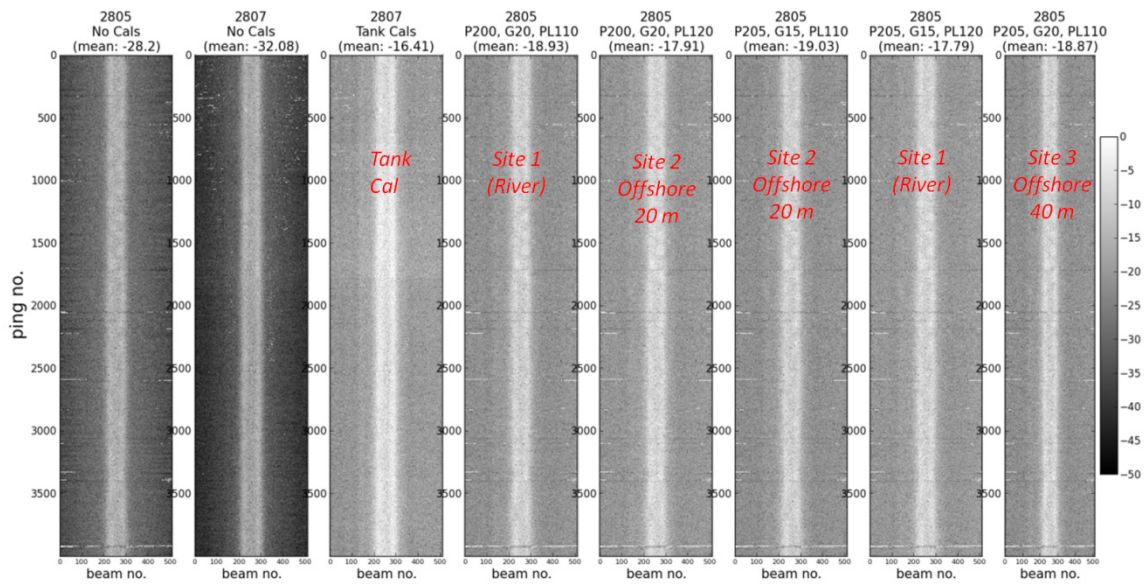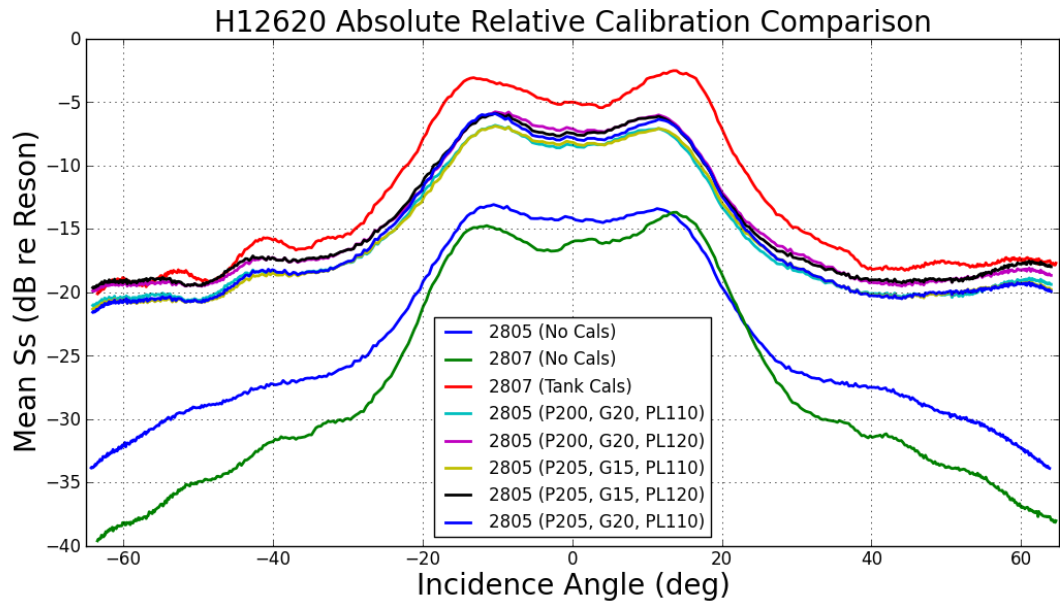
Figure 37: Launch 2805 and Launch 2807 system data processed without any calibration corrections, and Launch 2805 system data processed with five relative absolute field calibration sets and without any calibrations: beam averages (top), mosaics (bottom).

The blue and green beam means show the same initial case of applying no calibrations as was also shown in Figure 36. What is different is that the inclusion of the absolute tank calibration into the relative field calibration has shifted the data from both systems to an estimated absolute level. Again, the 5-7 dB initial difference between

88

systems is reduced to a dB or so by all realizations of the field calibration, but these all are now referenced to an estimated absolute level. Referencing all systems to an estimated absolute level is desirable because the reference level can be achieved with any calibrated MBES, thereby eliminating the need to retain a single arbitrary reference MBES against which all systems are relatively calibrated.

Discussion and Evaluation of Method and Findings

Though the *inter* and *intra* calibrations are meant to be used as a set, they can be evaluated for their individual contribution to the reduction of measurement inconsistency. There are also possible circumstances that might justify their individual use that are discussed here.

Inter Calibration: $C_{field}(\theta_s)$

The primary value of conducting a *inter* calibration is that it is a gauge of the largest component of the difference in the beam-to-beam central tendency between systems. The application of $C_{field}(\theta_s)$, with its associated SL_{field}, and G_{field} to hydrographic survey field data from California provides evidence that a beam-to-beam full swath difference can reduce backscatter measurement inconsistency to within a dB or so (Figure 36 and Figure 37). This implies that if systems are initially inconsistent by more than 1 to 2 dB, then this correction is worthwhile. If systems are initially inconsistent by less than 1-2 dB, such as was the case with the relative difference between the 200-kHz systems on Launch 2805 and Launch 2808 in 2012 (Figure 19), then there is little added benefit of applying the *inter* calibration results. The *intra* calibration may still be necessary if the slopes of the system responses about the same pivot settings are significantly different. It is inherently implied that if data from systems with different *intra* calibration slopes are acquired using the full range of settings (and

89

are not corrected), then the combined backscatter data will be inconsistent. Careful

attention should be paid to which calibrations are being applied and with what they are

paired with to avoid introducing beam pattern artifacts or incorrectly applying corrections

to the various system parameters.

The general across-swath beam pattern between systems appears consistent

between sites. However, the pattern appears less consistent near nadir and in the outer

beams. Further smoothing and/or exclusive use of select regions of greater stability

within the swath should also be considered.

Relative Calibration versus Relative Absolute Calibration

The primary value of referencing all systems to the tank calibrated system is that

in addition to theoretically resulting in more consistent measurements between systems,

all measurements are closer to absolute backscatter estimates. Considering that

$C_{default}$ is approximately off by 6 dB for 200 kHz and 9 dB for 400 kHz this is a

significant enhancement. Although acoustic seafloor backscattering models developed

by Mourad and Jackson have not been developed for 200- and 400-kHz frequencies yet,

Figure 38 shows that using the tank calibrations results in backscatter estimates that are

much closer to those predicted by the 100-kHz models presented in the University of

Washington Applied Physics Lab's Ocean Environmental Acoustic Models Handbook

(APL-UW, 1994), based on (Mourad and Jackson, 1989).

200 kHz 2807 Field Data from Site 3 Compared to 100 kHz Jackson Model for Medium and Course Grain Sand
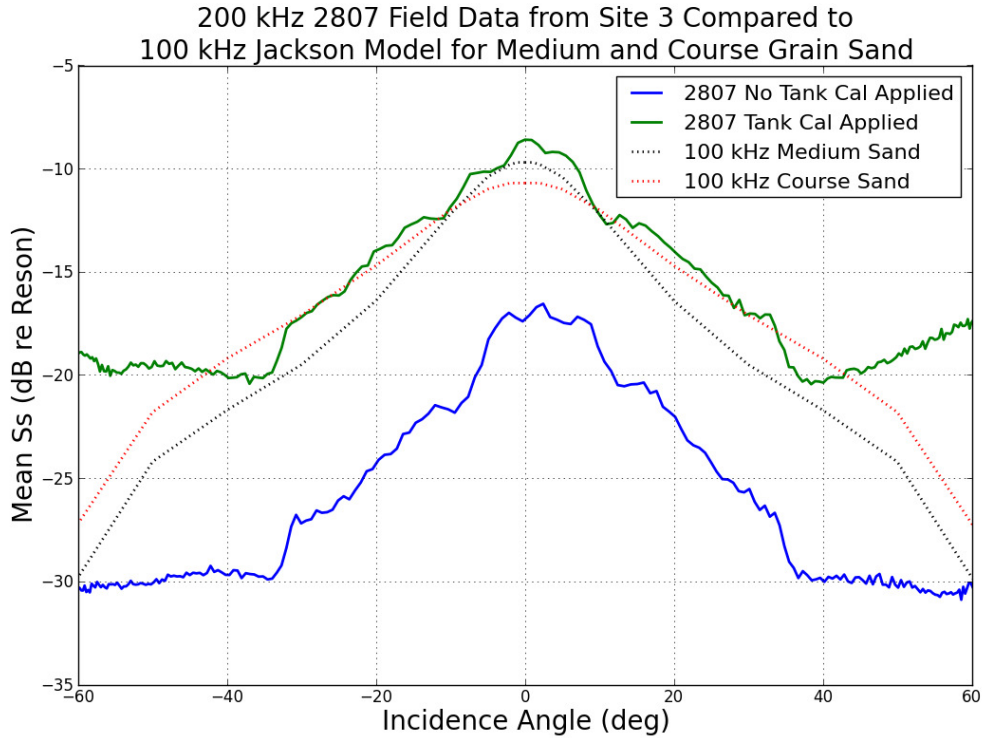
Figure 38: Beam averages from tank calibrated system, Launch 2807, at Site 3 with and without tank calibrations applied compared to 100 kHz Jackson models for medium and course sand.

However, applying tank calibration corrections have the potential to introduce beam pattern artifacts from $C_{tank}(\theta_s)$, $\psi_{\text{tx-tank}}$, and $\psi_{\text{rx-tank}}$, and systematic biases from applying SL_{tank} and G_{tank} to the reference system itself and all other systems referenced to it if the original tank calibration is inaccurate. A possible compromise between these two methods might be to change $C_{default}$ to a single representative value of the tank calibration such as the mean over a stable range of incidence angles, and pursue relative calibrations, thereby eliminating the introduction of beam pattern artifacts. Another option to consider is a single value calibration for all steering angles. The field calibration as proposed works well for oblique angles, but not as well for near nadir beams or extreme outer beams as indicated by the lower standard deviations for the oblique angle differences reported in Table 2. Certainly further investigation of how

91

accurate and stable each term is for both the tank and field calibrations and at which range of angles is warranted.

Intra Calibration: SL_{field} and G_{field}

The results of the *intra* calibration show that the slopes of the system responses to gain and power setting changes are not unity (as was observed in the tank as well) and therefore must be considered to achieve consistent backscatter measurements for all setting combinations. However, the variation between the *intra* calibrations is so wide, particularly for the gain settings, that perhaps the *intra* setting responses are not resolvable in the field. Further investigation into the cause of the variation between calibrations is necessary, particularly into the raw water column amplitude records and how the data are being treated by the processing algorithm described in Chapter 3, which itself may very well be introducing these inconsistent results. The filtering mechanism should be checked to ensure bottom detections were achieved for all beams and the linearity of the system response at very low gains should be inspected. The algorithm works backward from the highest setting down, and never discards gain settings below the pivot setting. Additional work is necessary to more carefully define the linear region of the system response about the pivot setting.

Considering the slopes of the SL_{field} and G_{field} calibrations relative to each other provides an indication of how much each correction will contribute to backscatter measurement consistency. For slopes other than unity, the magnitude of the backscatter measurement inconsistencies grow as settings further away from the pivot settings are used to operate the MBES. If the slopes of SL_{field} and G_{field} are unity, then their use does not contribute to consistent backscatter measurements since the correction line always passes through the pivot setting. Furthermore, if the slopes of the

92

SL_{field} and G_{field} for both the field calibrated system and reference system are the same, then the backscatter measurements for both systems will remain consistent for any settings used during MBES operation. The further the slopes of the SL_{field} and G_{field} LUTs are away from unity and the further the setting is away from the pivot setting, the greater the importance of correcting for them. Significant deviations from unity are cause for further investigation into the results of the test, and call into question the processing method, the conditions in which the test was conducted, and/or the general performance of the MBES.

The adjustment period after setting changes has not been addressed by this work. Though a slight rise in the raw data record for several pings after setting changes was observed in some of the raw *intra* calibration data, artifacts associated with sporadic setting change events are not easily perceptible in mosaics views. This indicates that they are not major, long-term contributors to backscatter measurement inconsistency.

Pulse Length Calibration, pseudo PL_{field}

The MBES system responses to pulse length setting changes that were reported by Lanzoni (2012) and also observed in the *intra* calibration field data are unusual in that higher amplitudes at pulse lengths below 200 μs are observed. The implication is that when systems are operated with pulse length settings both above and below 200 μs, regardless of how the amplitude records are sampled, inconsistent backscatter measurements on the order of 2-5 dB are expected as has been observed (Figure 27 and Figure 30). For this reason the pseudo PL correction has been proposed.

Looking more closely at the amplitude records from both the tank and field data around the target detections using different pulse length settings suggests the relationship between pulse length and amplitude might be related to the data sampling

rate. Figure 39 shows the nadir beam pulses recorded in the test tank at UNH, and in the field mounted on Launch 2807 alongside the pier using the same power and gain settings with different pulse length settings. The pulses from the tank data were generated by the calibration hydrophone (TC 4034) at a range of 12 m, and received and recorded by the tank-calibrated MBES. The pulses from the field data were transmitted and received by the same MBES mounted on Launch 2807 while alongside the NOAA pier in Newport, Oregon (15 amplitude samples centered about the seafloor detection were recorded). Higher amplitudes with shorter pulse lengths are observed in both cases. While each record of every beam and ping is unique, this plot shows the general tendency of the system response to different pulse length settings that were observed both in the tank and in the field for all systems and frequencies. The opposite effect (lower amplitude with shorter pulse lengths) was observed by a Reson 8125 (Parnum and Gavrilov, 2012).
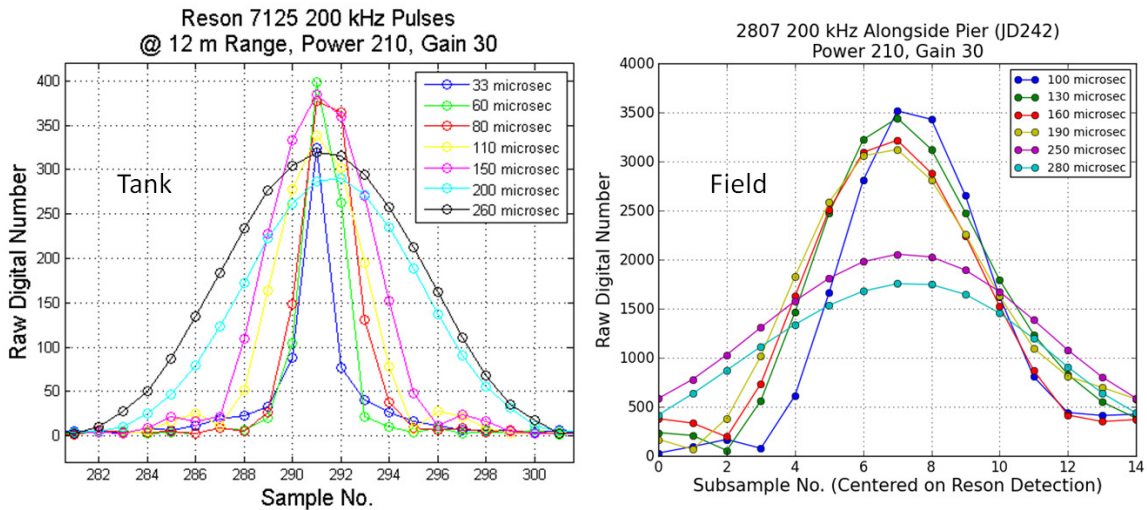

Figure 39: Recorded pulses of the nadir beam of the tank calibrated MBES in the tank (left) and in the field on Launch 2807 (right) using different pulse length settings.

The digital recording interval of the Reson 7125 is 29 μs. This implies that pulses generated with the lowest pulse length setting of 33 μs will be represented by one

to two samples, which is consistent with what is observed in the recorded data from the tank calibrations. The causes or reasons for higher amplitudes with shorter pulse lengths have not been further investigated or understood. This work goes only so far as to show the system response to different pulse length settings, and to propose a way to account for it in the backscatter reduction process in the form of a pseudo PL correction.

Stability

The question of how frequently the field calibrations should be repeated has not been well addressed. Ideally it is a question about the stability of the acoustic properties of each MBES-vessel pairing. This is expected to be directly related to the physical condition of the ceramic elements and the electronic components of the MBES, as well as any digital compensation for their variability due to environmental changes or material degradation over time; and the physical condition of the vessel. However, some of these changes may affect MBES-vessel pairings in a similar way such that the relative operational differences between systems are imperceptible using a relative calibration. For example, if the relative calibration measurements are performed in water temperatures of 20°C and are then the systems are operated in water temperatures of 10°C, the changes to the operational characteristics of the MBES are expected to change in the same way, so any measured differences will be roughly the same and imperceptible by this method. An absolute calibration is the only way to detect such changes, but is not considered important if the only goal is to achieve consistent measurements between systems operating in the same general location and time frame.

Changes to major hardware components such a receivers, projectors, and/or cables; changes to firmware, particularly those that might alter sampling, filtering, shading, beam-forming, or pulse shape; as well as major changes to the vessel that

might affect the acoustic properties of the platform such as alteration of the hull, propeller, generator, or engine, all might be cause for recalibration. The Reson normalization routine has been visually observed in real time to result in before and after changes in the raw digital number displays. (A comparison of an available collection of several normalization files is presented in Appendix B.) Additionally, degradation of hardware components may not happen in the same way over time to all systems, but has not been well studied with modern MBES components. The receiving response of Reson Seabat systems was estimated to change 0.5 dB/year (Pocwiardowski et al., 2006). Acoustic calibration of fisheries sonar using the on-axis standard sphere calibration method are typically performed before and after each survey, resulting in deviation in the backscatter measurements on the order of 2-6% (De Robertis et al., 2010). Experience with fisheries sonar systems have shown larger variation over time on the order of 0.3 to 0.6 dB, with larger variation shortly after production followed by more stability (De Robertis). This topic certainly requires further investigation. Until it is resolved, the full calibration should be repeated when the field calibrations no longer result in consistent backscatter measurements between systems (assuming the data from each system are processed nearly in real-time or at least daily).

CHAPTER 5

Conclusions

Four unique MBES-vessel pairings were observed to produce backscatter measurements with inconsistencies as low as a few tenths of a dB and as much as 5-7.5 dB in a fairly controlled field environment. A field calibration method was developed to produce *inter* and *intra* corrections relative to a single set of operational settings (power, gain, and pulse length) and to a single reference system that itself can either be used to produce absolute backscatter estimates by applying its tank calibration corrections to the data it records, or its own uncorrected backscatter estimates. The method was tested in a challenging location with reasonable results. The *inter* and *intra* corrections can be used as a full set (or as a subset if some calibrations are deemed unnecessary) for any setting combination to reduce inconsistencies to within a dB or so. This procedure informs when applying $C, SL, G,$ and pseudo PL corrections is worthwhile. This study has also explored alternate approaches for deriving and applying C.

As a true PL correction was explored during the development of the procedure, an unusual observation was made about how the Reson 7125 SV1 systems respond to changes in pulse length setting. This finding suggests that consistent backscatter measurements will not be achieved when multiple systems are operated using pulse length settings on either side of 200 µs unless a pseudo PL correction is used.

Also during development, the observation was made that as long as the physical components of the calibration environment can be controlled or shown to be sufficiently similar (i.e. effectively the same) for both vessels during the course of acquiring the calibration data, then the difference between the raw digital numbers can be used to derive $C_{field}(\theta_s)$ instead of going through the full backscatter reduction process. That is to say, it must be shown that the water column temperature, salinity, sound speed, acoustic interference and attenuation, and the sea surface conditions and vessel sea-keeping was nominally the same for both systems while the calibration was conducted. If this cannot be shown, then careful correction for these dynamics must be undertaken, otherwise they will be included in the calibration results as biases. In the future, inclusion of the 3D grazing angle corrections could improve the *inter* calibration such that aiming for ideal or similar conditions could be eliminated.

Finally, the development and implementation of tools in commercial software are necessary to 1) handle the application and meta data associated with both tank and field calibration corrections; 2) check that all the underlying assumptions to use DN differences are met and/or to make careful corrections for S_b beam-to-beam or incidence-angle-to-incidence-angle differences to create $C_{field}(\theta_s)$ for a set of pivot settings; and 3) create corrections for MBES responses at other operational settings. Comparative checks should include the before and after CTDs, the noise in the water column, the vessel attitude spectral densities, the beam to beam distributions, beam noise floors, and across-swath beam pattern shape for both systems. If any of these are not sufficiently similar, then corrections must be made to account for them. Most important is the ability for users to apply radiometric calibration corrections in commercial software in any appropriate way they choose, specifically $C(\theta_s)$, SL(power

setting), G(gain setting), $\psi_{tx}(\theta_s)$, $\psi_{rx}(\theta_s)$, τ(pulse length setting), or pseudo corrections such as that proposed for pulse length settings or possibly for beam pattern or MBES reference frame misalignment. Meta data to track the reference system and its level of calibration, the pivot settings or any other operational attribute combined in the field calibration output, and any other parameterized setting corrections is also necessary.

The calibration site and environmental conditions needed to conduct this method are primarily limited by the inability to measure and correct for the dynamics encountered in the field. However, the processing routine can and should be improved where possible to reduce the limiting factors on the calibration site and environmental conditions. First, accounting for the 3D slope of the seafloor and vessel pitch should improve the insonified area calculation, thereby improving the *inter* calibration. This would also allow the use of target seafloors with somewhat more complicated geometries, as well as MBES-vessel-systems with different hull designs and sensor mounting configurations.

This effort has also yet to identify a depth in which to achieve a complete *intra* calibration for the full range of setting combinations (or resolved whether or not such a depth exists), which is a severely limiting factor for achieving reasonable power and gain corrections, particularly gain. This work also does not address the immediate effects of changing settings, nor has it explored the uncertainty and stability of each calibration.

A second Reson 7125 SV1 has been calibrated in the UNH test tank, the results of which should be compared with the first system used in this work when they become available to gauge the consistency of the systems in a stable environment. Commercial and research Geocoder tools should consider changing the $C_{default}$ value they use for Reson 7125 SV1 system to values closer to the tank measurements for each frequency (e.g. ~-106 for 200-kHz projectors and ~109 for 400-kHz), particularly if the second tank

calibration results are similar to those of the first. This would result in commercially processed backscatter from uncalibrated systems resulting in measurements closer to absolute levels.

Further investigation into the cause of system inconsistency is also suggested, particularly through element level data comparisons both from the tank and field. The effect of Reson normalizations on backscatter consistency have not been well understood or quantified. Referencing the normalization values to a fixed reference for all systems would likely eliminate this concern. Finally, performing tank calibrations in such a way as to make it possible to resolve the beam pattern reference frames with the MBES reference frame is also a potential source of improvement in the realm of radiometric calibration corrections. These shortcomings are perceived to account for some portion of the remaining roughly one dB of inconsistency between systems that this method does not capture.

Though the tools to easily accomplish and utilize relative and/or absolute field calibrations of MBES do not currently exist in commercially available software, the NOAA mapping fleet can and should continue to pursue absolute calibration of backscatter data. The NOAA fleet can advocate to address some of the issues identified by this work such as the limitations imposed on the *intra* calibration by the limited dynamic range of the systems. The NOAA fleet could also acquire and maintain an absolutely calibrated system(s) on each coast of the United States and address the logistics, training, and coordination associated with operating all systems at the same time to measure the same section of seafloor from which to develop relative absolute calibrations. With improved intelligence regarding acoustic calibration and backscatter data acquisition, NOAA may have to adapt meta-data tracking standards for calibrated backscatter; and finally, could encourage commercial development of automated tools to

achieve absolute estimates of seafloor backscatter from MBES. In the long term, the seafloor characteristics that backscatter can help identify that relate to the stability and dynamics of the seafloor might also be used to inform resurvey and remapping efforts.

Overall this work quantified the problem of backscatter measurement inconsistency between four Reson 7125 SV1s, and developed a balanced alternative to absolute tank calibration for all MBES or simple relative calibrations. The method is an efficient compromise in terms of equipment, time, and expertise to relatively calibrate any number of systems to a single tank calibrated system. Although additional refinements are necessary, this work lays a foundation for achieving consistent backscatter measurements from many systems. As MBES data acquisition and processing techniques improve and the large-scale use of quality backscatter data increases, seamless backscatter products from multiple systems will remove the barriers to large-scale automated seafloor characterization.

LIST OF REFERENCES

AMIRI-SIMKOOEI, A., SNELLEN, M. & SIMONS, D. G. 2009. Riverbed sediment classification using multi-beam echo-sounder backscatter data. *The Journal of the Acoustical Society of America,* 126**,** 1724-1738.

APL-UW 1994. High-Frequency Ocean Environmental Acoustic Models Handbook. Seattle: University of Washington.

BROWN, C. J. & BLONDEL, P. 2009. Developments in the application of multibeam sonar backscatter for seafloor habitat mapping. *Applied Acoustics,* 70**,** 1242-1247.

BURDIC, W. S. 1984. *Underwater acoustic system analysis*, Prentice-HallEnglewood Cliffs, NJ.

CARIS 2012. HIPS and SIPS 7.0 User's Guide. Fredericton, NB, Canada.

CHEN, C. T. & MILLERO, F. J. 1977. Speed of sound in seawater at high pressures. *The Journal of the Acoustical Society of America,* 62**,** 1129-1135.

DARTNELL, P. & GARDNER, J. V. 2004. Predicting seafloor facies from multibeam bathymetry and backscatter data. *Photogrammetric engineering and remote sensing,* 70**,** 1081-1091.

DE MOUSTIER, C. & MATSUMOTO, H. 1993. Seafloor acoustic remote sensing with multibeam echo-sounders and bathymetric sidescan sonar systems. *Marine Geophysical Researches,* 15**,** 27-42.

DE ROBERTIS, A. Dec 18, 2013. *RE: Echosounder sphere calibration frequency.* Personal communication.

DE ROBERTIS, A., WILSON, C. D., WILLIAMSON, N. J., GUTTORMSEN, M. A. & STIENESSEN, S. 2010. Silent ships sometimes do encounter more fish. 1. Vessel comparisons during winter pollock surveys. *ICES Journal of Marine Science: Journal du Conseil,* 67**,** 985-995.

ETTER, P. C. 2013. *Underwater acoustic modeling and simulation*, CRC Press.

FONSECA, L. & CALDER, B. 2005. Geocoder: an efficient backscatter map constructor. *In:* Proceedings of the US Hydrographic Conference, 2005.

FONSECA, L. & MAYER, L. 2007. Remote estimation of surficial seafloor properties through the application Angular Range Analysis to multibeam sonar data. *Marine Geophysical Researches,* 28**,** 119-126.

FOOTE, K. G. 1982. Optimizing copper spheres for precision calibration of hydroacoustic equipment. *The Journal of the Acoustical Society of America,* 71**,** 742-747.

FOOTE, K. G. 1983. Maintaining precision calibrations with optimal copper spheres. *The Journal of the Acoustical Society of America,* 73**,** 1054-1063.

FOOTE, K. G., CHU, D., HAMMAR, T. R., BALDWIN, K. C., MAYER, L. A., HUFNAGLE, L. C. & JECH, J. M. 2005. Protocols for calibrating multibeam sonar. *The Journal of the Acoustical Society of America,* 117**,** 2013-2027.

FOOTE, K. G. & MACLENNAN, D. N. 1984. Comparison of copper and tungsten carbide calibration spheres. *The Journal of the Acoustical Society of America,* 75**,** 612-616.

FRANCOIS, R. & GARRISON, G. 1982. Sound absorption based on ocean measurements: Part I: Pure water and magnesium sulfate contributions. *The Journal of the Acoustical Society of America,* 72**,** 896-907.

GOFF, J. A., WHEATCROFT, R. A., LEE, H., DRAKE, D. E., SWIFT, D. J. P. & FAN, S. 2002. Spatial variability of shelf sediments in the STRATAFORM natural laboratory, Northern California. *Continental Shelf Research,* 22**,** 1199-1223.

GREENAWAY, S. 2010. *Linearity Tests of a Multibeam Echosounder* Master of Science, University of New Hampshire.

GREENAWAY, S., RICE, G. 2013. A Single Vessel Approach to Inter-Vessel Normalization of Seafloor Backscatter Data. *US Hydrographic Conference 2013.* New Orleans, L.A. .

HAMMERSTAD, E. 2000. EM Technical Note Backscattering and Seabed Image Reflectivity

HEAP, A. D., NICHOL, S. L. & BROOKE, B. P. 2014. Seabed mapping to support geological storage of carbon dioxide in offshore Australia. *Continental Shelf Research.*

HEATON, J. L., WEBER, T. C., RICE, G. & LURTON, X. 2013. Testing of an extended target for use in high frequency sonar calibration. *Proceedings of Meetings on Acoustics,* 19**,** -.

HSIAO, C., JAIN, A. & CHAHINE, G. 2006. Effect of gas diffusion on bubble entrainment and dynamics around a propeller. *In:* 26th Symposium on Naval Hydrodynamics. Rome, Italy, 2006.

HUGHES CLARKE, J., MAYER, L. & WELLS, D. 1996. Shallow-water imaging multibeam sonars: A new tool for investigating seafloor processes in the coastal zone and on the continental shelf. *Marine Geophysical Researches,* 18**,** 607-629.

KINNEY, J. W. F., ROGER D. 2006. Seabed Morphology off Southern Long Island: Studies of Artificial Reefs and Implications for Wind Farms. *Program for the Thirteenth Conference on Geology of Long Island and Metropolitan New York.*

KULM, L. D. 1965. *Sediments of Yaquina Bay, Oregon.* DOCTOR OF PHILOSOPHY, Oregon State University.

LANZONI, C. 2012. Reson Seabat 7125 Multibeam Sonar System Calibration Durham: University of New Hampshire.

LANZONI, J. C. & WEBER, T. C. 2011. A method for field calibration of a multibeam echo sounder. *In:* OCEANS 2011, 2011. 1-7.

LE ROUX, J. P. 2005. Grains in motion: A review. *Sedimentary Geology,* 178**,** 285-313.

LURTON, X. 2010. *An introduction to underwater acoustics: principles and applications*, Springer.

LURTON, X., DUGELAY, S. & AUGUSTIN, J. M. 1994. Analysis of multibeam echo-sounder signals from the deep seafloor. *In:* OCEANS '94. 'Oceans Engineering for Today's Technology and Tomorrow's Preservation.' Proceedings, 13-16 Sep 1994 1994. III/213-III/218 vol.3.

MAILLARD, E. 2010. SeaBat 7k series beamforming, beamspacing and imagery. Goleta: The RESON Group.

MASETTI, G. & CALDER, B. 2012. Remote identification of a shipwreck site from MBES backscatter. *Journal of Environmental Management,* 111**,** 44-52.

MITCHELL, N. C. & CLARKE, J. E. H. 1994. Classification of seafloor geology using multibeam sonar data from the Scotian Shelf. *Marine Geology,* 121**,** 143-160.

MONAHAN, E. C. & LU, M. 1990. Acoustically relevant bubble assemblages and their dependence on meteorological parameters. *Oceanic Engineering, IEEE Journal of,* 15**,** 340-349.

MOURAD, P. D. & JACKSON, D. R. 1989. High Frequency Sonar Equation Models For Bottom Backscatter And Forward Loss. *In:* OCEANS '89. Proceedings, 18-21 Sep 1989 1989. 1168-1175.

NOAA 2013a. Field Procedures Manual. National Oceanic and Atmospheric Administration Office of Coast Survey.

NOAA. 2013b. *Pacific Marine Environmental Lab Coastal Moorings* [Online]. Available: http://www.pmel.noaa.gov/co2/story/Coastal+Moorings [Accessed 2013].

NOAA 2013c. SOP Guidelines for Creating a Backscatter Mosaic. National Oceanic and Atmospheric Administration Office of Coast Survey.

NOAA SHIP FAIRWEATHER 2010 - 2013. Data Acquisition and Processing Report. U.S. Department of Commerce NOAA National Ocean Service http://www.ngdc.noaa.gov.

NOVARINI, J. C., KEIFFER, R. S. & NORTON, G. V. 1998. A model for variations in the range and depth dependence of the sound speed and attenuation induced by bubble clouds under wind-driven sea surfaces. *Oceanic Engineering, IEEE Journal of,* 23**,** 423-438.

PARNUM, I. M. & GAVRILOV, A. N. 2012. High-frequency multibeam echosounder measurements of seafloor backscatter in shallow water: Part 1—Data acquisition and processing. *Underwater Technology-Journal of the Societyfor Underwater Technology,* 30**,** 3.

PATON, M., MAYER, L. & WARE, C. 1997. Interactive 3D tools for pipeline route planning. *In:* OCEANS '97. MTS/IEEE Conference Proceedings, 6-9 Oct 1997 1997. 1216-1221 vol.2.

PEARCE, B., FARIÑAS-FRANCO, J. M., WILSON, C., PITTS, J., DEBURGH, A. & SOMERFIELD, P. J. Repeated mapping of reefs constructed by Sabellaria spinulosa Leuckart 1849 at an offshore wind farm site. *Continental Shelf Research.*

PENROSE, J. D., GAVRILOV, A. & PARNUM, I. M. 2008. Statistics of seafloor backscatter measured with multibeam sonar systems. *Journal of the Acoustical Society of America,* 123**,** 3628-3628.

POCWIARDOWSKI, P., YUFIT, G., MAILLARD, E. & ERIKSEN, P. 2006. Method for large sonar calibration and backscattering strength estimation. *In:* OCEANS 2006, 2006. IEEE, 1-5.

RESON 2011. SeaBat 7k Data Format. 2.20 ed. Slangerup.

RICE, G., GREENAWAY, S., WEBER, T., BEAUDOIN, J. 2012. Methods for Collecting and Using Backscatter Field Calibration Information for the Reson 7000 Series Multibeams. *Canadian Hydrographic Conference.* Niagra Falls, Canada.

SEA-BIRD ELECTRONICS, I. 2013. SBE 19plus V2 SeaCAT Profiler User's Manual. 11 ed. Bellevue, Washington.

SIMONS, D. G. & SNELLEN, M. 2009. A Bayesian approach to seafloor classification using multi-beam echo-sounder backscatter data. *Applied Acoustics,* 70**,** 1258-1268.

THORPE, S. A. 1982. On the Clouds of Bubbles Formed by Breaking Wind-Waves in Deep Water, and their Role in Air -- Sea Gas Transfer. *Philosophical Transactions of the Royal Society of London. Series A, Mathematical and Physical Sciences,* 304**,** 155-210.

THORPE, S. A. & HALL, A. J. 1983. The characteristics of breaking waves, bubble clouds, and near-surface currents observed using side-scan sonar. *Continental Shelf Research,* 1**,** 353-384.

URICK, R. J. (ed.) 1967. *Principles of Underwater Sound,* New York: McGraw-Hill.

WEBER, T. C., LYONS, A. P. & BRADLEY, D. L. 2005. An estimate of the gas transfer rate from oceanic bubbles derived from multibeam sonar observations of a ship wake. *Journal of Geophysical Research: Oceans,* 110**,** C04005.

WILSON, J. V., DEVISSER, A. & SUGIYAMA, B. 2009. Predicting the Mobility and Burial of Underwater Unexploded Ordnance (UXO) Using the UXO Mobility Model (ESTCP) 200417. DTIC Document.

APPENDICES

APPENDIX A

SUPPLEMENTAL FIELD TESTS

Several assumptions that were made in the formulation of this method were tested with other data sets and systems of opportunity. They are described and discussed here.

Beam-forming Mode

The assumption that the beam forming mode does not affect the result of the inter calibration was explored with data from a Reson 7125 SV2 on R/V Coastal Surveyor. Data were logged using the same ~300 m survey line off the coast of New Hampshire near Hampton Beach. The line was logged in both directions at a speed of 6 knots, once with roll stabilization enabled and again with it disabled at both frequencies in 18 m water depth. The vessel roll ranged from +/- 3° with period of a few seconds. Figure 40 and Figure 41 show the results of processing these lines with the research code with the nominal setting values applied.
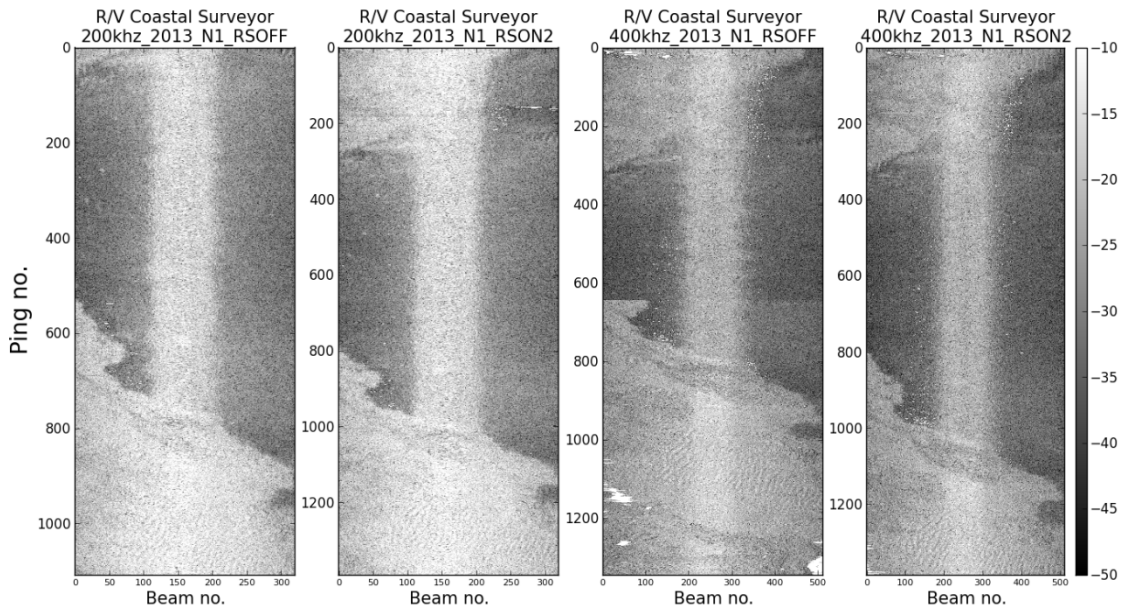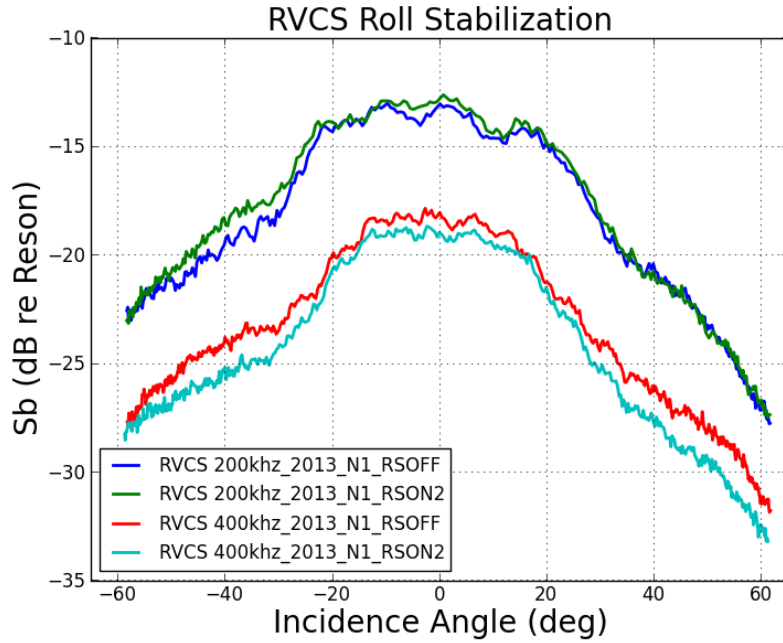
Figure 40: 200 kHz (bottom left) and 400 kHz (right bottom) data acquired in a northerly direction with roll stabilization disabled and enabled.
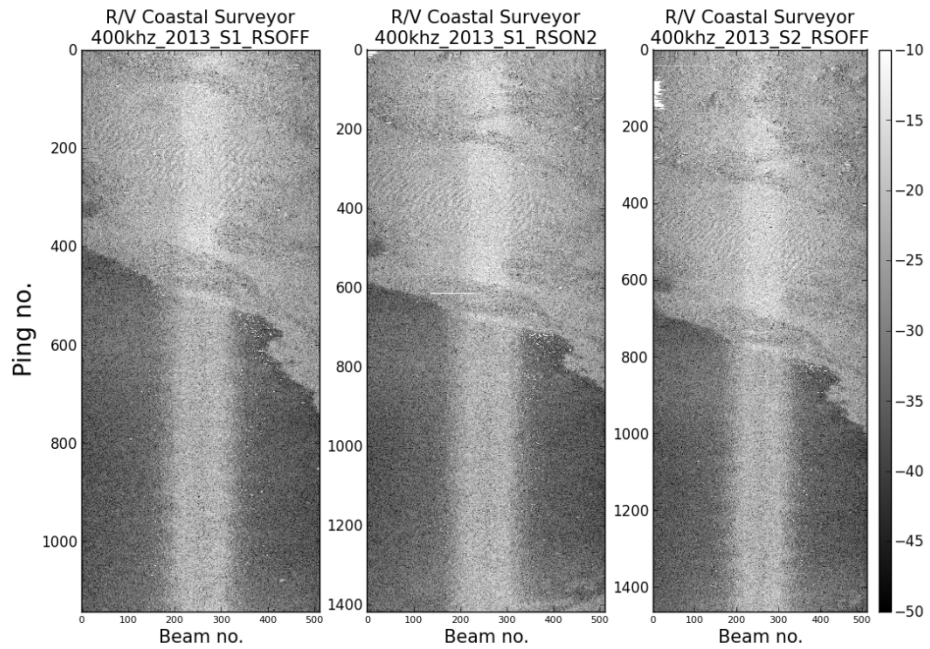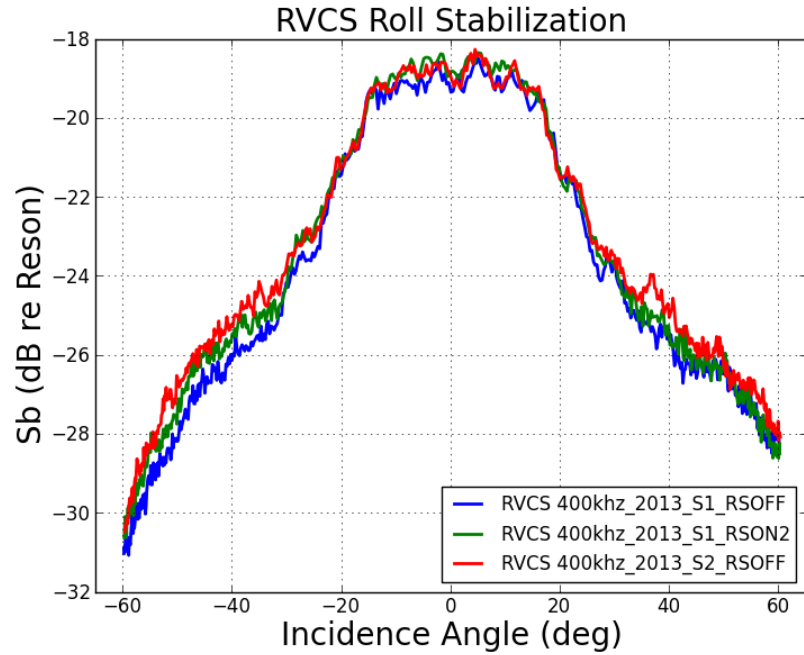
Figure 41: 400 kHz (bottom) data acquired in a southerly direction with roll stabilization disabled (bottom left and right) and enabled (bottom center).

These results appear consistent with what was observed in Duck Bay and Newport when running lines in opposite directions using the same operating settings

when roll stabilization was always enabled. Additionally, the technical note issued by Reson on beam forming supports this assumption (Maillard, 2010).

Linearity

The assumption that the systems are capable of operating in linear setting regimes for the range of possible settings (e.g. in deeper water and/or over softer sea beds) was explored with a Reson 7215 SV2 on NOAA Ship *Ferdinand R. Hassler* performing an *intra* calibration underway in 100 m water depth in Scantum Basin off the coast of New Hampshire. This assumption is important because it supports the extrapolation of the SL_{field} and G_{field} setting corrections through the high end setting options despite saturating in shallower depths. The results show operational setting combinations for which the gain is linear, but the power is not. Figure 42 shows an example of this. This does not mean the system cannot operate in an unsaturated condition for all settings, only that it has not been observed.
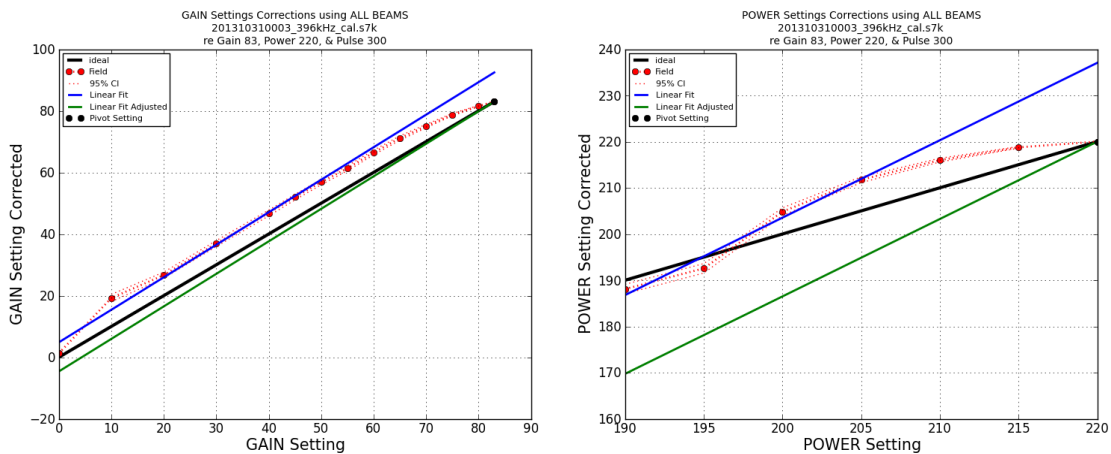

Figure 42: G_{field} LUT (left) and SL LUT (right) for highest possible pivot settings (Power 220, Gain 83, Pulse Length 300) from starboard Reson 7125 SV2 on Ferdinand R. Hassler in ~100 m of water.

Furthermore, Figure 43 shows the range of slopes that were observed for all pivot settings sampled. The SL_{field} slopes of *Hassler's* starboard Reson 7125 SV2 are nearly double what was observed with multiple Reson 7125 SV1, but the G_{field} slopes are consistent with the SV1s. These observations should be considered when calibrating Reson 7125 SV1s to SV2s, as well as any other comparable system.
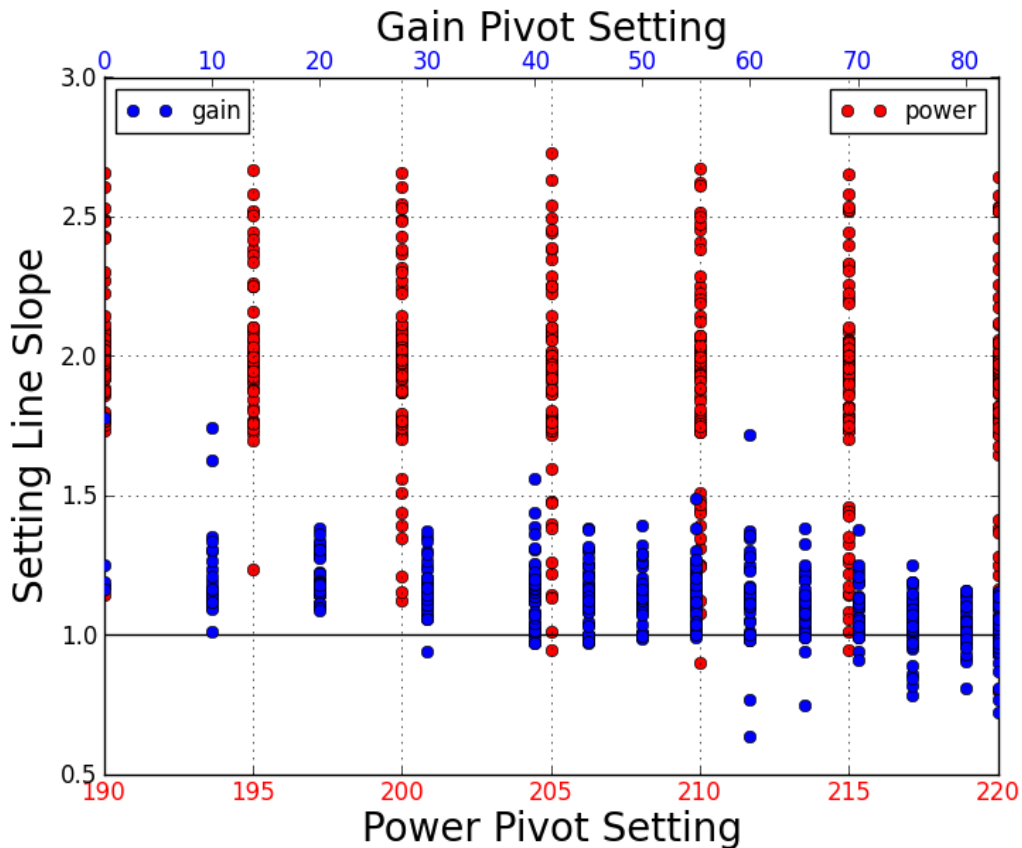

Figure 43: Comparison of intra calibration slopes for gain and power for NOAA Ship Ferdinand R. Hassler Starboard Reson 7125 SV2.

Reference Frame Misalignment between Systems and Along Track Incident Angle

Each system has four reference frames: the vessel reference frame, IMU reference frame, MBES reference frame, and beam pattern reference frame. By design,

113

the difference in beam amplitudes between systems that results from the ambiguity of the MBES reference frame misalignment with respect to the vessel and IMU reference frames between systems is captured in $C_{field}(\theta_s)$. Though all systems are similarly constructed, differences in loading from day to day (e.g. equipment, personnel, fuel levels, etc) and sea keeping at different speeds are to be expected. Because the *inter* calibration is only performed once at survey speed, the differences between beam amplitudes between systems due to dynamic reference frame misalignment is assumed to be negligible.

To explore the validity of this assumption, MBES data were logged while a launch was conducting ellipsoid-referenced dynamic draft measurements (ERDDM). The ERDDM measurements are derived by running a survey line in both directions, each set with increasing vessel engine RPMs (vessel speeds) for 3-5 minutes in each direction at each RPM (NOAA, 2013a). The backscatter data collected while running ERDDM lines near Site 1 in the Yaquina River with Launch 2807 were processed with the research code without any calibration corrections applied and compared with vessel pitch to estimate the effect of varying vessel alignment, particularly in the fore-aft direction. Figure 44 shows that a 2 dB spread in the central tendency of the backscatter measurements is possible in 8 m of water when the vessel pitch varies from roughly 0.5 to 5°. The implication is that ignoring vessel speed and attitude during the *inter* calibration can result in non-trivial biases in $C_{field}(\theta_s)$. Moreover, this confirms that backscatter measurement inconsistencies can result when the 3D beam angle of incidence, the components of which are the along-track and across-track incidence angles, is not accounted for in the backscatter reduction process.
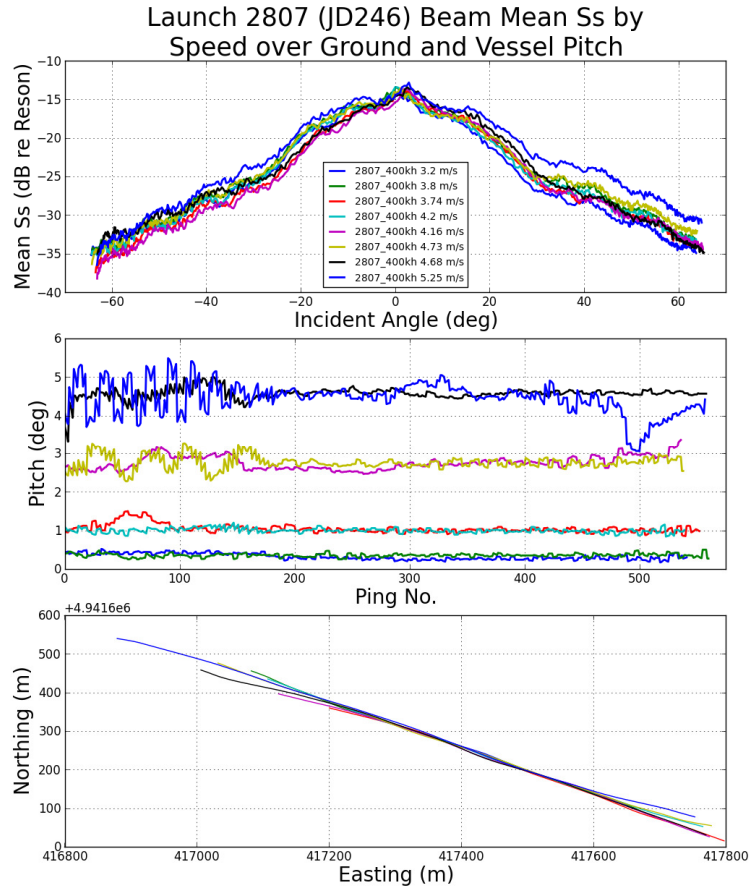
Figure 44: Comparison of beam mean S_b acquired by the same system over the same area near in time at varied speeds.

Other ways to pursue this issue and to possibly derive pseudo corrections for misalignment between beam pattern and MBES reference frames between systems might include looking at the beam amplitudes and IMU vessel orientation data while each vessel is alongside a pier and manually altered (pitched up and down in the longitudinal direction and rolled back and forth in the transverse direction). If the vessels are not operated in similar sea surface conditions and do not have similar sea keeping characteristics then accounting for the for-aft beam vector alignment with respect to vessel pitch and seafloor slope is necessary if this field calibration method is to be employed.

APPENDIX B

RESON NORMALIZATION FILE COMPARISON (.C7K FILES)

Reson Seabat 7P series MBES have the ability to normalize amplitude and phase differences between the receiver elements to reduce side lobe levels. After each normalization a .c7k file is created to store the results which are used during beam-forming. Visual changes in the raw data have been observed before and after normalizing the Reson 7125 SV1 MBES. An attempt was made to quantify the variability of the normalizations as a basis for understanding their contribution to backscatter measurement inconsistency. All available .c7k files from all systems were collected and compared to one another using a file reader provided by Reson and plotted in Figure 45, Figure 46, and Figure 47. While it is unknown how specifically these values are used during the beam-forming process, the variability suggests they are related to the observed changes in the displayed data before and after normalization.
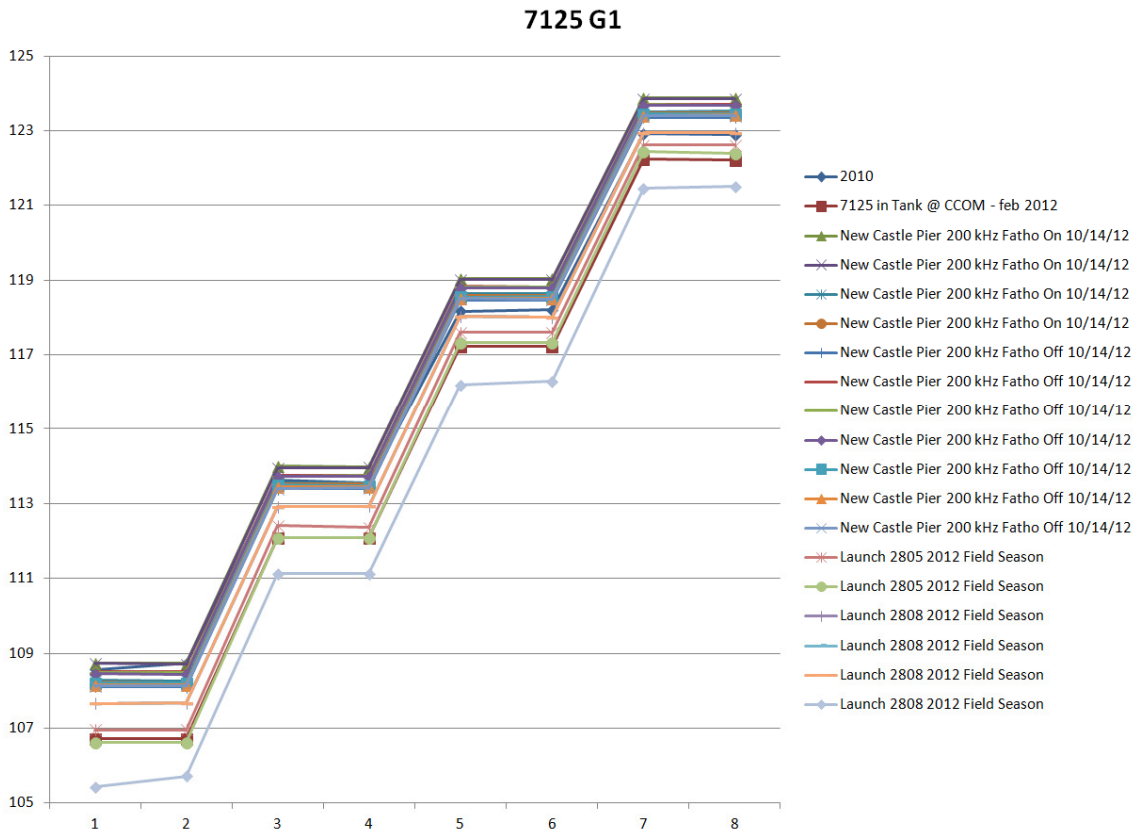
Figure 45: Reson .c7k file G1 values for systems on different vessels at different times in different locations.
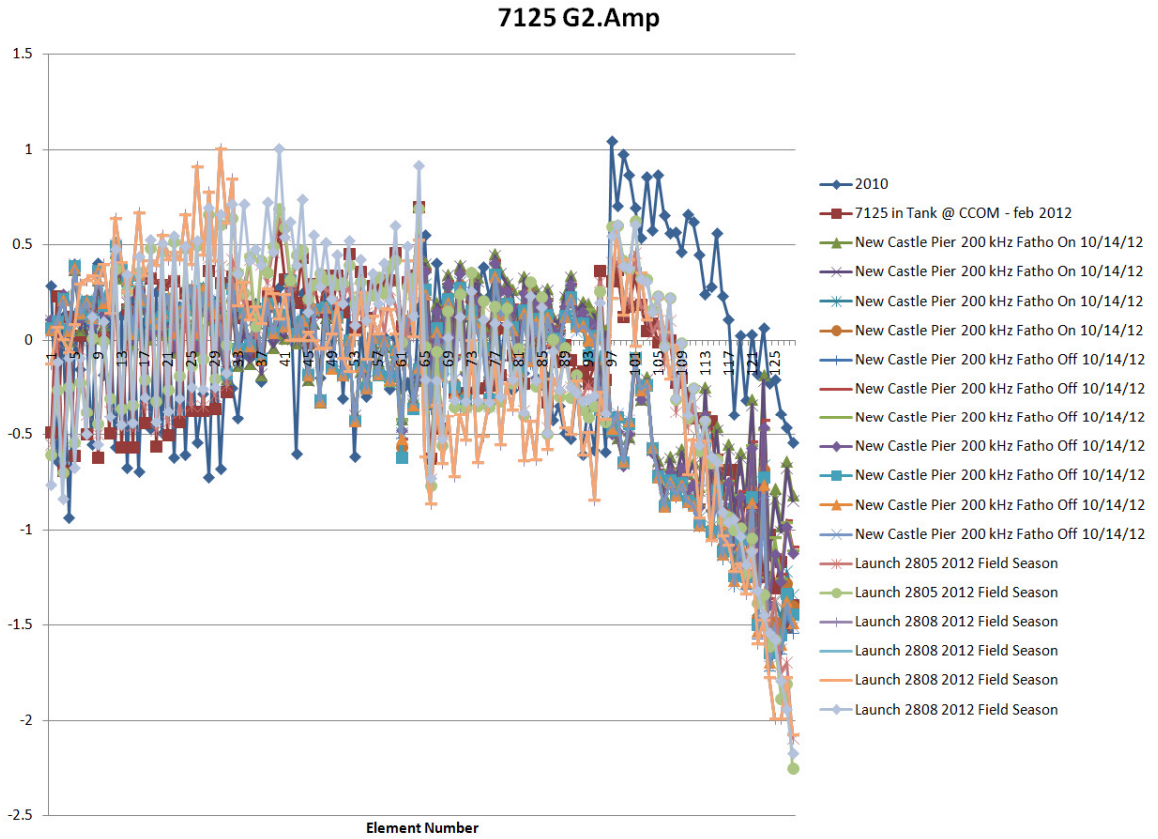
7125 G2.Amp

Figure 46: Reson .c7k file G2.Amp values for systems on different vessels at different times in different locations.

Figure 47: Reson .c7k file G2.Pha values for systems on different vessels at different times in different locations.
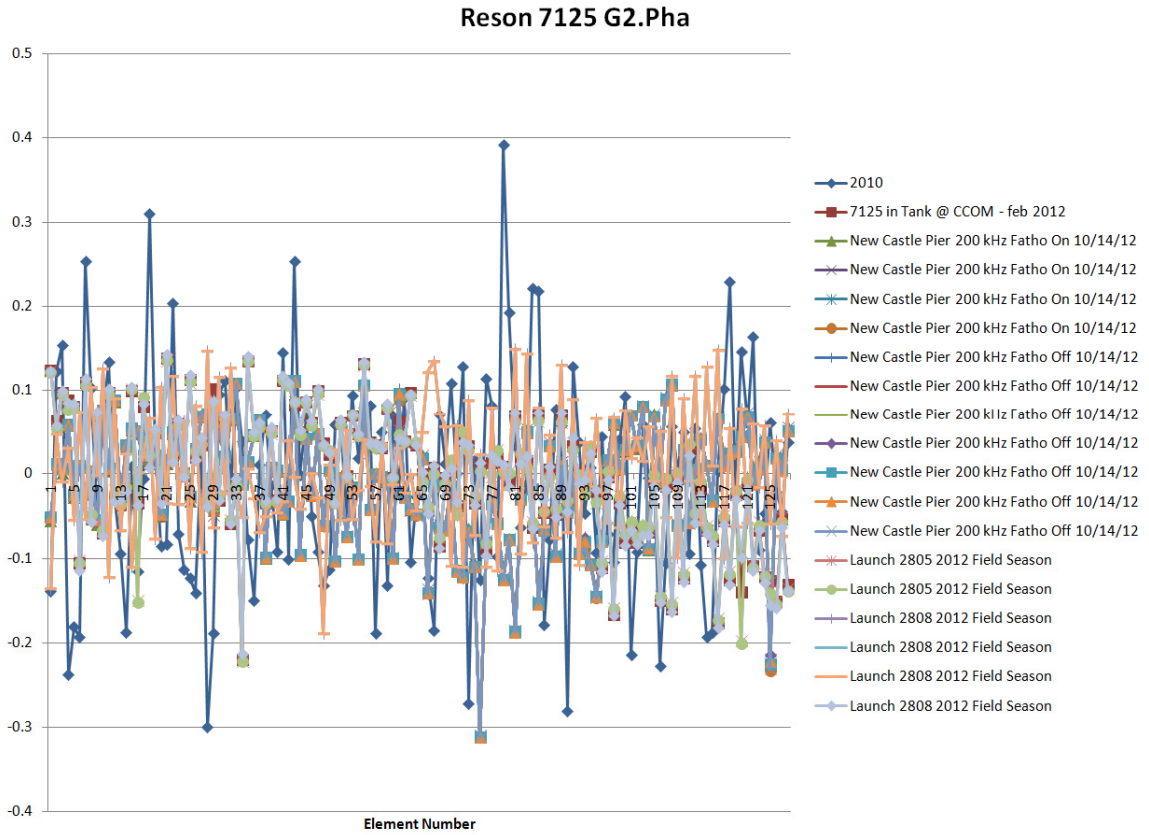
APPENDIX C

CONCEPTUALIZED CALIBRATION FILE SCHEMA

Figure 48 is a conceptualized framework for handling calibration files for a generic MBES for potential use with backscatter processing software.
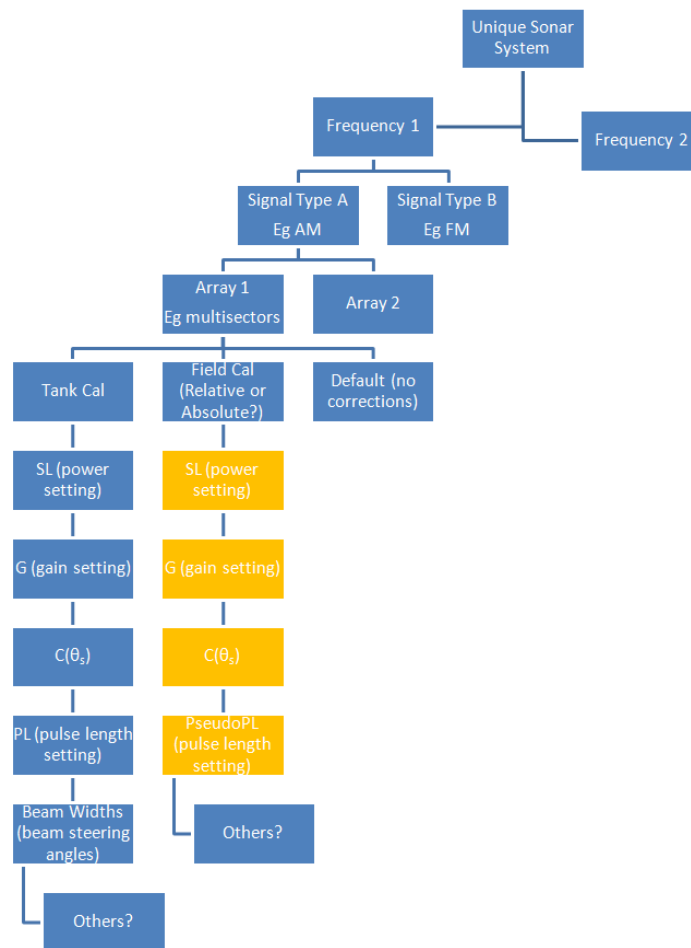

Figure 48: Conceptualized framework for calibration file handling.